

**WETTABILITY OF SILICON, SILICON DIOXIDE, AND ORGANOSILICATE GLASS**

Nelson Martinez, B.S.

Thesis Prepared for the Degree of  
**MASTER OF SCIENCE**

**UNIVERSITY OF NORTH TEXAS**

December 2009

**APPROVED:**

Richard F. Reidy, Major Professor and Interim  
Chair of the Department of Materials  
Science and Engineering

Witold Brostow, Committee Member

Jincheng Du, Committee Member

Srinivasan G. Srivilliputhur, Committee  
Member

Costas Tsatsoulis, Dean of the College of  
Engineering

Michael Monticino, Dean of the Robert B.  
Toulouse School of Graduate Studies

Martinez, Nelson. Wettability of Silicon, Silicon Dioxide, and Organosilicate Glass.

Master of Science (Materials Science and Engineering), December 2009, 106 pp., 26 tables, 48 illustrations, references 88 titles.

Wetting of a substance has been widely investigated since it has many applications to many different fields. Wetting principles can be applied to better select cleans for front end of line (FEOL) and back end of line (BEOL) cleaning processes. These principles can also be used to help determine processes that best repel water from a semiconductor device. It is known that the value of the dielectric constant in an insulator increases when water is absorbed. These contact angle experiments will determine which processes can eliminate water absorption. Wetting is measured by the contact angle between a solid and a liquid. It is known that roughness plays a crucial role on the wetting of a substance. Different surface groups also affect the wetting of a surface. In this work, it was investigated how wetting was affected by different solid surfaces with different chemistries and different roughness. Four different materials were used: silicon; thermally grown silicon dioxide on silicon; chemically vapor deposited (CVD) silicon dioxide on silicon made from tetraethyl orthosilicate (TEOS); and organosilicate glass (OSG) on silicon. The contact angle of each of the samples was measured using a goniometer. The roughness of the samples was measured by atomic force microscopy (AFM). The chemistry of each of the samples were characterized by using X-ray photoelectron spectroscopy (XPS) and grazing angle total attenuated total reflection Fourier transform infrared spectroscopy (FTIR/GATR). Also, the contact angle was measured at the micro scale by using an environmental scanning electron microscope (ESEM).

Copyright 2009

by

Nelson Martinez

## ACKNOWLEDGEMENTS

Twenty six years ago my father came to the U.S from El Salvador with dreams of providing a better life for me and my brothers. Twenty six years later I receive my Masters of Science in Engineering. Thanks to my father, Ramon Martinez, and my mother, Albertina Martinez, I have accomplished my dreams of being someone in life. I am eternally grateful for their support. I would also like to thank my siblings (David, Marby, Nancy, and Erick). To Dr. Rick Reidy, I thank him for being my advisor and friend for the time I was here. I couldn't have done this without his help. To Dr. Tom Scharf, Dr. Nigel Sheperd, Dr. Witold Brostow, Dr. Jincheng Du, and Dr. Srinivasan G. Srivilliputhur, I give thanks for the help I received from them and for the advice they gave me.

Last but not least, I would like to give thanks to all my friends. All were very supportive and made my time here a lot smoother. Thank you Fang-ling Kuo, Benedict, Eric, Ghare, Mohammed, Ming-Te, Amanda, Aaron, Wei-Lun, Tea, Marianna Pannico, Marianna Castro, Juliana Ricardo D'Souza (whom always was willing to talk to me when I would get bored in the lab), Francisco, Edwin, Sandeep, Nagarash, and anyone else who I considered my friend here at UNT. I would also like to give thanks to my friends in Houston, some whom I've known since I was a child. Thank you Walter Pacheco, Ruben, Angel, Lenin, Michael, Christel, Cintia. And finally I give thanks to my best friend Frank Franco, who always gave me his unconditional support and encouragement. If I've left any one out please accept my apologies.

## TABLE OF CONTENTS

ACKNOWLEDGEMENTS.....	iii
LIST OF TABLES .....	viii
LIST OF FIGURES .....	x
CHAPTER	
1. INTRODUCTION.....	1
1.1 Basic Principles of Wetting .....	1
1.2 Proposed Work on Contact Angle .....	1
2. WETTING, ROUGHNESS, AND CHEMICAL FUNCTIONALIZATION .....	3
2.1 Wetting .....	3
2.1.1 Adhesive and Cohesive Forces .....	3
2.1.2 Young's Equation .....	3
2.1.3 Harmonic and Geometric Model .....	4
2.2 Roughness .....	6
2.2.1 Cassie-Baxter and Wenzel's Model.....	6
2.3 Chemical Functionalization.....	7
2.3.1 Hydroxyl, Hydrogen, and Trimethylsilyl Termination .....	7
2.3.2 Hydroxyl Termination.....	7
2.3.3 Hydrogen Termination .....	8
2.3.4 Trimethylsilyl Termination .....	8
3. SILICON, TOX, TEOS, and OSG .....	12
3.1 Materials.....	12
3.2 TOX .....	12

3.3 TEOS.....	13
3.4 OSG .....	14
3.5 Previous Work on Wettability of SiO <sub>2</sub> .....	14
3.6 Previous Work on Wettability of OSG .....	15
4. EXPERIMENTAL .....	17
4.1 Etching and Supercritical Treatments .....	17
4.2 Contact Angle .....	18
4.2.1 Purpose of Measuring Contact Angle .....	18
4.2.2 Goniometer .....	19
4.2.3 Contact Angle Procedure.....	20
4.3 FTIR/GATR .....	20
4.3.1 Infrared Spectroscopy Theory .....	20
4.3.2 FTIR/GATR Apparatus and Procedure of Measurements .....	22
4.4 XPS .....	23
4.4.1 XPS Theory .....	23
4.4.2 Apparatus and Procedure of Measurements .....	24
4.5 AFM.....	25
4.5.1 AFM Theory .....	25
4.5.2 Apparatus and Procedure of Measurements .....	27
4.6 ESEM.....	27
4.6.1 ESEM Theory .....	27
4.6.2 ESEM Apparatus and Procedure of Measurements .....	28
5. RESULTS .....	29

5.1 Silicon Results .....	29
5.1.1 Contact Angle and Surface Energy Results.....	29
5.1.2 Silicon FTIR/GATR.....	31
5.1.3 Silicon XPS .....	33
5.1.4 Silicon AFM Results .....	34
5.1.5 Conclusions for Silicon .....	38
5.2 TOX Results .....	39
5.2.1 TOX Contact Angle and Surface Energy .....	39
5.2.2 TOX FTIR/GATR.....	42
5.2.3 TOX XPS.....	50
5.2.4 AFM TOX .....	51
5.2.5 Conclusions for TOX .....	55
5.3 TEOS Results .....	56
5.3.1 TEOS Contact Angle and Surface Energy .....	56
5.3.2 TEOS FTIR/GATR.....	59
5.3.3 TEOS XPS.....	67
5.3.4 TEOS AFM.....	68
5.3.5 Conclusions for TEOS .....	72
5.4 OSG Results .....	73
5.4.1 OSG Contact Angle and Surface Energy .....	73
5.4.2 GATR/FTIR for OSG.....	76
5.4.3 OSG XPS .....	81
5.4.4 OSG AFM.....	82

5.4.5 Conclusions for OSG .....	86
6. FURTHER EXPERIMENTATION .....	87
6.1 Wetting after Dynamic Contact.....	86
6.2 Wetting in ESEM vs. Goniometer.....	90
7. CONCLUSIONS AND FUTURE WORK .....	93
7.1 Conclusion.....	93
7.2 Future Work .....	93
BIBLIOGRAPHY .....	95

## LIST OF TABLES

	Page
<b>Table 5-1</b> Surface Energies for Etched Si and Etched + HMDS Si .....	30
<b>Table 5-2</b> Wavenumber and Band Assignment for Etched Si and Etched + HMDS Si .....	32
<b>Table 5-3</b> Carbon, Silicon, and Oxygen Percentages for Each Sample .....	33
<b>Table 5-4</b> AFM Summary of Etched Si.....	35
<b>Table 5-5</b> AFM Summary of Etched + HMDS Si.....	37
<b>Table 5-6</b> Surface Energies for the TOX Samples .....	41
<b>Table 5-7</b> Wavenumber and Band Assignment for TOX Samples .....	49
<b>Table 5-8</b> Carbon, Silicon, and Oxygen Percentages for Each Sample .....	50
<b>Table 5-9</b> Wavelength, RMS, and Peak Height for Received TOX .....	51
<b>Table 5-10</b> Wavelength, RMS, and Peak Height for Etched TOX .....	52
<b>Table 5-11</b> Wavelength, RMS, and Peak Height for HMDS TOX .....	53
<b>Table 5-12</b> Wavelength, RMS, and Peak Height for Etched + HMDS TOX.....	54
<b>Table 5-13</b> Surface Energy for TEOS .....	58
<b>Table 5-14</b> Wavenumber and Band Assignment for TEOS Samples .....	66
<b>Table 5-15</b> XPS Data for TEOS.....	67
<b>Table 5-16</b> Wavelength, RMS, Peak Heights of Received TEOS .....	68
<b>Table 5-17</b> Wavelength, RMS, Peak Heights of Etched TEOS .....	69
<b>Table 5-18</b> Wavelength, RMS, Peak Heights of HMDS TEOS .....	70
<b>Table 5-19</b> Wavelength, RMS, Peak Heights of Etched + HMDS TEOS .....	71
<b>Table 5-20</b> Surface Energy for OSG .....	75
<b>Table 5-21</b> Wavenumber and Band Assignment for OSG Samples .....	76

<b>Table 5-22</b> XPS Data for OSG.....	81
<b>Table 5-23</b> Wavelength, RMS, Peak Heights of Received OSG .....	82
<b>Table 5-24</b> Wavelength, RMS, Peak Heights of Etched OSG.....	83
<b>Table 5-25</b> Wavelength, RMS, Peak Heights of HMDS OSG .....	84
<b>Table 5-26</b> Wavelength, RMS, Peak Heights of Etched + HMDS OSG .....	85

## LIST OF FIGURES

	Page
<b>Figure 2-1</b> The CO <sub>2</sub> Phase Diagram as a Function of Temperature and Pressure .....	9
<b>Figure 2-2 a)</b> Hydroxyl Termination.....	11
<b>b)</b> Hydrogen Termination .....	11
<b>c)</b> TrimethylsilylTermination .....	11
<b>Figure 4-1</b> Contact Angle Gonimeter Rame-Hart Model 250 .....	19
<b>Figure 4-2</b> FTIR Nexus 470 E.S.P Spectrometer .....	21
<b>Figure 4-3</b> GATR Using a Ge Crystal with 65° .....	23
<b>Figure 4-4</b> XPS PHI 5000 Versa Probe.....	24
<b>Figure 4-5</b> Force vs. Distance for Contact and Non Contact.....	26
<b>Figure 4-6</b> Veeco (Digital Instruments) Multimode Nanoscope III .....	26
<b>Figure 4-7</b> FEI Quanta 200 ESEM.....	28
<b>Figure 5-1</b> Contact Angle for Etched Si and Etched + HMDS Si .....	30
<b>Figure 5-2</b> FTIR Peaks for Etched Si and Etched + HMDS Si .....	32
<b>Figure 5-3</b> Number of Events vs. Height for the Etched Si.....	35
<b>Figure 5-4</b> 3-D Image of the Etched Si Sample .....	35
<b>Figure 5-5</b> Number of Events vs. Heights of Etched + HMDS Si .....	37
<b>Figure 5-6</b> 3-D Image of the Etched + HMDS Si Sample.....	37
<b>Figure 5-7</b> Contact Angle for TOX Samples .....	41
<b>Figure 5-8 a)</b> Received TOX FTIR/GATR Spectrum.....	42
<b>b)</b> Received TOX FTIR/GATR Spectrum Wavelengths 950 cm <sup>-1</sup> -1300 cm <sup>-1</sup> .....	42

<b>Figure 5-9 a)</b> Etched TOX FTIR/GATR Spectrum .....	44
<b>b)</b> Etched TOX FTIR/GATR Spectrum Wavelengths	
$900\text{ cm}^{-1}$ - $1300\text{ cm}^{-1}$ .....	44
<b>Figure 5-10 a)</b> HMDS TOX FTIR/GATR Spectrum .....	46
<b>b)</b> HMDS TOX FTIR/GATR Spectrum Wavelengths	
$1000\text{ cm}^{-1}$ - $1300\text{ cm}^{-1}$ .....	46
<b>Figure 5-11 a)</b> Etched + HMDS TOX FTIR/GATR Spectrum .....	48
<b>b)</b> Etched + HMDS TOX FTIR/GATR Spectrum Wavelengths	
$950\text{ cm}^{-1}$ - $1300\text{ cm}^{-1}$ .....	48
<b>Figure 5-12</b> Peak Heights for Received TOX.....	51
<b>Figure 5-13</b> Peak Heights for Etched TOX .....	52
<b>Figure 5-14</b> Peak Heights for HMDS TOX .....	53
<b>Figure 5-15</b> Peak Heights for Etched + HMDS TOX .....	54
<b>Figure 5-16</b> Number of Events vs. Height for TOX .....	55
<b>Figure 5-17</b> Contact Angles for TEOS.....	58
<b>Figure 5-18 a)</b> Received TEOS FTIR/GATR Spectrum .....	59
<b>b)</b> Received TEOS FTIR/GATR Spectrum Wavelengths	
$900\text{ cm}^{-1}$ - $1300\text{ cm}^{-1}$ .....	59
<b>Figure 5-19 a)</b> Etched TEOS FTIR/GATR Spectrum.....	61
<b>b)</b> Etched TEOS FTIR/GATR Spectrum Wavelengths	
$950\text{ cm}^{-1}$ - $1300\text{ cm}^{-1}$ .....	61

<b>Figure 5-20 a)</b> HMDS TEOS FTIR/GATR Spectrum .....	63
<b>b)</b> HMDS TEOS FTIR/GATR Spectrum Wavelengths	
$900\text{ cm}^{-1}$ - $1300\text{ cm}^{-1}$ .....	63
<b>Figure 5-21 a)</b> Etched + HMDS TEOS FTIR/GATR .....	65
<b>b)</b> Etched + HMDS TEOS FTIR/GATR Spectrum Wavelengths	
$900\text{ cm}^{-1}$ - $1300\text{ cm}^{-1}$ .....	65
<b>Figure 5-22</b> Peak Heights for Received TEOS .....	68
<b>Figure 5-23</b> Peak Heights for Etched TEOS.....	69
<b>Figure 5-24</b> Peak Heights for HMDS TEOS .....	70
<b>Figure 5-25</b> Peak Heights for Etched + HMDS TEOS .....	71
<b>Figure 5-26</b> Number of Events vs. Height for TEOS.....	72
<b>Figure 5-27</b> Contact Angles for OSG.....	75
<b>Figure 5-28 a)</b> Received OSG FTIR/GATR Spectrum.....	77
<b>b)</b> Received OSG FTIR/GATR Spectrum Wavelengths	
$900\text{ cm}^{-1}$ - $1300\text{ cm}^{-1}$ .....	77
<b>Figure 5-29 a)</b> Etched OSG FTIR/GATR Spectrum.....	78
<b>b)</b> Etched OSG FTIR/GATR Spectrum Wavelengths	
$950\text{ cm}^{-1}$ - $1300\text{ cm}^{-1}$ .....	78
<b>Figure 5-30 a)</b> HMDS OSG FTIR/GATR Spectrum .....	79
<b>b)</b> HMDS OSG FTIR/GATR Spectrum Wavelengths	
$950\text{ cm}^{-1}$ - $1300\text{ cm}^{-1}$ .....	79
<b>Figure 5-31 a)</b> Etched + HMDS OSG FTIR/GATR Spectrum .....	80
<b>b)</b> Etched + HMDS OSG FTIR/GATR Spectrum Wavelengths	

900 cm <sup>-1</sup> -1300 cm <sup>-1</sup> .....	80
<b>Figure 5-32</b> Peak Heights for the Received OSG .....	82
<b>Figure 5-33</b> Peak Heights for the Etched OSG .....	83
<b>Figure 5-34</b> Peak Heights of HMDS OSG .....	84
<b>Figure 5-35</b> Peak Heights for the Etched + HMDS OSG .....	85
<b>Figure 5-36</b> Number of Events vs Height for OSG .....	86
<b>Figure 6-1 a)</b> Water Contact Angle Before and After Dynamic Contact.....	89
<b>b)</b> DIM Contact Angle Before and After Dynamic Contact.....	89
<b>Figure 6-2</b> Water Contact Angle on Goniometer and ESEM .....	90
<b>Figure 6-3 a,b,c,d)</b> Images of Water Droplet on the Environmental Scanning Electron Microscope as the Drop Starts to Condense and Grow on the Samples .....	92

# CHAPTER 1

## INTRODUCTION

### 1.1 Basic Principles of Wetting

Wetting of a substance has been widely investigated since it has many applications in many different fields; from the semiconductor industry, to biological applications, to coatings, and to many other fields. However, the main focus of interest has been on its applications to the cleaning of semiconductor materials. Wetting by definition is how much a liquid attracts a solid surface. Wetting is measured by the contact angle between a solid and a liquid. The equation commonly used to quantify the wetting of a substance is Young's equation [1-6]

$$\cos \theta_{\text{young}} = \frac{\gamma_{\text{sv}} - \gamma_{\text{sl}}}{\gamma_{\text{lv}}} \quad (\text{Eq. 1-1}).$$

However, this equation is based on the assumption that the solid is perfectly flat. It is known that this is not the case since any surface at the microscopic level will show some sort of roughness. To accommodate this limitation, we have to make use of other wetting models that take into consideration the roughness of a surface. One such model was first described by Wenzel, and the other is the Cassie-Baxter model [3-4, 7-13]. The Wenzel model makes the assumption that the liquid penetrates the surface roughness. The Cassie-Baxter model makes the assumption that surface asperities trap air beneath the surface liquid.

### 1.2 Proposed Work on Contact Angle

In this work I studied how wetting was affected by different solid surfaces with different chemistries and different roughness. It is known that as the roughness of a material increases, the more hydrophobic (the more it repels water) the material is. Also, it is known that different surface chemistries can affect the contact angle between a surface and a liquid. Four different materials were used: silicon; thermally grown silicon dioxide (thermal oxide, TOX) on silicon;

chemically vapor deposited (CVD) silicon dioxide on silicon made from tetraethyl orthosilicate (TEOS); and organosilicate glass (OSG) on silicon. After cutting the respective samples into 1 and 2 inch pieces, one set of these materials was etched with a mixture of hydrofluoric (HF) acid and deionized water. The ratio was 1:50. Another set was etched with dilute HF and then were placed in a supercritical chamber to functionalize them with hexamethyldisilazane (HMDS). A third set was only functionalized by HMDS. The contact angle of each of the samples was measured using a goniometer. The roughness of the samples was measured by atomic force microscopy (AFM). The chemistry of each of the samples was characterized using X-ray photoelectron spectroscopy (XPS) and grazing angle total attenuated total reflection Fourier transform infrared spectroscopy (FTIR/GATR). A dynamic contact angle mechanism was done on the samples and the contact angle was measured afterwards to see if water had penetrated the surface. Also, the contact angle was measured at the micro scale by using an environmental scanning electron microscope (ESEM).

## CHAPTER 2

### WETTING, ROUGNESS, AND CHEMICAL FUNCTIONALIZATION

#### 2.1 Wetting

##### 2.1.1 Adhesive and Cohesive Forces

Wetting is usually measured by observing the contact angle a liquid makes with a solid surface. The contact angle is the angle that the liquid/vapor interface makes with a solid/liquid interface. There are two main forces involved in the interaction between liquid and solid; adhesive and cohesive [1-2]. The adhesive force is the force that causes a liquid to spread across a solid surface--the force of attraction between a solid and a liquid. The cohesive force prevents a liquid from spreading over a solid surface. This force is the attraction between the molecules within the liquid. It causes the liquid droplet to ball up avoiding contact with the solid. The resultant of these two forces is the measured contact angle between the solid and liquid. When the contact angle is less than 90°, the liquid will spread over a large area of the solid and is commonly termed a hydrophilic surface. When the contact angle is greater than 90°, the liquid is repelled by the solid surface limiting the contact area between the solid and liquid. This is commonly referred to as a hydrophobic surface.

##### 2.1.2 Young's Equation

The theory of wetting usually makes the use of Young's equation

$$\cos \theta_{\text{young}} = \frac{\gamma_{\text{sv}} - \gamma_{\text{sl}}}{\gamma_{\text{lv}}} \quad (\text{Eq. 1-1}) [1-6].$$

Where  $\gamma_{\text{sv}}$  is the interfacial energy between the solid and the vapor (usually termed surface free energy),  $\gamma_{\text{sl}}$  is the interfacial energy between the solid and the liquid, and  $\gamma_{\text{lv}}$  is the interfacial energy between the liquid and the vapor (this is usually termed surface tension). Interfacial

energy is the excess energy that exists between these two phases. It usually arises from an imbalance of the forces of the molecules at the interface (units are J/m<sup>2</sup>).

### 2.1.3 Harmonic and Geometric Model

When measuring the surface energy of the solid/liquid interface, there are two different methods that are used to interpret these data: harmonic and geometric [14]. Before there is any explanation on either of these methods, we have to understand work of cohesion and work of adhesion [1-2]. Work of cohesion is the work required to separate a liquid into two separate parts, and it is given by the equation

$$W_{\text{cohesion}} = 2\gamma_{\text{lv}}, \quad (\text{Eq. 2-1})$$

where  $\gamma_{\text{lv}}$  is the surface tension of the liquid. The work of adhesion is the work required to separate a liquid from a solid surface, and it is given by the equation

$$W_{\text{adhesion}} = \gamma_{\text{lv}} + \gamma_{\text{sv}} - \gamma_{\text{sl}} \quad (\text{Eq. 2-2})$$

which simplifies to the Young-Dupree equation

$$W_{\text{adhesion}} = \gamma_{\text{lv}}(1 + \cos \theta) \quad (\text{Eq. 2-3}).$$

Both the geometric and the harmonic methods employ the assumption that when using different liquids on the same surface, it is possible to calculate different components of the surface energy when the different components of the liquids are known. These different components (i.e polar, dispersive, hydrogen bonding, induction force, etc...) are additive. That means the total surface energy is given by the equation

$$\gamma_{\text{total}} = \gamma^{\text{d}} + \gamma^{\text{p}} + \gamma^{\text{h}} + \dots \quad (\text{Eq. 2-4}).$$

In both the geometric and the harmonic means, we make use of two different liquids to measure the work of adhesion: a polar liquid (deionized water) and a dispersive liquid (diiodomethane). The geometric model uses

$$W_{\text{adhesion}} = 2(\gamma_{\text{lv}}^{\text{d}} \gamma_{\text{sv}}^{\text{d}})^{1/2} + 2(\gamma_{\text{lv}}^{\text{p}} \gamma_{\text{sv}}^{\text{p}})^{1/2} \quad (\text{Eq. 2-5})$$

for the work of adhesion. It then sets this equation equal to the Young Dupree eqn. to get the following equation

$$\gamma_{\text{lv}}(1 + \cos \theta) = 2(\gamma_{\text{lv}}^{\text{d}} \gamma_{\text{sv}}^{\text{d}})^{1/2} + 2(\gamma_{\text{lv}}^{\text{p}} \gamma_{\text{sv}}^{\text{p}})^{1/2} \quad (\text{Eq. 2-6}).$$

However since we are using two liquids than the two equations become

$$\gamma_{\text{lvH20}}(1 + \cos \theta_{\text{H20}}) = 2(\gamma_{\text{lvH20}}^{\text{d}} \gamma_{\text{sv}}^{\text{d}})^{1/2} + 2(\gamma_{\text{lvH20}}^{\text{p}} \gamma_{\text{sv}}^{\text{p}})^{1/2} \quad (\text{Eq. 2-7})$$

and the second equation becomes

$$\gamma_{\text{lvDIM}}(1 + \cos \theta_{\text{DIM}}) = 2(\gamma_{\text{lvDIM}}^{\text{d}} \gamma_{\text{sv}}^{\text{d}})^{1/2} + 2(\gamma_{\text{lvDIM}}^{\text{p}} \gamma_{\text{sv}}^{\text{p}})^{1/2} \quad (\text{Eq. 2-8})$$

the 2 equations are then linearized to get

$$\frac{(\gamma_{\text{lvH20}}^{\text{d}})^{1/2}}{\gamma_{\text{lvH20}}} (\gamma_{\text{sv}}^{\text{d}})^{1/2} + \frac{(\gamma_{\text{lvH20}}^{\text{p}})^{1/2}}{\gamma_{\text{lvH20}}} (\gamma_{\text{sv}}^{\text{p}})^{1/2} = \frac{(1 + \cos \theta_{\text{H20}})}{2} \quad (\text{Eq. 2-9})$$

$$\frac{(\gamma_{\text{lvDIM}}^{\text{d}})^{1/2}}{\gamma_{\text{lvDIM}}} (\gamma_{\text{sv}}^{\text{d}})^{1/2} + \frac{(\gamma_{\text{lvDIM}}^{\text{p}})^{1/2}}{\gamma_{\text{lvDIM}}} (\gamma_{\text{sv}}^{\text{p}})^{1/2} = \frac{(1 + \cos \theta_{\text{DIM}})}{2} \quad (\text{Eq. 2-10})$$

These equations are then solved for  $(\gamma_{\text{sv}}^{\text{p}})^{1/2}$  and  $(\gamma_{\text{sv}}^{\text{d}})^{1/2}$ .

For the harmonic mean, the work of adhesion is determined by the equation

$$W_{\text{adhesion}} = \frac{4\gamma_{\text{lv}}^{\text{d}} \gamma_{\text{sv}}^{\text{d}}}{\gamma_{\text{lv}}^{\text{d}} + \gamma_{\text{sv}}^{\text{d}}} + \frac{4\gamma_{\text{lv}}^{\text{p}} \gamma_{\text{sv}}^{\text{p}}}{\gamma_{\text{lv}}^{\text{p}} + \gamma_{\text{sv}}^{\text{p}}} \quad (\text{Eq. 2-11}).$$

This equation is set equal to the Young-Dupree equation using two different liquids to get two equations to solve

$$\gamma_{\text{lvH20}}(1 + \cos \theta_{\text{H20}}) = \frac{4\gamma_{\text{lvH20}}^{\text{d}} \gamma_{\text{sv}}^{\text{d}}}{\gamma_{\text{lvH20}}^{\text{d}} + \gamma_{\text{sv}}^{\text{d}}} + \frac{4\gamma_{\text{lvH20}}^{\text{p}} \gamma_{\text{sv}}^{\text{p}}}{\gamma_{\text{lvH20}}^{\text{p}} + \gamma_{\text{sv}}^{\text{p}}} \quad (\text{Eq. 2-12})$$

$$\gamma_{\text{lvDIM}}(1 + \cos \theta_{\text{DIM}}) = \frac{4\gamma_{\text{lvDIM}}^{\text{d}} \gamma_{\text{sv}}^{\text{d}}}{\gamma_{\text{lvDIM}}^{\text{d}} + \gamma_{\text{sv}}^{\text{d}}} + \frac{4\gamma_{\text{lvDIM}}^{\text{p}} \gamma_{\text{sv}}^{\text{p}}}{\gamma_{\text{lvDIM}}^{\text{p}} + \gamma_{\text{sv}}^{\text{p}}} \quad (\text{Eq. 2-13}).$$

Solving these two equations permits us to solve for  $(\gamma_{\text{sv}}^{\text{p}})^{1/2}$  and  $(\gamma_{\text{sv}}^{\text{d}})^{1/2}$ .

To obtain the contact angle, we must take into account the adhesive and cohesive forces.

The assumption used for this case is that the solid surface is flat; however, even the smoothest

surfaces will have some degree of roughness at the micro scale. Therefore, the surface energy models used in these must account for rough surfaces.

## 2.2 Roughness

### 2.2.1 Cassie-Baxter and Wenzel's Model

To deal with inherent roughness, Wenzel or Cassie-Baxter models of wetting are to be used [3, 8-9]. The difference between these two models is that the Wenzel model makes the assumption that water penetrates the surface while the Cassie-Baxter model assumes that air can be trapped between the peaks or pillars of the material while the liquid rests on top of the air/peaks. The Wenzel model also makes the assumption that the solid is a homogenous surface. The equation used for Wenzel's model is

$$\cos \theta' = r \cos \theta_{\text{young}} \quad (\text{Eq. 2-14})$$

where  $\theta'$  is the contact angle at the rough surface,  $\theta_{\text{young}}$  is the Young contact angle, and  $r$  is the roughness coefficient. The  $r$  constant is a measure of how surface roughness affects a material and is defined as the ratio between the true area of a solid surface and the apparent area. The Cassie-Baxter model on the other hand makes the assumption that we have a heterogeneous surface composed of solid-liquid and solid-vapor interfaces. The equation for the Cassie-Baxter model is

$$\cos \theta' = f_1 \cos \theta_1 + f_2 \cos \theta_2 \quad (\text{Eq. 2-15})$$

where  $f_1$  is the surface area fraction of one material with contact angle  $\theta_1$ , and  $f_2$  is the surface area fraction of the second material with contact angle  $\theta_2$ . If  $f_2$  represents the area fraction of trapped air then we know that the contact angle on a liquid drop on air would be  $180^\circ$  we can set  $\cos \theta_2$  equal to 1, and since the  $f_1 + f_2 = 1$  the equation becomes

$$\cos \theta' = f_1 \cos \theta_1 + (1 - f_1) \cos 180^\circ \Rightarrow \cos \theta' = f_1 \cos \theta_1 + f_1 - 1. \quad (\text{Eq. 2-16})$$

## 2.3 Chemical Functionalization

### 2.3.1 Hydroxyl, Hydrogen, and Trimethylsilyl Termination

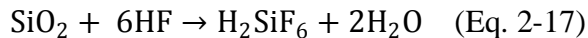
The chemical effect on contact angle was studied by varying surface chemistries on a surface with a known roughness. The samples were terminated by hydroxyls, hydrogen, and trimethylsilyls. These terminations will affect the contact angle of the two liquids being investigated.

### 2.3.2 Hydroxyl Termination

Hydroxyl termination often results from manufacturing processing [15]. The thermal oxide grown on the silicon sample is amorphous, so it does not have a specifically defined bravais lattice crystal structure. However, there is short range order in which the silicon is at the center of 4 oxygen atoms arranged in the form of a tetrahedron. These tetrahedral are linked together by shared or bridging oxygen atoms. Long range order is not present in this material because there is no regular three dimensional arrangements of the tetrahedral. But there are also oxygen atoms that are shared between two called non-bridging oxygen atoms. Since there is oxygen atoms that are not being shared, then there will be many tetrahedral not connected to neighboring tetrahedral. This means that such a material will have a more open structure meaning that impurities can easily penetrate the material. One of the impurities that are introduced is hydroxyls ( $\text{OH}$ ). Hydroxyls are formed when water is introduced into the network; water molecules convert the bridging oxygen site to two hydroxyls. Hydroxyls are known to be hydrophilic since the oxygen on the molecule is highly electronegative making this functionality polar, and therefore, attracted to water molecules. Figure 2-2a shows a hydroxyl terminated surface.

### 2.3.3 Hydrogen Termination

To create a hydrogen terminated surface, the samples were etched in a mixture of de-ionized water and hydrofluoric acid (HF) [16-21]. The HF has the ability to attack silicon dioxide at room temperature; however, it is never used in full concentration because it etches SiO<sub>2</sub> very rapidly. The reaction for this case is



where H<sub>2</sub>SiF<sub>6</sub> is water soluble. What tends to happen in the etching of a SiO<sub>2</sub> layer is:

1. Free protons are absorbed into the oxygen atoms.
2. This causes the oxygen to positively charge and will need to neutralize.
3. Silicon neutralizes the oxygen by donating an electron.
4. The electron density around silicon reduces as a cause of donating an electron, and this causes the Si – O bond to break.
5. A positive charge on the silicon is left.
6. This causes HF<sub>2</sub><sup>-</sup> to react and allows the etching process to take place; which removes the oxygen and leaves a hydrogen termination [19, 22-23].

Hydrogen termination is known to exhibit hydrophilic properties. Figure 2-2b shows a hydrogen terminated surface.

### 2.3.4 Trimethylsilyl Termination

Functionalizing a surface with HMDS can leave a surface with trimethylsilyl (CH<sub>3</sub>)<sub>3</sub>Si – O groups. But before we start talking about functionalizing a surface with HMDS, we need to talk about supercritical fluids [24-26]. A fluid is in a supercritical state when the fluid reaches and surpasses its critical point and it lies in that region defined by its phase diagram (figure 2-1).

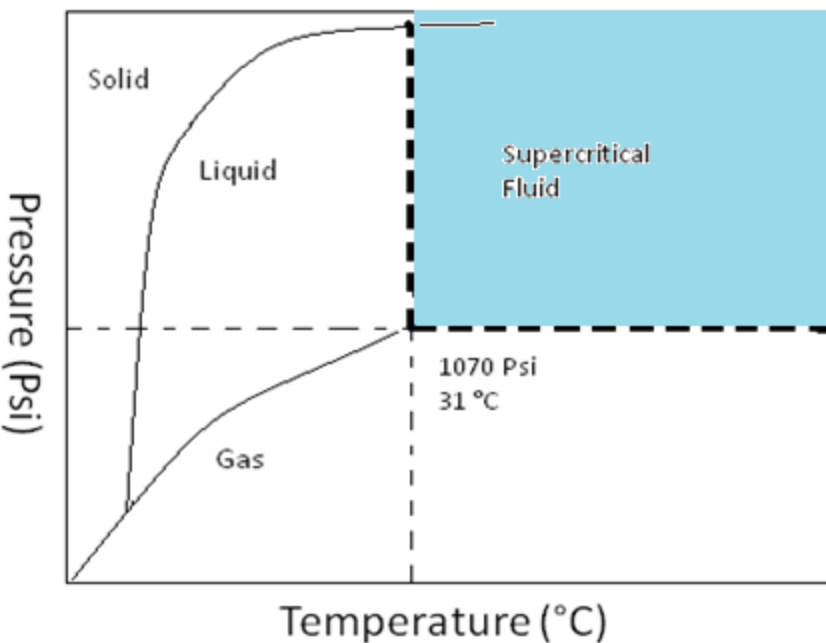
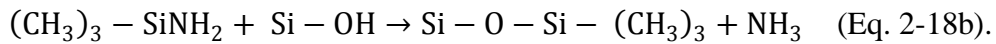
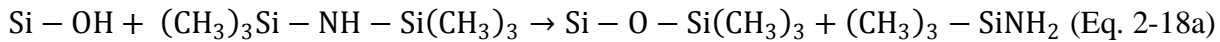


**Figure 2-1** The CO<sub>2</sub> Phase Diagram as a Function of Temperature and Pressure

In this region the fluid is neither a liquid nor a gas, it is in a state that will exhibit both liquid and gas properties. Supercritical fluids have a lot of applications ranging from the food industry to the pharmaceutical industry [27]. However, there is a lot of interest on the application to the cleaning of semiconductor materials, as well as, functionalizing samples using a supercritical treatment [28-31]. The fluid that is usually used for these processes is CO<sub>2</sub>. There are many reasons why CO<sub>2</sub> is the chosen fluid:

1. It has gas-like transport properties and near liquid density that make it very useful when processing porous low k dielectrics.
2. Supercritical CO<sub>2</sub> is non toxic.
3. It has a low critical temperature and pressure, 1070 Psi and 31° Celsius.
4. Varying pressure, temperature, and co-solvents allow the control of solvating capability in the supercritical state.

Functionalizing a surface with HMDS under supercritical conditions is faster and more efficient than liquid and vapor functionalization methods. There are two things that go on during silylation in supercritical CO<sub>2</sub>: first, water is removed from the substrate; and second, it places hydrophobic functionalities on the substrate. In this case, trimethylsilyl (CH<sub>3</sub>)<sub>3</sub>Si – O replaces a hydroxyl group. Figure 2-2c shows a trimethylsil terminated surface. A two-step reaction occurs in this case [32]



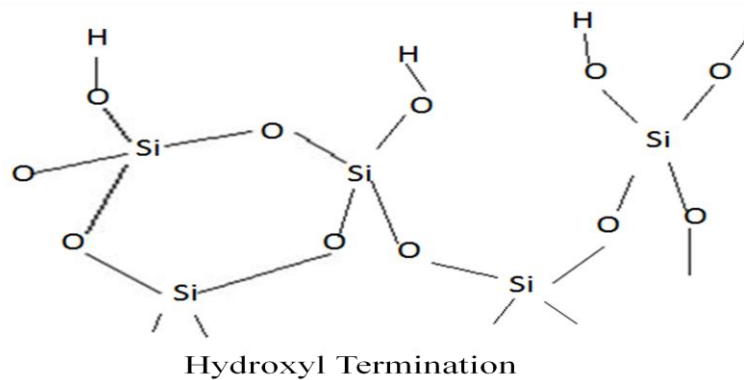


**Figure 2-2a**

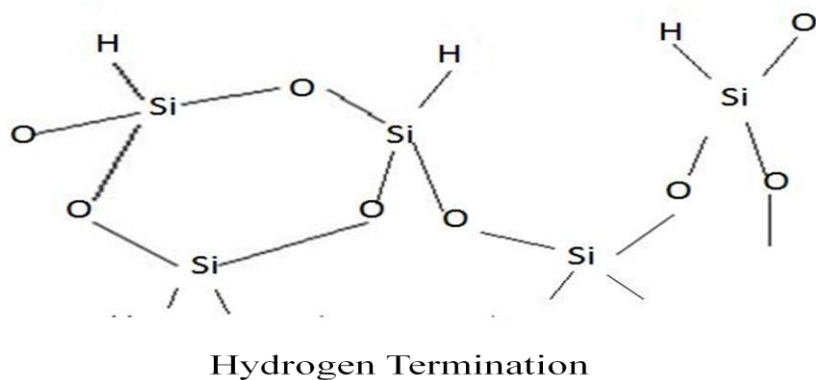


**Figure 2-2b**

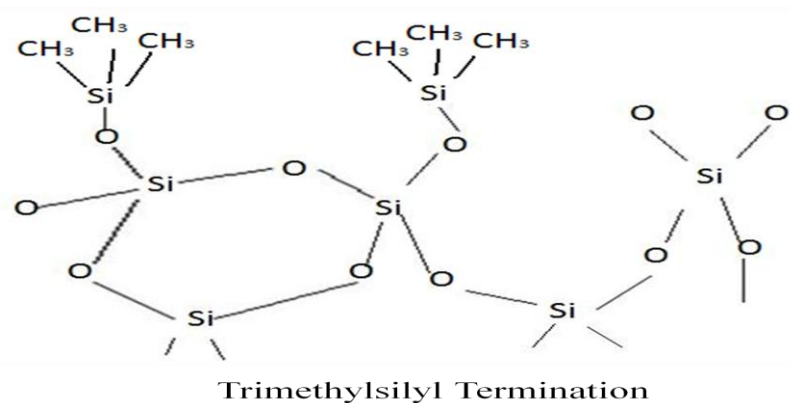


**Figure 2-2c**

**Figure 2-2 a)** Hydroxyl Termination **b)** Hydrogen Termination **c)** Trimethylsilyl Termination

## CHAPTER 3

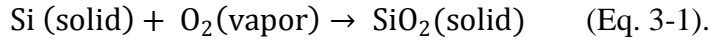
### SILICON, TOX, TEOS, AND OSG

#### 3.1 Materials

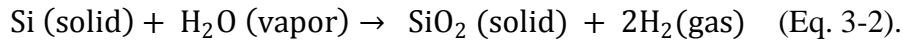
The materials used for this work were: silicon; thermally grown silicon dioxide on silicon (these will be termed TOX); silicon dioxide deposited by chemical vapor deposition (CVD) using a tetraethyl orthosilicate (TEOS) precursor on silicon (these will be termed TEOS); and organosilicate glass (OSG) on silicon (these will be termed OSG). These layers are expected to have different roughness. The pure silicon surface is expected to have a native oxide in the surface that forms upon exposure to environmental oxygen. Silicon dioxide layers are heavily used in the semiconductor industry because it is  $\text{SiO}_2$  is essential to building an integrated circuit. It passivates the silicon surface which prevents leakage paths among the devices on the piece of silicon.

#### 3.2 TOX

There are two common oxidation processes for silicon: dry oxidation and wet oxidation [33]. During dry oxidation, oxygen is introduced under a dry environment at an elevated temperature, and the reaction is



During wet oxidation, the silicon is placed in a water vapor environment at high temperature, and the reaction is



To form high quality  $\text{SiO}_2$  layers, a silicon wafer must be exposed to oxygen at temperatures of 800-1200°C. The Deal-Grove model is used to describe the oxide growth rate

and the oxide thickness. However, this model is most accurate for films thicker than 300 Å, but can be used for films as thin as 100 Å. There are two assumptions in using this model [33]:

1. the chemical reaction happens on the surface of the wafer, and
2. the rate at which oxygen or water molecules pass the oxide film on the wafer and the rate at which the silicon and oxygen react at the silicon surface will have an effect in the oxide growth.

The equation [33] given is

$$X_{ox}(t) = A/2 \left[ \left( 1 + \frac{[t+\tau]}{\left[ \frac{A^2}{4B} \right]} \right)^{1/2} - 1 \right] \quad (\text{Eq. 3-3})$$

where  $t$  is the time,  $B$  and  $A$  are constants, and  $\tau$  is used to account for any oxidation already present.

### 3.3 TEOS

TEOS is also a thin layer of  $\text{SiO}_2$  on silicon, made using chemical vapor deposition (CVD) [34]. This process uses plasma to fracture the TEOS. CVD involves several steps to place a thin film on a wafer:

1. Reactant gases are passed through a chamber in the form of a flow of gas that comes very close to the wafers inside the chamber.
2. The gases are transported to the wafer surface through diffusion where the reactants are absorbed.
3. These adsorbed species reach the surface of the wafer to places called growth sites, where the reactants form the  $\text{SiO}_2$  film.

### 3.4 OSG

The OSG (organosilicate glass) samples are a new type of films that are of interest because of their low dielectric constant (2.85) [35]. These films are of interest for the semiconductor industry because they are used as interlayer dielectric in interconnecting structures. These films are often called SiOCH films because silicon, oxygen, carbon, and hydrogen comprise these films. These films are made using a process called Plasma Enhanced Chemical Vapor Deposition (PECVD). Tetramethylcyclotetrasiloxane (TMCTS) is the precursor used to manufacture this film.

### 3.5 Previous Work on Wettability of SiO<sub>2</sub>

There have been some studies on the wetting of silicon dioxide [4, 6, 12, 36-44]. The studies have ranged from measuring contact angle of a tin droplet on a SiO<sub>2</sub> surface to modifying the surface at the nanometer scale to observe super hydrophobic effects, to studying the wettability of SiO<sub>2</sub> using an environmental scanning electron microscope (ESEM). A lot of this work shows that the contact angles on a silicon dioxide layer vary considerably. This is due to variations in impurities, roughness, and homogeneity. All these properties will affect the resulting measured contact angle, thus, explaining why different researchers observe different contact angles for the same liquid and material. Pierre Letellier points this out in his paper [4].

There is a great deal of work on the wettability of SiO<sub>2</sub>. Richard Thomas points out [43] that a SiO<sub>2</sub> surface becomes more wettable with the formation of silanols on the SiO<sub>2</sub> layer. This is relevant to this work because silanol terminated surfaces are the subject of one of our studies. Jeung Ku Kang and Charles B. Musgrave describe what happens when silicon dioxide is exposed to a HF/H<sub>2</sub>O mixture [19]. They point out that etching will leave a hydrogen terminated surface; however, they do not discuss the resulting contact angle. The contact angle will be investigated

in this work. The work done previously on functionalizing a surface with HMDS will make a surface more hydrophobic [21-24]. It is expected that this will also be the case for SiO<sub>2</sub> samples.

There have also been studies on the wettability of SiO<sub>2</sub> using an ESEM. Daniel Aronov and Gil Rosenman [6] point out that the wettability of SiO<sub>2</sub> in this environment and in micro or nano scale droplets is affected by line tension. They state that when they observe a positive line tension, the surface is more hydrophilic, and when the line tension is negative, the surface is more hydrophobic. This is of interest because contact angles will be measured in an ESEM in this work.

The roughness effect on the contact angle is of importance [3, 8-9]. The roughness on silicon dioxide shows that as a surface is made rougher it will repel water more. Soeno suggests [12] that by controlling the surface structure of a surface, a substrate can be made superhydrophobic. He points out that rougher surfaces repel water more intensely.

All this information is important because it is needed to better understand the effect of chemistries and roughness on the wetting of silicon dioxide. Once there is a clear understanding, these principles can be applied to better select cleans for front end of line (FEOL) and back end of line (BEOL) cleaning processes. Also, these principles can be used to help determine processes that best repel water from a semiconductor device. The value of the dielectric constant in an insulator increases when water is absorbed. These contact angle experiments will also help to determine which processes can eliminate water absorption.

### 3.6 Previous Work on Wettability of OSG

OSG has a different structure than SiO<sub>2</sub> [28] and shows improved dielectric properties over SiO<sub>2</sub> [35, 45-50]. As I already stated OSG is composed of an amorphous arrangement of Si,C,O, and H atoms. This is the reason they are termed SiOCH. It should be pointed out that

HF etching of OSG has shown some increase in the size of the pores, but it does not affect the chemical makeup of the OSG [49]. Silylation of a surface affect the contact angle.

All this information is important because it is needed to better understand the interaction between chemistries and roughness on the wetting of organosilicate glass. Organosilicate glass is currently employed in 65nm back end structures, because OSG has a low dielectric constant. Understanding the effect of wetting and roughness on these films is important because the interaction with water will affect the dielectric constant low-k films. Consequently, it is important to know what processes can be used to prevent water absorption in these films.

## CHAPTER 4

### EXPERIMENTAL

#### 4.1 Etching and Supercritical Treatments

There are many methods to study the interactions between a fluid and a material. However, depending on what subject one is interested in and what is trying to be determined, one makes the measurements that best suit each case. For our case, the interest was studying roughness and chemistry effects on the wetting of different materials. In addition we were interested in how the size of a liquid droplet affects the contact angle it makes with the solid surface, and if this liquid penetrates the surface of the samples. Silicon wafers with three different films (TOX, TEOS, and OSG) were studied. These materials had different intrinsic roughness and were modified with different agents to change their surface chemistries. Each where etched in a mixture of de-ionized water and hydrofluoric acid in order to remove oxide and create hydrogen terminated surface [16-21]. A set of the samples were treated with supercritical HMDS/CO<sub>2</sub> to functionalize the surface with trimethylsilyls ( (CH<sub>3</sub>)<sub>3</sub>Si – O) [24-26, 28-32, 51]. Samples were treated as follows:

1. Silicon
  - a. Etched with HF in a 20:1 water/HF mixture for 90 sec
  - b. Etched with HF in a 20:1 water/HF mixture for 90 sec and left over night in HMDS(20%) and n-hexane(80%)
2. Thermal oxide (TOX)
  - a. As received treated with an HMDS/CO<sub>2</sub> supercritical treatment
  - b. Etched with HF in a 50:1 water/HF mixture for 30 sec

- c. Etched with HF in a 50:1 water/HF mixture for 30 sec and treated with an HMDS/CO<sub>2</sub> supercritical treatment
- 3. SiO<sub>2</sub> from CVD of TEOS
  - a. As received treated with an HMDS/CO<sub>2</sub> supercritical treatment
  - b. Etched with HF in a 50:1 water/HF mixture for 30 sec
  - c. TEOS was etched with HF in a 50:1 water/HF mixture for 30 sec and treated with an HMDS/CO<sub>2</sub> supercritical treatment
- 4. Organosilicate glass (OSG)
  - a. As received treated with an HMDS/CO<sub>2</sub> supercritical treatment
  - b. Etched with HF in a 50:1 water/HF mixture for 30 sec
  - c. Etched with HF in a 50:1 water/HF mixture for 30 sec and treated with an HMDS/CO<sub>2</sub> supercritical treatment.

#### 4.2 Contact Angle

##### 4.2.1 Purpose of Measuring Contact Angle

Measuring the contact angle of a surface is rather a simple process; however, the contact angle can provide a great deal of information about the surface being studied [3-6, 12, 38, 41-44]. Two different liquids were used to measure the contact angles; de-ionized water and diiodomethane (DIM). The purpose of doing this is to see how contact angle is affected when using a liquid that interacts through dispersive forces with the surface (the DIM) and using a liquid that is affected by polar forces (de-ionized water). These results could be used, to measure surface energies [7]. Wetting of a substrate was studied by measuring the ascending and receding contact angle of each liquid on the samples. Ascending contact angle is the angle at which the liquid is in contact with the sample and there is an addition of liquid to the surface,

causing the contact angle to increase. Receding contact angle is the angle at which the liquid is in contact with the sample and the liquid is removed from the surface, causing the contact angle to decrease. Our main interest did not lie on the hysteresis of the sample, which is the difference between the ascending contact angle and the receding contact angle. The interest in doing this was to see if doing ascending and receding contact angles on a surface will cause the surface to become more hydrophilic. This mechanism can cause the material to be more hydrophilic because after this mechanism the liquid would penetrate the surface roughness. Hence, there will be a decrease in contact angle. To determine this, the contact angle was measured after doing ascending and receding motion on the samples.

#### 4.2.2 Goniometer

Static contact angles and dynamic contact angles were measured using the Rame-Hart Model 250 Standard Goniometer with Dropimage Advanced v 2.3 (Figure 4-1).

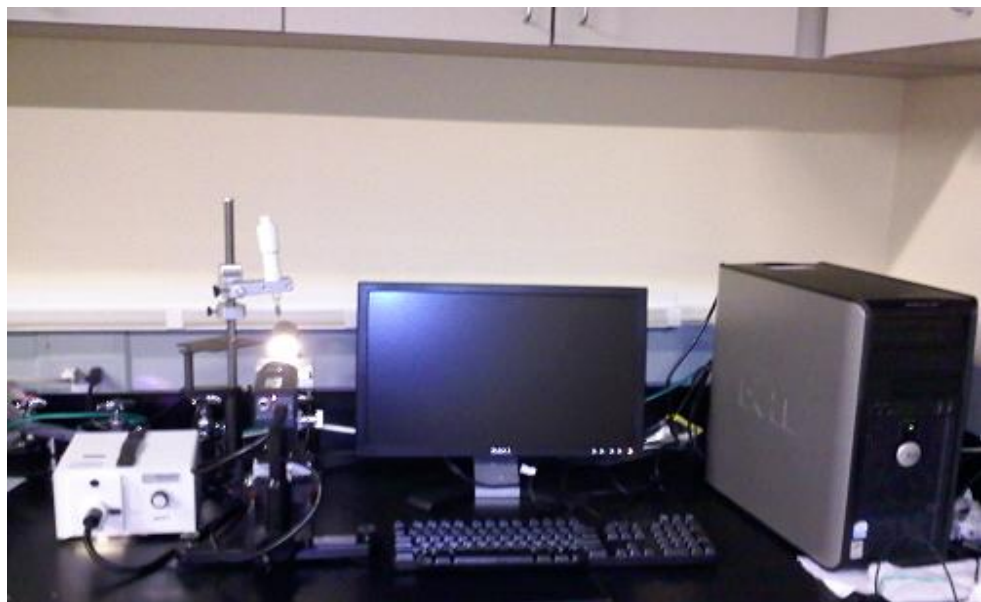


**Figure 4-1** Contact Angle Gonimeter Rame-Hart Model 250

#### 4.2.3 Contact Angle Procedure

Prior to beginning the contact angle measurement, the software was calibrated and the alignment of the stand was checked. The DI water was changed every day that a measurement was taken. The DIM was not changed every day, but a black tape was placed around the syringe so that light wouldn't affect the DIM since DIM is sensitive to light. 8 to 10 drops were placed on different areas of the samples, and the contact angles were averaged. The drops were around .01 micro liters, and the drops size was around 2 to 3 mm.

### 4.3 FTIR/GATR

#### 4.3.1 Infrared Spectroscopy Theory

Infrared spectroscopy has been used for almost a century for the purpose of analyzing the chemical bonds in a material [52-53]. An infrared experiment will measure changes in the intensity of the infrared radiation beam as a function of wavelength or frequency as it passes through a sample. Infrared Spectroscopy makes use of the asymmetrical molecular vibration of molecules. These vibrations lead to changes in molecular net dipole moments. This is essential for the molecule to be infrared active. The frequency of vibration between bonds can be explained by Hooke's Law. This approximation makes use of the harmonic oscillator where two masses are attached to a spring. The vibration frequency is given by the equation

$$f = \frac{1}{2\pi} \sqrt{\frac{k}{\mu}} \quad (\text{Eq. 4-1})$$

where  $\mu$  is the reduced mass given by the equation

$$\mu = \frac{m_1 m_2}{m_1 + m_2} \quad (\text{Eq. 4-2})$$

and  $k$  is the force constant. The masses of the atoms in the bond are given by  $m_1$  and  $m_2$ . When the vibration frequency of a molecule is equal to the frequency of the incident infrared radiation, the molecule will absorb the infrared energy.

The FTIR spectrophotometer is the dominant tool in infrared spectroscopy. The FTIR uses the Michelson interferometer to disperse the infrared radiation. The frequencies that are emitted will follow the same optical path, but the frequencies will be sent at different times. The interferometer will split the infrared radiation into two beams. The two beams will bounce off different mirrors and eventually recombine again at the beam splitter. The new beam is now called an interferogram, it has all the infrared frequencies encoded into it. The interferogram is what actually hits the sample, and it is the signal after the interaction that is unique to each sample. The detector picks up the resulting signal and sends it to a computer where it is decoded using Fourier Transformation mathematical techniques and then gives the transmittance or absorption vs. frequency (or wavenumber) spectrum.

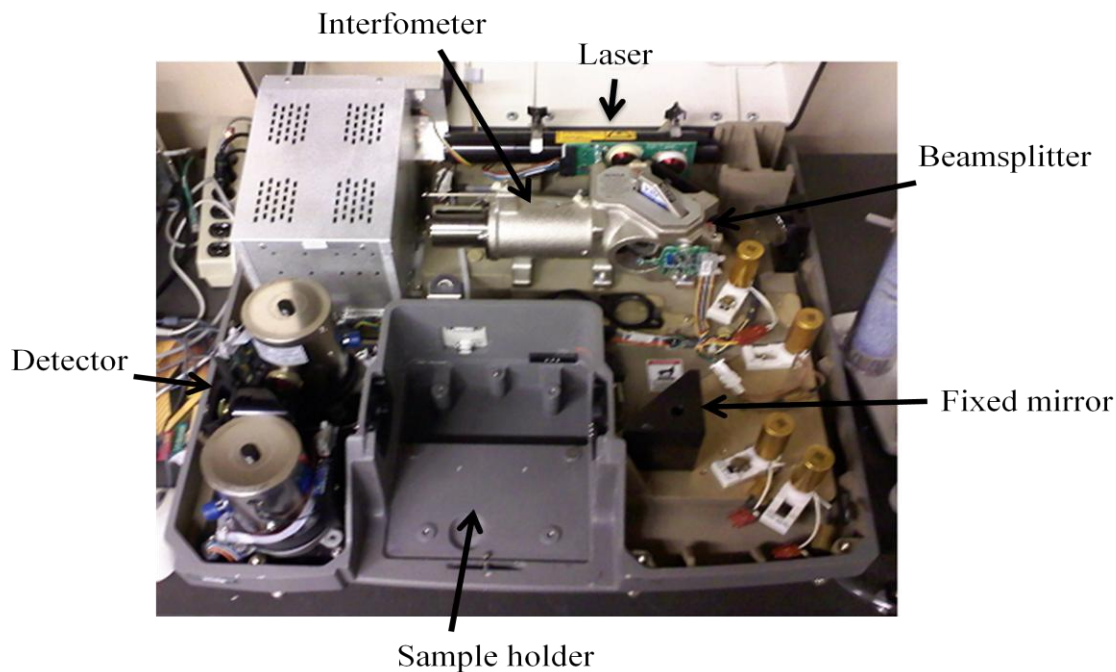


**Figure 4-2** FTIR Nexus 470 E.S.P Spectrometer

The spectrum given uses the equation

$$T_w = \left( \frac{I_t}{I_o} \right)_w \quad (\text{Eq. 4-3})$$

where  $I_t$  is the intensity of light after it has interacted with the sample, the  $I_0$  is the intensity of light incident upon the sample and  $w$  is the frequency of the incident beam. If the absorbance vs. frequency (or wave number) spectrum is desired than we use Beer-Lambert Law given by the equation

$$A_w = -\log T_w \quad (\text{Eq. 4-4})$$

#### 4.3.2 FTIR/GATR Apparatus and Procedure of Measurements

The spectra obtained were acquired using a NEXUS 470 FT-IR (Figure 4-2) spectrometer and a grazing angle total attenuated reflection accessory (GATR). The GATR is useful for analyzing thin films on a substrate. The film is sandwiched between the silicon and the germanium crystal. It focuses the beam onto the sample and forces it bounce several times between the germanium and the film. This gives a range of incident angles, making it suitable for a film.

GATR is ideal for analyzing the surface of a sample. This GATR accessory uses a germanium crystal and a  $65^\circ$  angle of incidence (Figure 4-3). The beam penetrates the germanium crystal, and it bounces several times due to the change in the refractive index. The evanescent wave is the wave that actually comes into contact with the film. It extends beyond the surface of the crystal and bounces between the film and the germanium crystal. It then exits the crystal into the detector.

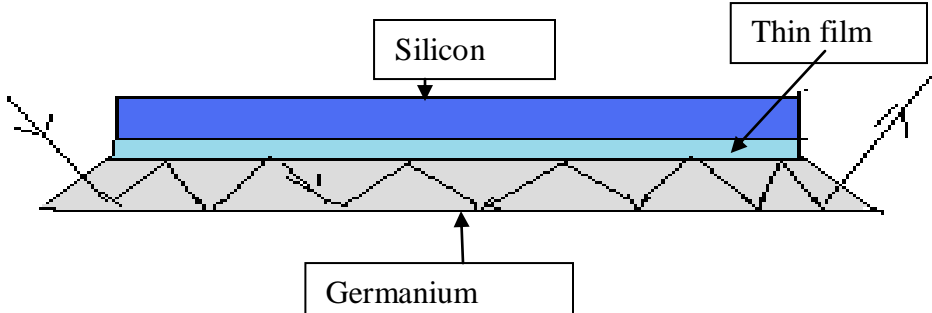


**Figure 4-3** GATR Using a Ge Crystal with 65°

The samples were placed on the Ge crystal and tightened with a torque screwdriver. It was tighten to a pressure of 30 oz/in. The number of scans taken was 64 and the resolution was  $4 \text{ cm}^{-1}$ .

#### 4.4 XPS

##### 4.4.1 XPS Theory

X-Ray photoelectron spectroscopy [54-55] makes use of Einstein's photoelectric law to analyze the surface of a sample. Einstein's photoelectric law states that when a photon hits a surface with certain energy, it will transfer the energy to an atom of the surface and remove an electron. The electron will have a kinetic energy equal to the energy of the photon that hits the surface minus the binding energy of the electron to the atom.

$$K.E = h\nu - B.E \quad (\text{Eq. 4-5})$$

This equation comes from atomic electron shells. From basic chemistry, we know that the electrons in a neutral atom will equal to the number of protons in the nucleus. It is also known that two electrons of opposite spin can occupy each orbital. The energy levels of each atomic orbital will be discrete. However, a given orbital, will experience different electrostatic attraction depending on the atom since the attraction will be different for each atomic nucleus. When using XPS, there is more interest in the core electrons of an atom. The reason is that the

binding energies of the core electrons are what provide the unique signature of the elements present. All elements are identified using their core electron binding energies with the exception of hydrogen and helium since these elements have no core electrons. XPS can penetrate a depth of 2 to 20 atomic layers of the sample being analyzed.

#### 4.4.2 Apparatus and Procedure of Measurements

For elemental analysis the XPS PHI 5000 Versa Probe was used (Figure 4-4); it was purchased through Physical Electronics. The measurements were conducted by Eric Osei-Yiadom.



**Figure 4-4** XPS PHI 5000 Versa Probe

## 4.5 AFM

### 4.5.1 AFM Theory

An atomic force microscope (AFM) [56-57] allows us to measure roughness or texture of a sample surface. As it has already been mentioned, roughness plays a critical role in the contact angle between a surface and a liquid. AFM works by allowing a fine sharp tip attached to the micro-scale cantilever to come into contact or very close contact to a sample. The sample is placed under the tip, and different forces attract or repel the tip deflecting the cantilever according to Hooke's law. A laser is used to measure this deflection by bouncing off the top surface of the cantilever into a position sensitive detector. These deflections are then measured and processed by the computer.

There are several interactive forces that are involved in AFM, such as the capillary force that is caused by a buildup of water on the tip, and the force caused by the cantilever itself. However, it is the van der Waals force that is of main interest because it is this force that the tip and the sample experience when the distance between the two is beyond the chemical bonding distance. This force is estimated to be approximately 1-20 nN. To explain this force, we use a force vs. distance graph (Figure 4-5). When analyzing the sample in the contact mode, the tip and the sample are a few angstroms apart, and the force between them is considered repulsive. In non-contact mode, the tip and the sample are 10-100 angstroms apart, and the force is considered attractive. The tapping mode analyzes the sample by making use of both the contact and non-contact region, fluctuating between the two. The force processed by the computer deflects the cantilever. This force is given by Hook's law.

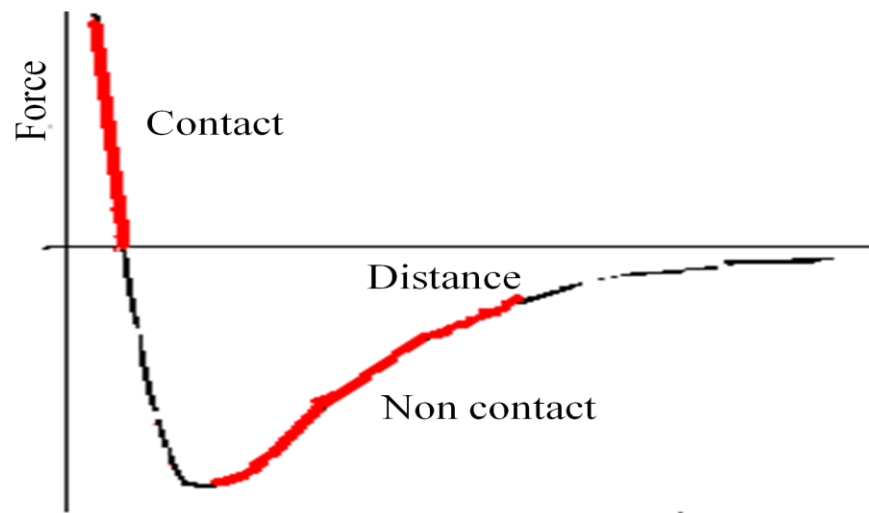


**Figure 4-5** Force vs. Distance for Contact and Non Contact



**Figure 4-6** Veeco (Digital Instruments) Multimode Nanoscope III

#### 4.5.2 Apparatus and Procedure of Measurements

Surface topography measurements were made using a Veeco (Digital Instruments) Multimode Nanoscope III operated in tapping mode using Si probes (Tap300, Budget Sensors) at room temperature, humidity and pressure (figure 4-6). The measurements were made by Maia Romanes.

### 4.6 ESEM

#### 4.6.1 ESEM Theory

An environmental scanning electron microscope (ESEM) allows us to study a substrate with very high magnification. The ESEM works similar in a similar fashion to the scanning electron microscope (SEM). However, the ESEM allows us to control the temperature and pressure inside the chamber allowing other measurements to be conducted in the chamber.

The theory behind an ESEM is very straight forward [58-59]. A beam of electrons penetrates through the water vapor, which was introduced through a separate vacuum pump. The beam hits the surface of the sample. When the electrons hit the surface, there is an emission of electrons or photons from the surface of the sample. These are termed secondary electrons. These electrons collide with the water molecules, and cause the vapor to emit secondary electrons of their own. The secondary electrons produced by the water molecules also produce secondary electrons in adjacent water molecules. All these secondary electrons are picked up by the gaseous secondary electron detector (GSED), and turned into images sent to the computer screen.

One of the things that allow the formation of water droplets on the surface of a sample is the cooling stage. The cooling stage allows the control of the temperature of the sample. As you

cool the stage and the sample, it allows the condensation of water to take place on top of your sample.

#### 4.6.2 ESEM Apparatus and Procedure of Measurements

Measurements were done using the FEI QUANTA 200 (Figure 4-7). The measurements were taken by placing the samples on a cooling stage and lowering the temperature from 1 °C to 4 °C. The pressure was kept constant at 6 Torr; the detector used was a gaseous secondary electron detector, and the spot size was kept at 4. The voltage ranged from 20 kV to 25 kV, depending on the sample.



**Figure 4-7** FEI Quanta 200 ESEM

## CHAPTER 5

### RESULTS

#### 5.1 Silicon Results

In this section the results for the experiments done on the silicon wafers are given. These experiments were done to study the effects of roughness and chemistries on the contact angles. Silicon was used because it is a pretty flat substrate in comparison to the other samples that were used in this work. One silicon set was etched in HF/de-ionized water (1:20) mixture for 90 sec (designated etched Si). This was done to remove the native oxide that forms on silicon as a result of it being exposed to the environment, and it was done to leave a hydrogen termination on the surface. A second set was etched in HF/de-ionized water (1:20) and functionalized by leaving it over night on a mixture of 20%HMDS and 80% n-hexane [60] (designated etched + HMDS Si). This was done to measure the change in the surface energy or contact angle of the wafers when placing trimethylsilyls on the surface.

##### 5.1.1 Contact Angle and Surface Energy Results

Figure 5-1 shows that the measured contact angles for both etched and etched/silylated samples are near 90 degrees. The water contact angle for the HMDS-treated silicon was a little bit higher than the silicon etched wafer. This is likely because the trimethylsilyls are actually repelling the water more than hydrogen terminated silicon. The DIM contact angle for the HMDS silicon is significantly higher than the etched wafer. This is a good indication that the roughness does affect the interaction between dispersive liquid and the surface, since the RMS roughness for the etched + HMDS Si was a lot higher (1.69 nm) than the etched Si (.532nm).

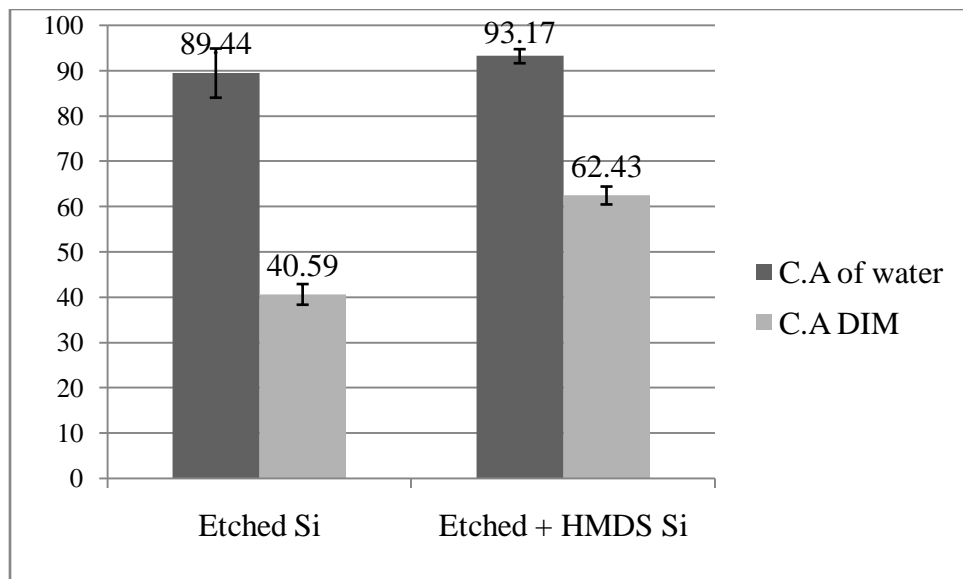


**Figure 5-1** Contact Angle for Etched Si and Etched + HMDS Si

**Table 5-1** Surface Energies for Etched Si and Etched + HMDS Si

SURFACE ENERGY	Polar ( $\frac{J}{m^2}$ )	Dispersive ( $\frac{J}{m^2}$ )	Total ( $\frac{J}{m^2}$ )
Geometric of Etched Si	$1.1 \pm .27$	$39.31 \pm .31$	$40.40 \pm .37$
Harmonic of Etched Si	$4.67 \pm .53$	$39.88 \pm .27$	$44.56 \pm .58$
Geometric of Etched + HMDS Si	$2.0 \pm .12$	$27.07 \pm .3$	$29.07 \pm .27$
Harmonic of Etched + HMDS Si	$5.19 \pm .16$	$29.2 \pm .25$	$34.39 \pm .25$

The surface energies for the samples are given in Table 5-1. As expected, the surface energies of the etched Si are higher than the surface energies for the etched + HMDS Si. This is expected because the water contact angle is lower for the etched Si than for the etched + HMDS Si. Meaning that the surface with the highest surface energy will disperse the liquid more, and this will cause the liquid to spread over the surface instead of balling up into a drop. As has already been mentioned, the harmonic and the geometric models use different work of adhesion equations to determine the surface energies. This is the reason the surface energy values differ for the same sample/liquid measurements. However, the trends are the same.

### 5.1.2 Silicon FTIR/GATR

The FTIR peaks for the etched silicon wafer are given in figure 5-2. The peaks of interest are at wave numbers  $1036\text{ cm}^{-1}$  [61-62],  $2930\text{ cm}^{-1}$  [63-64], and  $3735\text{ cm}^{-1}$  [65-66]. The assignments of these peaks are given in table 5-3. The peak at  $1036\text{ cm}^{-1}$  reveals that we have the Si – O asymmetric stretch bond [61-62]. This tells us that we do have  $\text{SiO}_2$ , but the absorbance tells us that we do not have very much. At  $2930\text{ cm}^{-1}$ , it shows that there was  $\text{CH}_2$  stretching vibrations present in the wafer [63-64]. This might be coming from the air or from etching. The peak  $3735\text{ cm}^{-1}$  is recognized as a terminal or isolated Si – OH group [65-66]. This is pointing out that hydroxyls were present on the wafer.

The FTIR peaks for the etched + HMDS Si wafer are also given below. The peaks of interest for this case are also the wave-numbers at  $1036\text{ cm}^{-1}$  [61-62],  $2930\text{ cm}^{-1}$  [63-64], and  $3735\text{ cm}^{-1}$  [65-66]. The peaks for this case are around the same region as for the etched silicon wafer. It was expected that we would observe some Si –  $\text{CH}_3$  peaks on the etched + HMDS wafer. The reason we are not seeing these peaks has to do with the fact that the concentration of HMDS used was very low, so the FTIR/GATR is not picking up any of these peaks.

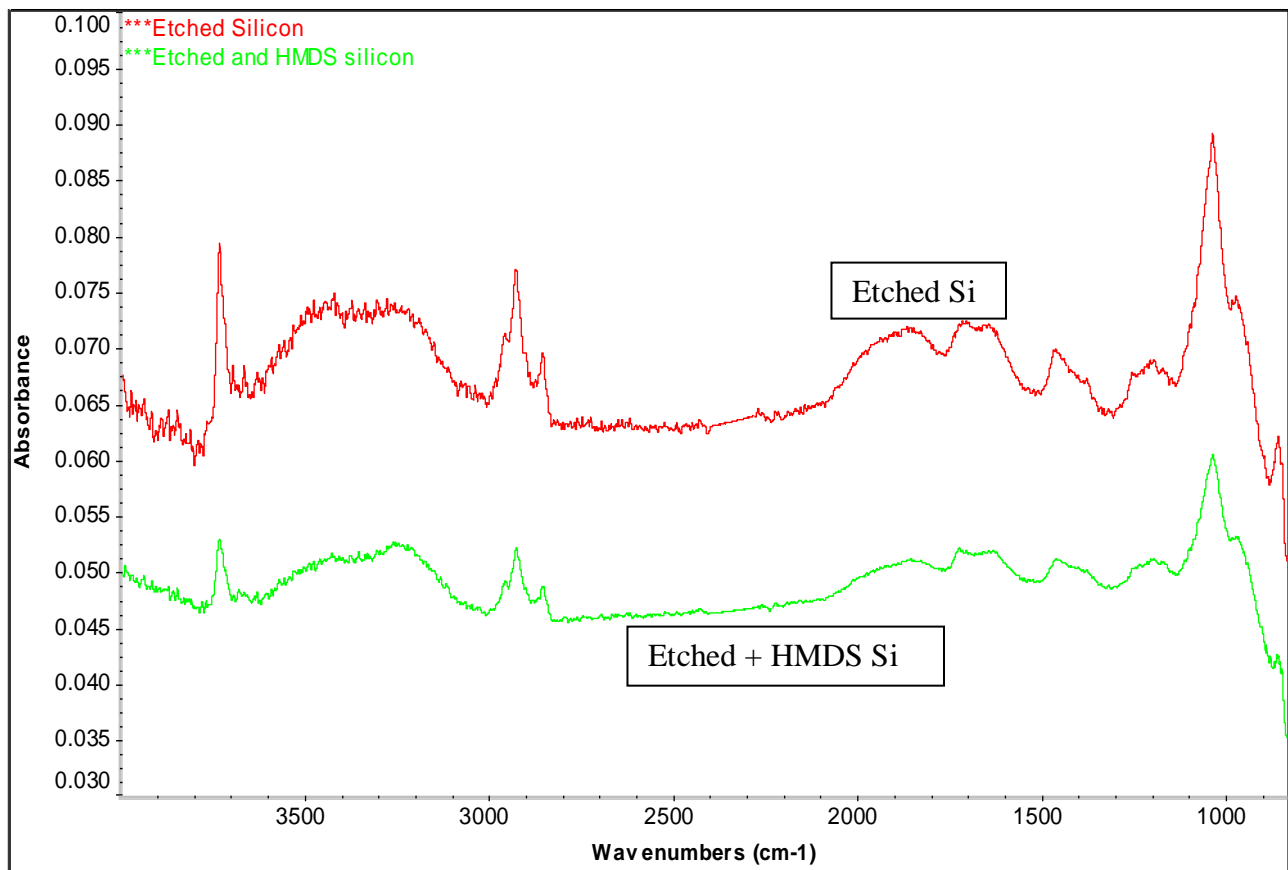


**Figure 5-2** FTIR Peaks for Etched Si and Etched + HMDS Si

**Table 5-2** Wavenumber and Band Assignment for Etched Si and Etched + HMDS Si

Wavenumber $cm^{-1}$	Band assignment	Reference
1036	Si–O asymmetric stretch bond	[61-62]
2930	CH <sub>2</sub> stretching vibrations	[63-64]
3735	Terminal Si – OH group	[65-66]

### 5.1.3 Silicon XPS

XPS was done on these wafers to determine the elemental composition of the wafers. XPS was essential for this project because XPS helped identify the groups that were placed on the surfaces. It was also used to remove trimethylsilyls from the surface of the etched + HMDS Si through argon sputtering. Argon sputtering removed some of the layers of the surface of the sample. Once the sample was sputtered cleaned, XPS measurements were taken again. The argon sputtered sample for the etched + HMDS Si was compared to the original etched + HMDS Si. The point was to see if sputtering removed the trimethylsilyls from the surface.

The data (Table 5-3) showed that there is carbon, oxygen, and silicon present for both the etched Si sample and the etched + HMDS Si sample. The data (Table 5-3) shows that the ratio between the oxygen and silicon for the etched Si and the etched + HMDS Si sputter cleaned sample is very low. This is an indication that the samples didn't have an oxide layer on them. The table below shows the amount of carbon, silicon, and oxygen present in each of the wafers. They are as one might expect. The etched Si has less carbon and oxygen than the etched + HMDS Si sample [67] suggesting that the extra carbon and oxygen present is due to the addition of trimethylsilyl  $(CH_3)_3Si - O$  groups [67]. Hydrogen cannot be measured in these samples by XPS because hydrogen does not have core electrons. The etched + HMDS Si samples that were sputter cleaned showed that there is the same amount of carbon, silicon, and oxygen as the etched Si. The values in the table are with the margin of error for the XPS. This means that the trimethylsilyls that were placed on the etched + HMDS Si were removed after the clean.

**Table 5-3** Carbon, Silicon, Oxygen Percentages for Each Sample

SAMPLE	C 1s	Si 2p	O 1s	O/Si
Etched Si	4	93.8	2.2	0.02
Etched + HMDS Si (sputter clean)	4.6	93.5	1.9	0.02
Etched + HMDS Si (no sputter clean)	14.2	64.3	21.5	0.33

#### 5.1.4 Silicon AFM Results

An atomic force microscope allows us to measure roughness that can play a critical role in the contact angle between a surface and a liquid. AFM is essential for this experiment because it will help determine how the surface changes when modifying it with the different chemistries. The height vs. number of events (asperities) for the etched Si is given in for the entire scanned area and a selected “flat” region (Fig 5-3). We can see that there are areas where there is less than the mean height known as valleys, and regions where they are greater than mean height known as peaks. This is visible by looking into the 3-D image of the sample given in figure 5-4 (this is a representative image). As can be seen, the hillocks are higher than the flat area of the wafer. They are 4.1 nm in height. Examining Figures 5-3 and 5-4, one can observe that a considerable fraction of the roughness of the sample comes from large peaks. These peaks are believed to be impurities on the wafer that may have come from etching or the subsequent rinse of etchant. The Root Mean Square (RMS) roughness is determined by taking the deviation in height between the peaks and the valleys within a specific area. Greater deviations describe a rougher surface. The RMS roughness is .532 nm for the etched Si. The wavelength is a measure of the distance between asperities. The wavelength of the sample is 14 nm. This means that the asperities are reasonably close to each other.

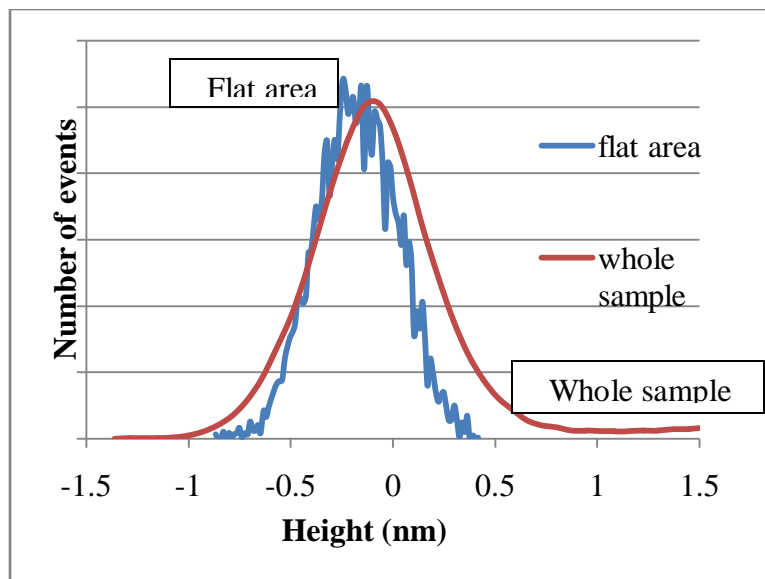


**Figure 5-3** Number of Events vs. Height for the Etched Si

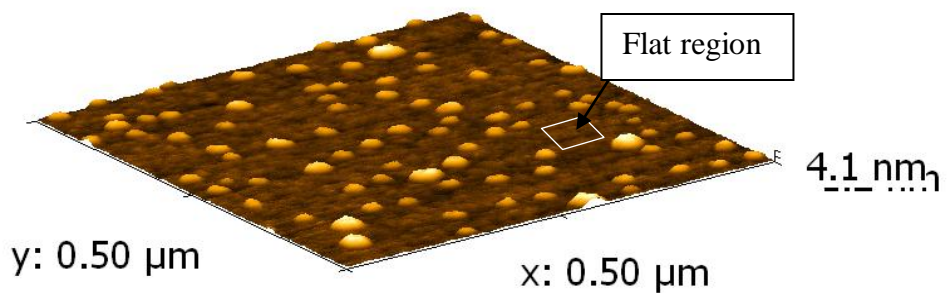


**Figure 5-4** 3-D Image of the Etched Si Sample

**Table 5-4** AFM Summary of Etched Si

Scan	Wavelength (nm)	RMS (nm)
1	13.1	0.52
2	15.45	0.53
3	14.25	0.5
4	11.93	0.53
5	15.23	0.59
Average	$13.99 \pm 1.48$	$0.53 \pm .03$

The number of events vs. height for the etched + HMDS Si is given in figure 5-5. As we can see for this case, it is also visible that the flat area as compared to the whole sample has less height. This means that the roughness of the sample comes from these peaks, which are actually coming from the etching and the HMDS treatment of the surface. By looking into the 3-D image (figure 5-6), it tells us that it is rougher than the etched silicon. As can be seen, the peaks are actually 7.3 nm. This is telling us that the stuff is actually being placed on the peaks rather than on the flat areas. The wavelength for this case is 11.66 nm, and the average Root Mean Square roughness is 1.69 nm. In comparison to the etched Si sample, this tells us that the distance between asperities are closer, and the sample is a lot rougher. This value tells us that the HMDS actually roughened the surface a lot more and this might be the reason the contact angle was higher. The wavelength and RMS roughness are given in the table 5-5.

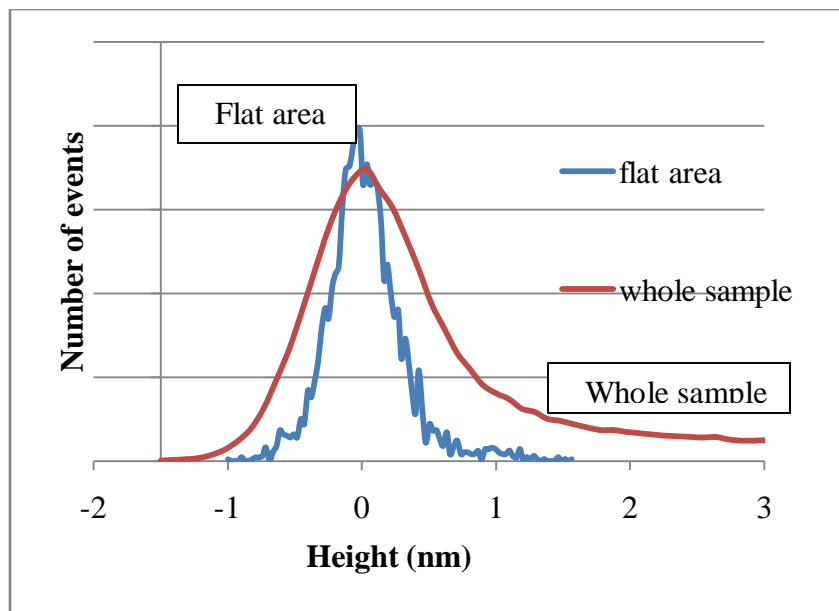


**Figure 5-5** Number of Events vs. Heights of Etched + HMDS Si

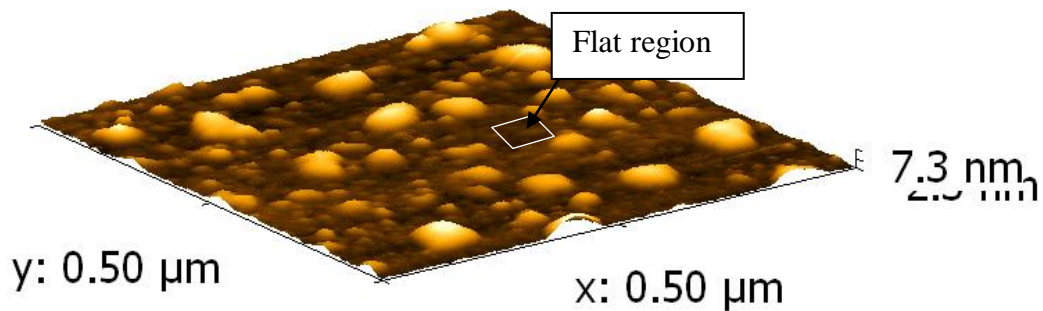


**Figure 5-6** 3-D Image of the Etched + HMDS Si Sample

**Table 5-5** AFM Summary of Etched + HMDS Si

Scan	Wavelength (nm)	RMS (nm)
1	10.6	2.02
2	11.23	1.67
3	12.13	1.87
4	12.88	1.47
5	11.48	1.42
Average	$11.66 \pm .87$	$1.69 \pm .26$

### 5.1.5 Conclusions for Silicon

The de-ionized water contact angles for the etched Si and etched + HMDS Si were very close. However, the DIM contact angles were very different. This suggests that the roughness has an effect on the contact angle of the DIM. However, the roughness showed no effect on the water contact angle. The water contact angle was mostly affected by the surface chemistries. From the data it showed that the RMS roughness on the etched Si was .532 nm, and the RMS roughness for the etched + HMDS Si was 1.69 nm. These values are significantly different, so it is very likely that the DIM was more affected by the roughness, since the contact angle for the DIM on etched Si was  $49.59^\circ$  and the DIM contact angle for the etched + HMDS SI was  $62.43^\circ$ . As for the water contact angle, it showed values of  $89.44^\circ$  for the etched Si and  $93.17^\circ$  for the etched + HMDS Si. As can be seen these values are closer compared to the DIM contact angles. The data for the XPS shows that the wafers did have the native oxide removed after etching them. XPS also proved that there were trimethylsilyls left on the etched + HMDS Si. The FTIR/GATR data didn't show that there was any trimethylsilyls on the surface of the etched + HMDS Si wafer, but this could be due to the fact that the amount of concentration used to functionalize the wafer was very low. So, the FTIR/GATR didn't observe these peaks. However, XPS and AFM do show that there was a change in surface so it is concluded that trimethylsilyls were added to the surface of the wafer. This proves that the contact angle was affected by the trimethylsilyls. It increased the contact angle as the chemistries with the addition of trimethylsilyls. The analyses of the other samples are needed in order to make generalized conclusions.

## 5.2 TOX Results

These experiments were done to study the effects of roughness and chemistries on the contact angle. TOX was used because it offers a reasonably flat surface compared to the other silicon dioxide sample made with CVD and the organosilicate glass. Four different sets of samples were used in this case. One TOX set was studied as-received (received TOX). One TOX set was etched in HF/de-ionized water (1:50) mixture for 30 sec (etched TOX). The purpose of etching the sample was to remove hydroxyls and replace them with hydrogen. A third set was placed in the supercritical chamber as received and functionalized with HMDS (HMDS TOX). This was done to replace hydroxyls with trimethylsilyls. The fourth set was etched and functionalized with HMDS in supercritical CO<sub>2</sub> (etched + HMDS TOX). The etching was done to replace the hydroxyls with hydrogen, and functionalizing with HMDS was done to replace available hydroxyls with trimethylsilyls. This was supposed to leave a surface with both hydrogen and trimethylsilyls. The goal was to observe how two hydrophobic surfaces would repeal a liquid.

### 5.2.1 TOX Contact Angle and Surface Energy

The results for the contact angle are shown in figure 5-7. The water contact angle for the received TOX sample was 48.35°, and for the etched TOX sample, the water contact angle came out to be 18.44°. This is a very interesting result because the etched sample was expected to increase the contact angle between the water drop and the surface. This decrease in contact angle may be due to the removal of a semi-hydrophobic layer exposing a more hydroxylated layer on the “new” surface. The sample HMDS TOX (91.59°) gave a higher water contact angle which is expected since trimethylsilyls are being placed on the samples (this will be confirmed with XPS and FTIR data). The etched + HMDS TOX (86.22°) water contact angle is higher

relative to the received TOX and etched TOX, but it is a little lower than the HMDS TOX. This indicates that etching created hydroxyls, and since the sample was functionalized with the same concentration as the HMDS TOX than the ratio of hydroxyls to trimethylsilyls was higher for the etched + HMDS TOX. This is why a lower contact angle relative to the HMDS TOX is observed.

The DIM contact angle measurements show some differences with the respective water contact angles. One difference is that the etching did not reduce the contact angle for the DIM as much as it did for the water contact angle. The DIM contact angles for received TOX and etched TOX was  $50.18^\circ$ , and  $41.77^\circ$ , respectively. This makes sense because the DIM is not heavily affected by the hydroxyls since DIM is a dispersive liquid. A non-polar liquid will not respond to the high polarity of the hydroxyls on the surface of the sample. The other difference is that the DIM contact angle for the etched + HMDS TOX ( $67.88^\circ$ ) was two degrees higher than the HMDS TOX ( $65.82^\circ$ ). However, this is within the standard deviation error, so it can be assumed to be the same value.

Surface energies are given in table 5-6. These values correlate very well with the values observed for the contact angles. The samples with the contact angle with the lowest values have the highest surface energies. Etched TOX is of interest because it has a very high surface energy. This is due to the addition of hydroxyls after etching.

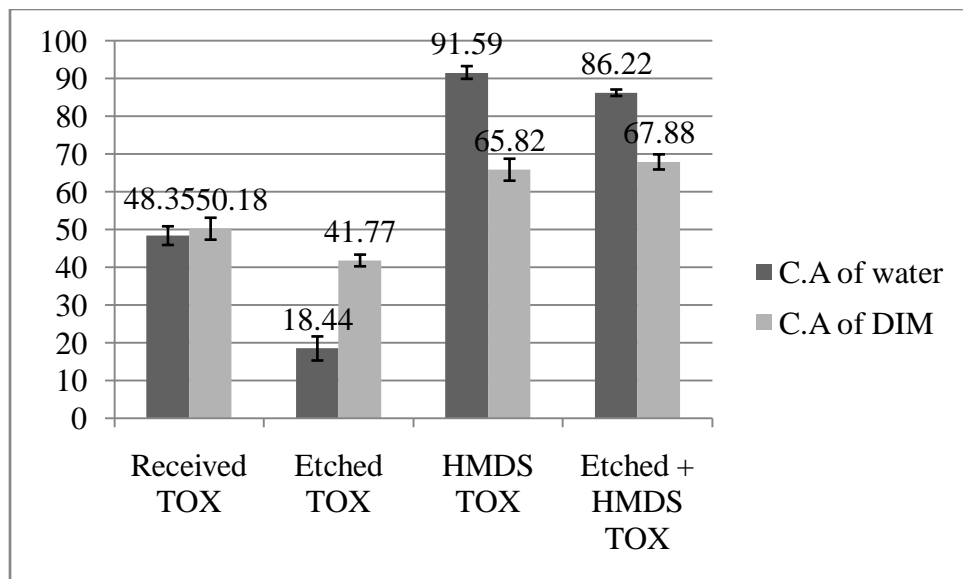


**Figure 5-7** Contact Angle for TOX Samples

**Table 5-6** Surface Energies for the TOX Samples

SURFACE ENERGY	Polar ( $\frac{\text{J}}{\text{m}^2}$ )	Dispersive ( $\frac{\text{J}}{\text{m}^2}$ )	Total ( $\frac{\text{J}}{\text{m}^2}$ )
Geometric of Received TOX	$21.74 \pm .31$	$34.71 \pm .29$	$55.91 \pm .3$
Harmonic of Received TOX	$25.09 \pm .25$	$35.32 \pm .32$	$60.41 \pm .3$
Geometric of Etched TOX	$34.42 \pm .28$	$38.68 \pm .14$	$73.11 \pm .28$
Harmonic of Etched TOX	$37.01 \pm .25$	$39.33 \pm .13$	$76.33 \pm .26$
Geometric of HMDS TOX	$2.79 \pm .16$	$25.24 \pm .43$	$28.04 \pm .36$
Harmonic of HMDS TOX	$6.18 \pm .19$	$27.65 \pm .36$	$33.82 \pm .32$
Geometric of Etched + HMDS TOX	$4.96 \pm .12$	$24.04 \pm .29$	$29.00 \pm .22$
Harmonic of Etched + HMDS TOX	$8.67 \pm .12$	$26.63 \pm .25$	$35.3 \pm .2$

### 5.2.2 TOX FTIR/GATR

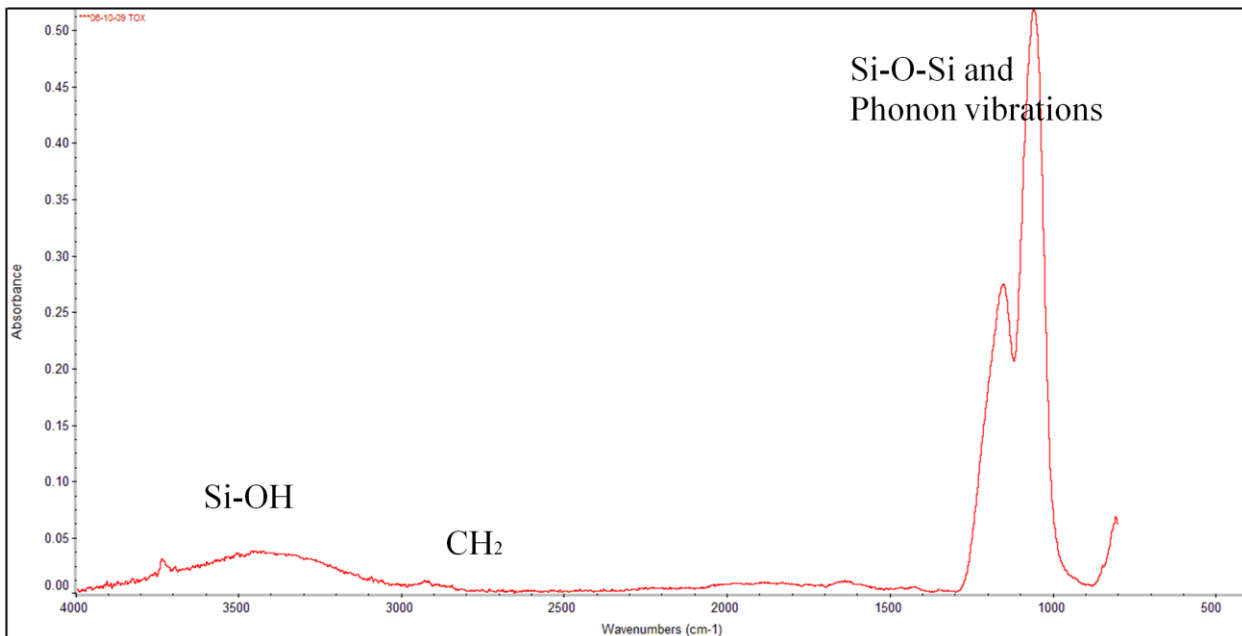


**Figure 5-8 a)** Received TOX FTIR/GATR Spectrum

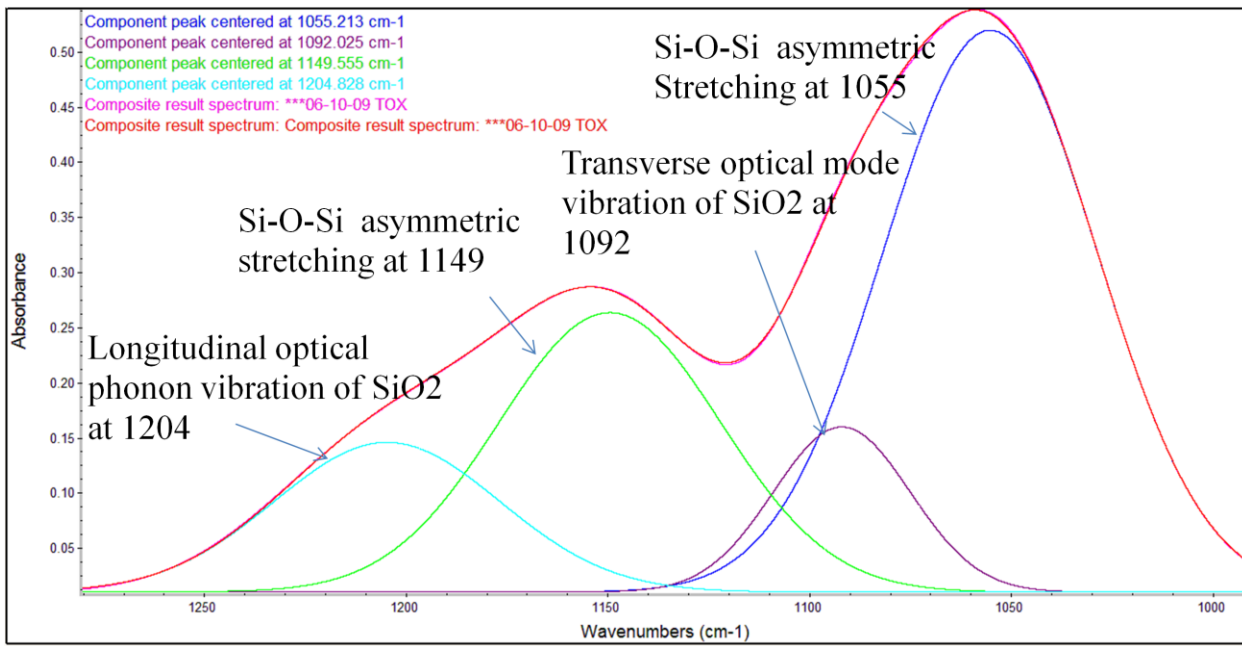


**Figure 5-8 b)** Received TOX FTIR/GATR Spectrum Wavelengths  $950 \text{ cm}^{-1}$ - $1300 \text{ cm}^{-1}$

FTIR data for the received TOX sample (figure 5-8a) shows that it does come with hydroxyls. The peaks at  $3738\text{ cm}^{-1}$  are considered isolated Si – OH groups [65-66]. The peak at  $2930\text{ cm}^{-1}$  suggests that there are some  $\text{CH}_2$  impurities in the sample [63-64]. The peaks of interest for  $\text{SiO}_2$  are at wavelengths from  $950\text{ cm}^{-1}$ - $1300\text{ cm}^{-1}$  (figure 5-8b):  $1055\text{ cm}^{-1}$  [68-72],  $1092\text{ cm}^{-1}$  [73-75],  $1149\text{ cm}^{-1}$  [70, 76-77], and  $1204\text{ cm}^{-1}$ [78-81]. The  $1204\text{ cm}^{-1}$  peak is considered a longitudinal optical phonon vibration of  $\text{SiO}_2$  [78-81]. The  $1149\text{ cm}^{-1}$  [70, 76-77] peak is considered Si – O – Si asymmetric stretching [70, 76-77]. The  $1092\text{ cm}^{-1}$  [73-75] peak corresponds to the transverse optical mode vibration of  $\text{SiO}_2$  [73-75]. And the  $1055\text{ cm}^{-1}$  peak is also Si – O – Si asymmetric stretching [68-72].

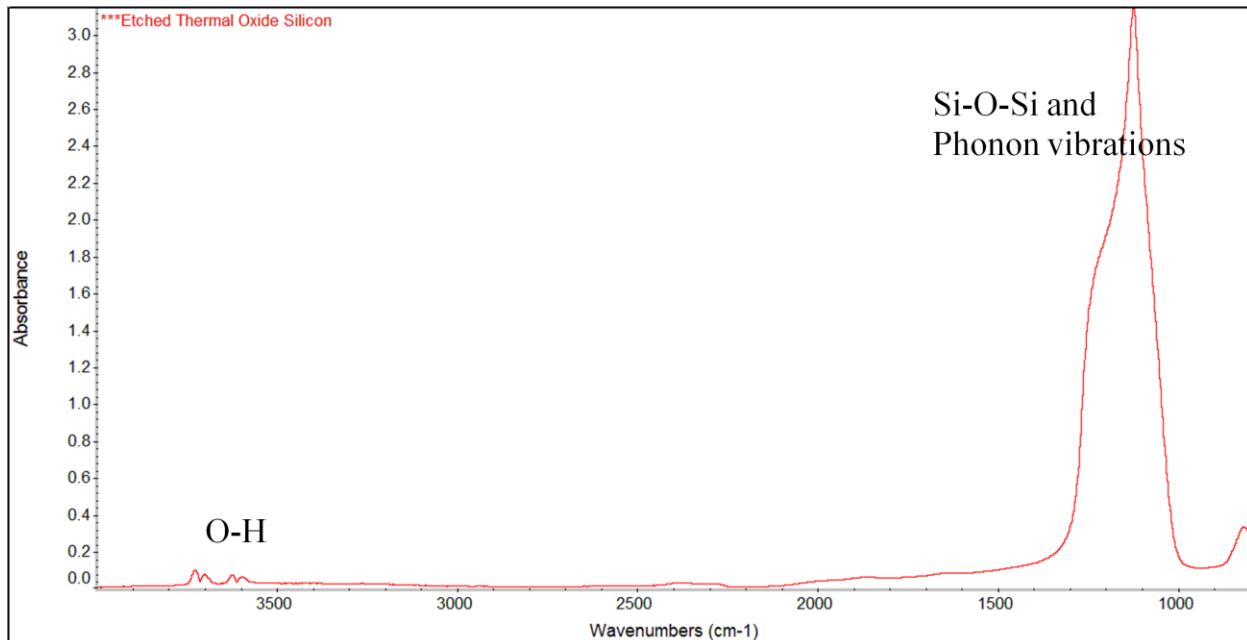


**Figure 5-9 a)** Etched TOX FTIR/GATR Spectrum

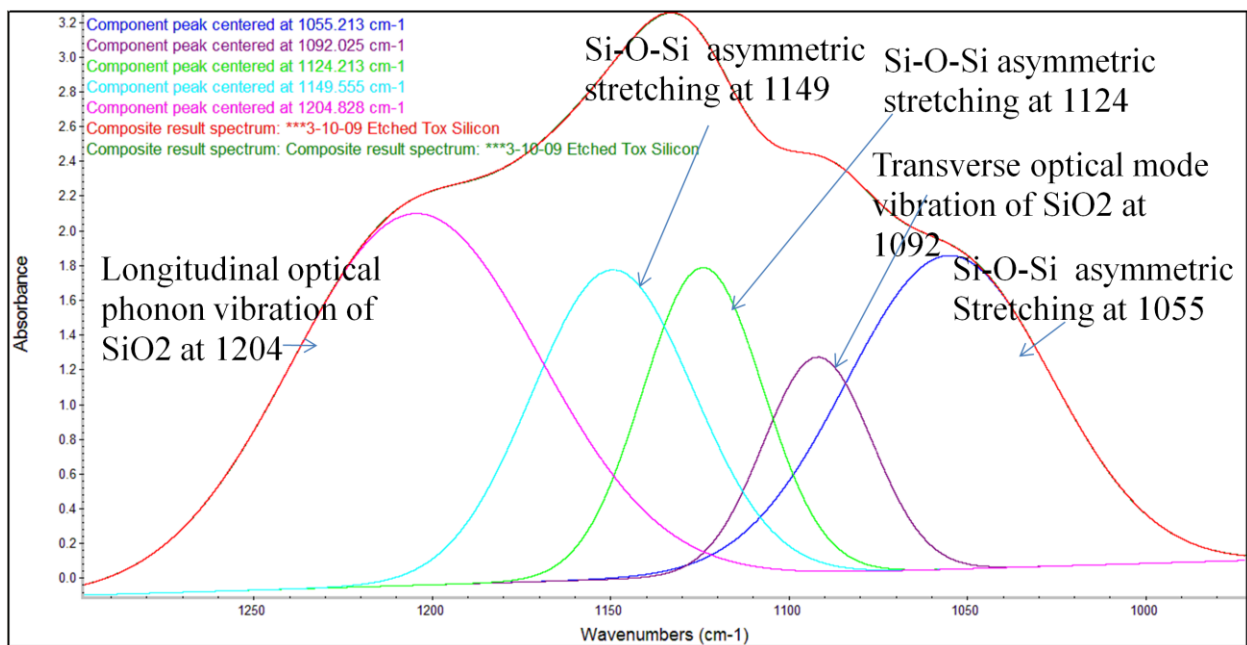


**Figure 5-9 b)** Etched TOX FTIR/GATR Spectrum Wavelengths 900 cm<sup>-1</sup>-1300 cm<sup>-1</sup>

The FTIR data for the etched TOX (figure 5-9a) sample shows that there are hydroxyls left on the surface. However, there is a difference between the hydroxyls in this sample as compared to the received TOX. The peaks at  $3730\text{ cm}^{-1}$  and  $3700\text{ cm}^{-1}$  correspond to the Si – OH terminal group [65-66]. The peaks at  $3600\text{ cm}^{-1}$  and  $3626\text{ cm}^{-1}$  are considered hydrogen bonded or vicinal Si – OH groups [82-83]. The silicon dioxide is definitely present because the Si – O – Si peaks are very clearly shown. Figure 5-9 b shows the silicon dioxide peak only. The peaks are at the same place as the received TOX sample:  $1055\text{ cm}^{-1}$  [68-72],  $1092\text{ cm}^{-1}$  [73-75],  $1149\text{ cm}^{-1}$  [70, 76-77], and  $1204\text{ cm}^{-1}$  [78-81]. However, there is an extra peak that is observed for the etched TOX. The peak is located at  $1124\text{ cm}^{-1}$ . It is considered a Si – O – Si asymmetric stretching vibration [84]. There were no Si – H peaks. These peaks are expected to be from range  $2000\text{ cm}^{-1} – 2300\text{ cm}^{-1}$ . This suggests that the etching did not leave a hydrogen terminated surface although a single monolayer of SiH may not be detectable by GATR-FTIR. However, the low measured contact angle would indicate that hydrophobic Si – H terminal groups were not present.

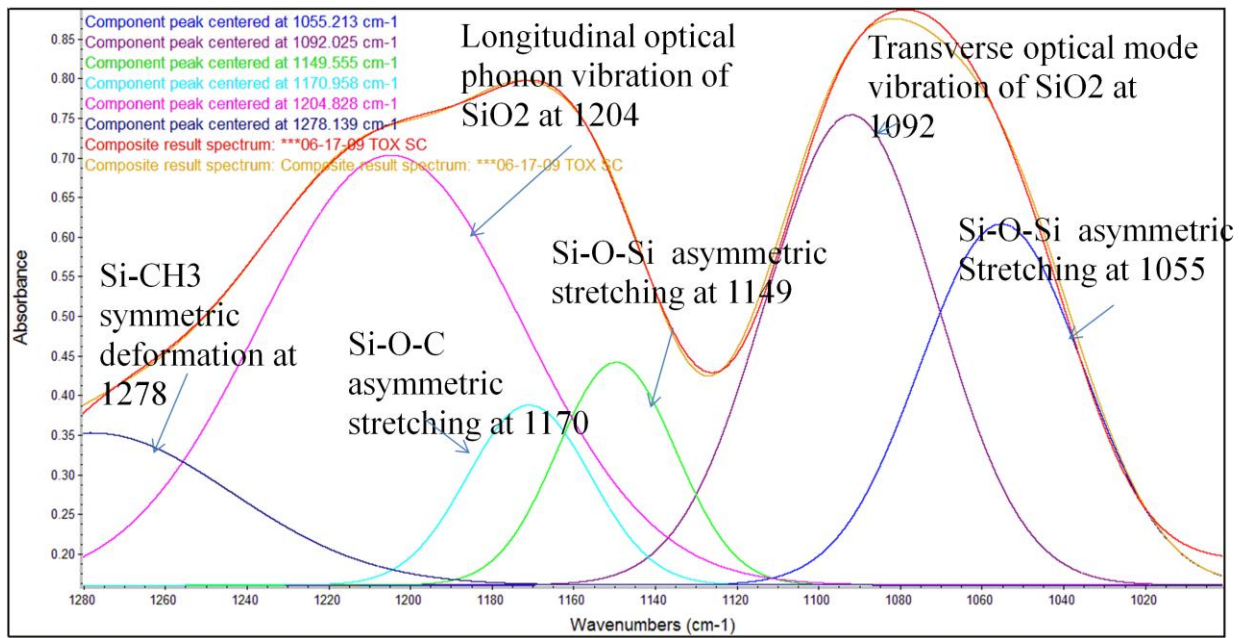
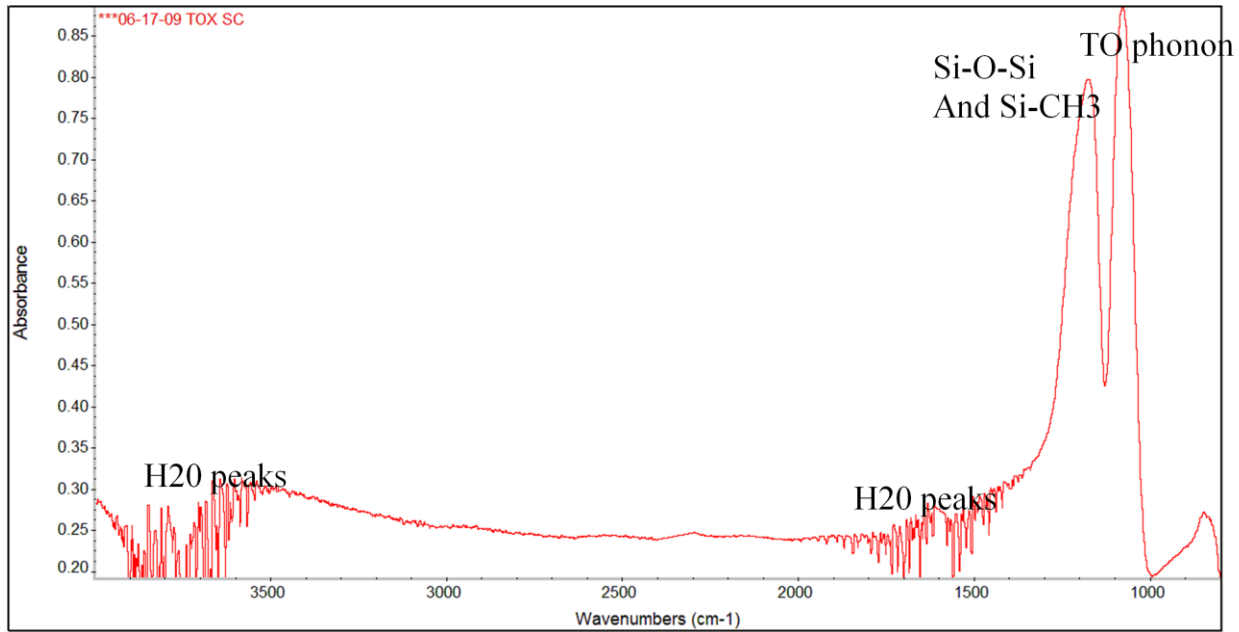
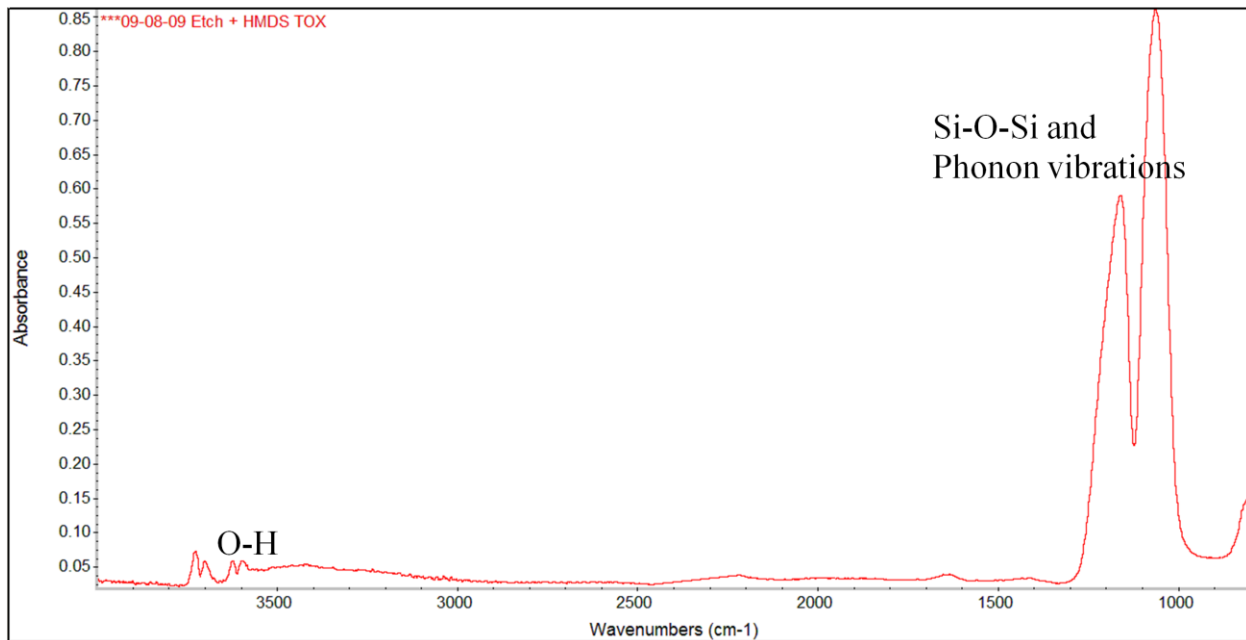
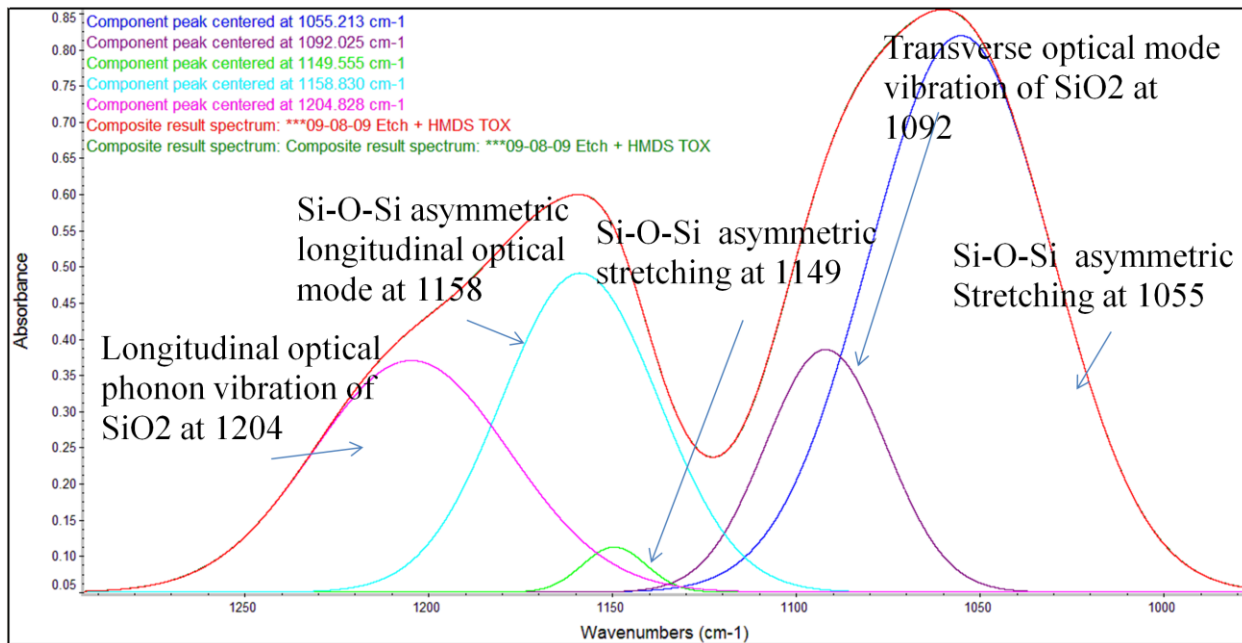


Figure 5-10 b) HMDS TOX FTIR/GATR Spectrum Wavelengths  $1000 \text{ cm}^{-1}$ - $1300\text{cm}^{-1}$

The FTIR data for the HMDS TOX is given in figure 5-10 a) and figure 5-10 b). There are water peaks at  $3500\text{ cm}^{-1}$  to  $4000\text{ cm}^{-1}$  wavelengths and at wavelengths  $1300\text{ cm}^{-1}$ - $2000\text{ cm}^{-1}$ . There are four main peaks at  $1055\text{ cm}^{-1}$  [68-72],  $1092\text{ cm}^{-1}$  [73-75],  $1149\text{ cm}^{-1}$  [70, 76-77], and  $1204\text{ cm}^{-1}$  [78-81]. These are the same peaks as in the received TOX. However, there are two extra peaks that are present in this sample. They are the  $1170\text{ cm}^{-1}$  and the  $1278\text{ cm}^{-1}$ . The  $1170\text{ cm}^{-1}$  peak shows that there is Si – O – C asymmetric stretching [32, 60]. However, the  $1278\text{ cm}^{-1}$  peak tells us that we have trimethylsilyl groups [28-31, 46, 50, 60, 69]. The peak is a Si – CH<sub>3</sub> symmetric deformation vibration. Due to the fact that we saw increase in contact angles, the XPS showed higher carbon (this will be presented in the next section), and we saw one peak in the FTIR/GATR of Si – CH<sub>3</sub>, it is reasonable to conclude that some trimethylsilyls were added to the film surface.



**Figure 5-11 a)** Etched + HMDS TOX FTIR/GATR Spectrum



**Figure 5-11 b)** Etched + HMDS TOX FTIR/GATR Spectrum Wavelengths

$$950 \text{ cm}^{-1} - 1300 \text{ cm}^{-1}$$

The FTIR data for the etched + HMDS TOX is given in figure 5-11a) and figure 5-11b).

There are four main peaks are at  $1055\text{ cm}^{-1}$  [68-72],  $1092\text{ cm}^{-1}$  [73-75],  $1149\text{ cm}^{-1}$  [70, 76-77], and  $1204\text{ cm}^{-1}$  [78-81]. These are the same peaks as in the received TOX. The  $1158\text{ cm}^{-1}$  peak corresponds to the Si – O – Si asymmetric vibration [70, 76-77]. A Si – CH<sub>3</sub> peak was expected, but none was observed. Since the XPS and XPS sputtering do show signs of trimethylsilyl (this will be confirmed in the next section) and the contact angle increased than the evidence do point out that there were trimethylsilyl on the surface.

The FTIR data showed evidence that there were trimethylsilyls present for the HMDS TOX, but there was no evidence of trimethylsilyls present for the etched + HMDS TOX. Also there were no Si – H peaks present for the etched TOX sample. The XPS data will be used in the next section to find evidence of trimethylsilyls. The band assignments and wavenumbers are summarized in table 5-7.

**Table 5-7** Wavenumber and Band Assignment for TOX Samples

Wavenumber $\text{cm}^{-1}$	Band assignment	Reference
1055	Si – O – Si asymmetric stretching	[68-72]
1092	Transverse optical mode vibration of SiO <sub>2</sub>	[73-75, 78, 85]
1124	Si – O – Si asymmetric stretching	[84]
1149	Si – O – Si asymmetric stretching	[70, 76-77]
1158	Si – O – Si asymmetric stretching	[70, 76-77]
1170	Si – O – C asymmetric stretching	[32, 60]
1204	Longitudinal optical phonon vibration of SiO <sub>2</sub>	[78-81]
1278	Si – CH <sub>3</sub> symmetric deformation	[28-31, 35, 46, 50, 60, 69]
2930	CH <sub>2</sub> stretching vibrations	[63-64]
3600 & 3626	Hydrogen bonded OH groups	[82-83]
3700 & 3730	Terminal Si – OH group	[65-66]
3738	Terminal Si – OH group	[65-66]

### 5.2.3 TOX XPS

XPS experiments were essential to monitor the surface chemistry of the films and to identify functional groups added on the surfaces. Through sputtering, XPS was also used to remove trimethylsilyls from the surface of the HMDS TOX and the etched + HMDS TOX films. This analysis helped confirm that these surfaces were successfully silylated with HMDS.

Table 5-8 shows the amount of carbon, silicon, and oxygen present in each of the samples. The chemistries are as we expect. The received TOX and the etched TOX has less carbon than the etched + HMDS TOX sample and the HMDS TOX. This could mean that the addition of carbon is coming in the form of the trimethylsilyl  $(CH_3)_3Si - O$ . The reason the hydrogen is not indicated here is because XPS cannot identify this element since it doesn't have core electrons. Also it is clear that the etched TOX has less oxygen than the received TOX, but this is not a significant amount. What I think is happening here is that the etching removed some of the hydroxyls but the subsequent rinse of the etching might have placed a new group of hydroxyls on the sample. However, there isn't as many newly placed hydroxyls as there was in the beginning, this is why we see that there is a little less oxygen than the received TOX sample. The sputter cleaned HMDS TOX shows there was some reduction in carbon. This is indicating that the sputtering removed some of the trimethylsilyls off the surface but not all of them. This is also observed with the etched + HMDS TOX sample that was sputtered cleaned.

**Table 5-8** Carbon, Silicon, and Oxygen Percentages for Each Sample

Samples	C 1s	O 1s	Si 2p	O/Si
Received TOX	0.5	69.4	30.1	2.31
Etched TOX	0.5	68.4	31	2.21
HMDS TOX (No sputter)	5.8	64.2	29.9	2.15
HMDS TOX (Sputter clean)	1.8	64.2	31.4	2.04
Etched + HMDS TOX (No sputter)	6.3	64.3	29.4	2.19
Etched + HMDS TOX (Sputter clean)	2.7	67.4	29.9	2.25

#### 5.2.4 AFM TOX

An AFM image for the TOX is shown below (figure 5-12). There were 5 different scans of the sample taken, and the average heights of the peaks for the different scans were similar in height. This indicates that unlike the silicon samples there was not much residue or debris on the surface. The wavelength for this case is 12.72 nm, and the average Root Mean Square roughness is .22 nm indicating that the asperities are reasonably close to each other and TOX is less rough than silicon. The wavelength, RMS, and the hillock heights are given in the table 5-9.

**Table 5-9** Wavelength, RMS, and Peak Height for Received TOX

Scan	Wavelength (nm)	RMS (nm)	Peak height (nm)
1	12.63	0.22	1.1
2	13.9	0.22	1
3	12.8	0.21	.9
4	12.6	0.22	1
5	11.68	0.21	1
Average	$12.72 \pm .79$	$0.22 \pm .01$	$1 \pm .07$

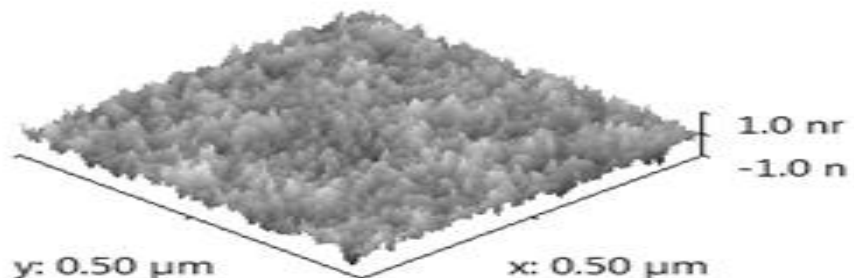


**Figure 5-12** Peak Heights for Received TOX

An etched TOX AFM image is given below (figure 5-13). The heights of the peaks are a little bit higher than the TOX, but not significantly. The number of events vs. height graph was used to compare the height difference between the received and etched TOX. The wavelength for this sample is 10.64 nm, less than the received TOX. I think it reduced because the etching may have removed the surface layer heterogeneously. Average Root Mean Square roughness is 0.25 nm. In comparison to the TOX sample, this is a little rougher. The wavelength, RMS roughness, and peak heights are given in the table 5-10.

**Table 5-10** Wavelength, RMS, and Peak Height for Etched TOX

Scan	Wavelength (nm)	RMS (nm)	Peak height (nm)
1	10.08	0.25	1.1
2	11.15	0.26	2.2
3	10.98	0.25	1.2
4	10.23	0.25	1.5
5	10.8	0.24	1.3
Average	$10.64 \pm .47$	$0.25 \pm .01$	$1.46 \pm .44$

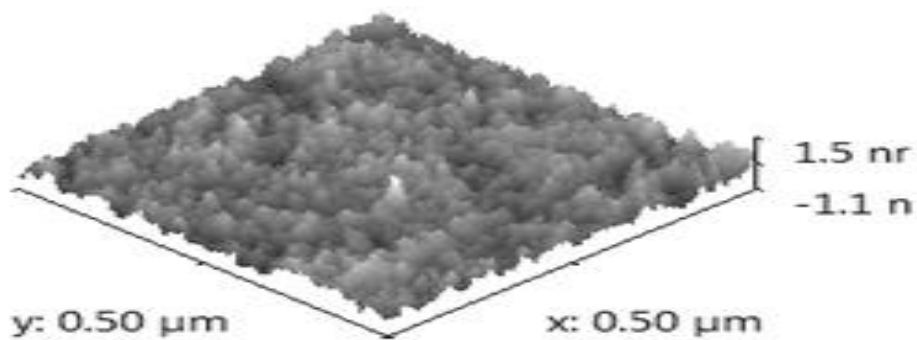


**Figure 5-13** Peak Heights for Etched TOX

An AFM image for the HMDS TOX is given in figure 5-14. The peaks do show an increase in height. This is a good indication that the surface may be silylated by trimethylsilyls. However, the numbers of events vs. height graph will be used to verify if the peaks increased in height. The wavelength for this case is 10.16 nm. It decreased in comparison to the received TOX. The trimethylsilyls were likely added to the peaks rather than the valleys due to steric limitations; consequently, thus, adding both height and width to the peaks decreasing the distance between asperities. The average RMS roughness is .26 nm. This is a little rougher than the received TOX and etched TOX samples. The water and the DIM contact angles increased for the HMDS TOX and etched + HMDS TOX, as compared to the received TOX and etched TOX. This is due to changes in the chemistries and the roughness. The wavelength, RMS roughness, and the peak heights are given in the table below.

**Table 5-11** Wavelength, RMS, and Peak Height for HMDS TOX

Scan	Wavelength (nm)	RMS (nm)	Peak Heights (nm)
1	10	0.32	4.8
2	9.95	0.25	2.1
3	10.03	0.25	2.6
4	10.77	0.28	3.3
5	10.05	0.23	2.0
Average	$10.16 \pm .34$	$0.26 \pm .04$	$2.96 \pm 1.15$

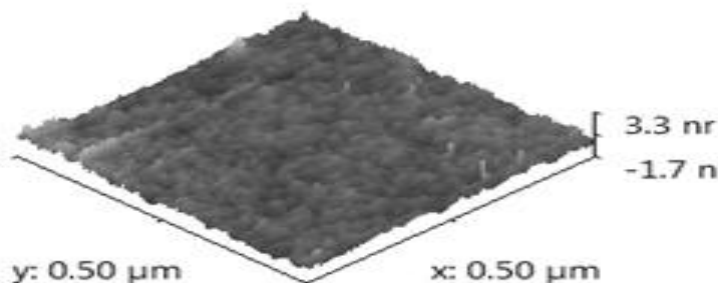


**Figure 5-14** Peak Heights for HMDS TOX

The AFM image for the etched + HMDS TOX is given below (figure 5-15). The height of the peaks did not change relative to the HMDS TOX. This suggests that trimethylsilyls were added to the surface. The wavelength is 10.89 nm. I think it reduced because the etching may have removed the surface layer heterogeneously. Also, placing trimethylsilyls on the peaks will add the  $(CH_3)_3Si - O$  groups. I think this is also why the asperities are closer to each other. The average Root Mean Square roughness is .42 nm. This sample is rougher than the received TOX, etched TOX, and HMDS TOX samples. The wavelength, RMS roughness, and peak heights are given in the table below (table 5-12).

**Table 5-12** Wavelength, RMS, and Peak Height for Etched + HMDS TOX

Scan	Wavelength (nm)	RMS (nm)	Peak Height (nm)
1	9.93	0.41	2.8
2	11.25	0.42	2.0
3	10.45	0.42	2.0
4	11.1	0.50	6.3
5	11.7	0.44	1.9
Average	$10.89 \pm .70$	$0.42 \pm .04$	$3 \pm 1.88$

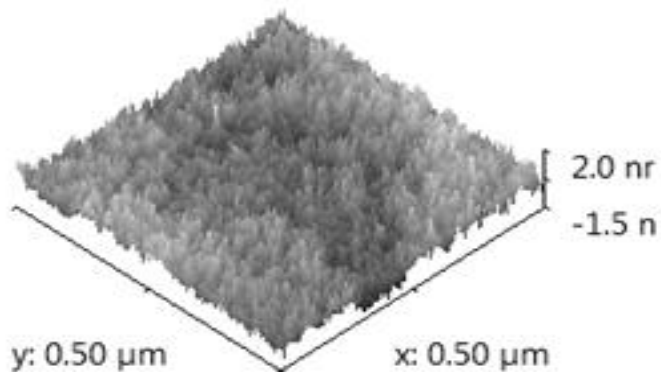


**Figure 5-15** Peak Heights for Etched + HMDS TOX

The number of events vs. height for all the samples is given below (figure 5-17). This data shows that the peaks increased by etching the sample, by adding HMDS, and by etching and adding HMDS. However, the peak height for the etched TOX is not significantly different from the received TOX. The right side of the graphs indicates the addition of stuff to the samples. Which in our case were would be trimethylsilyls.

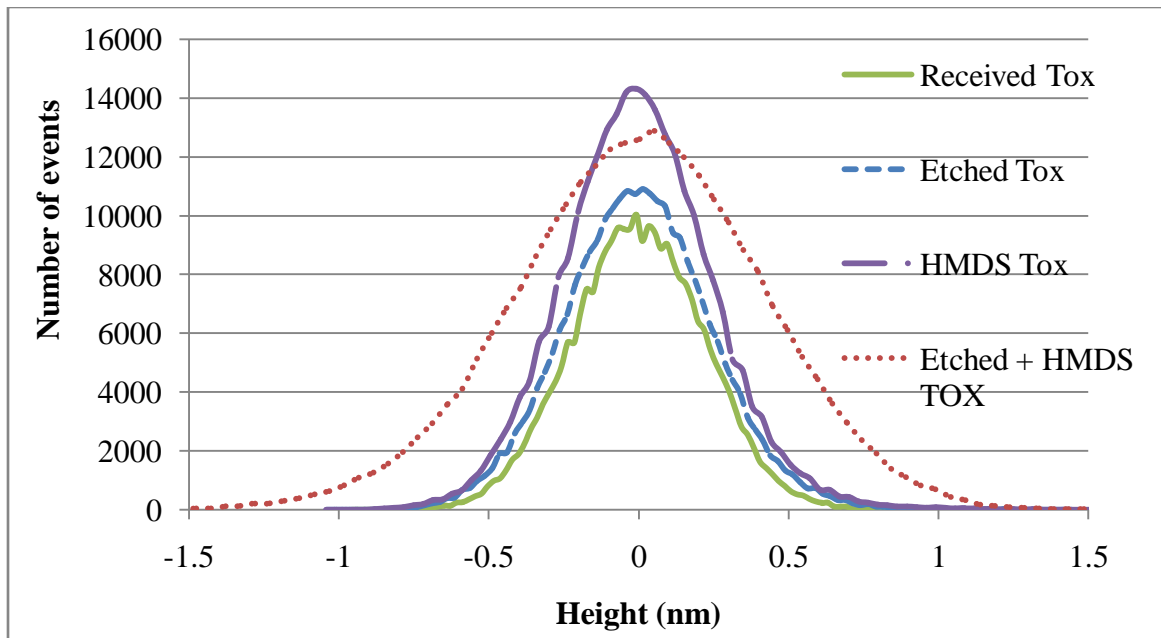


**Figure 5-16** Number of Events vs. Height for TOX

### 5.2.5 Conclusions for TOX

There exists a clear correlation between the contact angle and surface chemistries. The FTIR data and contact angle proved that there were more hydroxyls after the etching. Hence, the more hydroxyls a surface has the more it attracts water. The XPS and AFM proved that the HMDS placed trimethylsilyls after the supercritical treatment. And the trimethylsilyls groups on the sample increased the contact angle. However, DIM showed similar trends to the water contact angle but it showed that it is not heavily affected by the hydroxyls.

### 5.3 TEOS Results

In this section the results for the silicon dioxide made by chemical vapor deposition (CVD) (TEOS) will be given. TEOS was used because it offers a rougher surface compared to the TOX sample. However, this sample is not as rough as the OSG. Four different sets of samples were used in this case. One TEOS set was used as it was received (received TEOS). One TEOS set was etched in HF/de-ionized water (1:50) mixture for 30 sec (etched TEOS). The purpose of etching the sample was to remove hydroxyls and replace them with hydrogen. A third set was functionalized by HMDS in supercritical CO<sub>2</sub> (HMDS TEOS). This was done to remove hydroxyls and replace them with trimethylsilyls. The fourth set was etched and then functionalized with HMDS in supercritical CO<sub>2</sub> (etched + HMDS TEOS). The etching was done to replace the hydroxyls with hydrogen, and functionalizing with HMDS was done to replace any remaining hydroxyls with trimethylsilyls. The purpose was to study the contact angle of a liquid when it was placed on a surface that exhibited two different forms of hydrophobic functional groups.

#### 5.3.1 TEOS Contact Angle and Surface Energy

The results for the contact angle are as follows (figure 5-17). The water contact angle for the received and etched TEOS samples were 43.3° and 28.3°, respectively. The contact angle was expected to be hydrophobic. It appears that the etching of the samples added more hydroxyls, thus, lowering the contact angle as compared with the received TEOS. The HMDS TEOS sample had a higher water contact angle because trimethylsilyls have been added to the film surface. The water contact angle for the etched + HMDS TEOS (88.25°) sample is higher than the received TEOS and etched TEOS, but slightly less than the HMDS TEOS (92.29°). This indicates that etching added more hydroxyls to the film providing more sites for silylation.

Because both HMDS TEOS and etched + HMDS TEOS films were functionalized with the same HMDS concentration, etched + HMDS TEOS will form more trimethylsilyls than HMDS TEOS. However, the additional un-reacted silanols make the etched + HMDS TEOS film slightly less hydrophobic than the HMDS TEOS.

The DIM contact angles show similar trends as the water contact angles with one main difference; etching did not reduce the DIM contact angle. The received TEOS and etched TEOS DIM contact angles were nearly identical:  $43.83^\circ$  and  $41.97^\circ$ , respectively. This makes sense because the DIM is not heavily affected by the hydroxyls since DIM is a dispersive liquid. A dispersive liquid won't react towards hydroxyls since it is a non polar liquid. The other contact angles follow the same pattern as the water contact angles. They increase for the HMDS TEOS and the etched + HMDS TEOS. This increase in contact angle is also due to the trimethylsilyls present on the surface of the samples. The samples repel the DIM, causing an increase in contact angle.

Surface energies for the TEOS samples are given in table 5-13. The contact angles and the surface energies follow similar pattern. The contact angles reduce for the samples that exhibit the highest surface energies and the contact angles increase for the samples that exhibit the lowest surface energies.

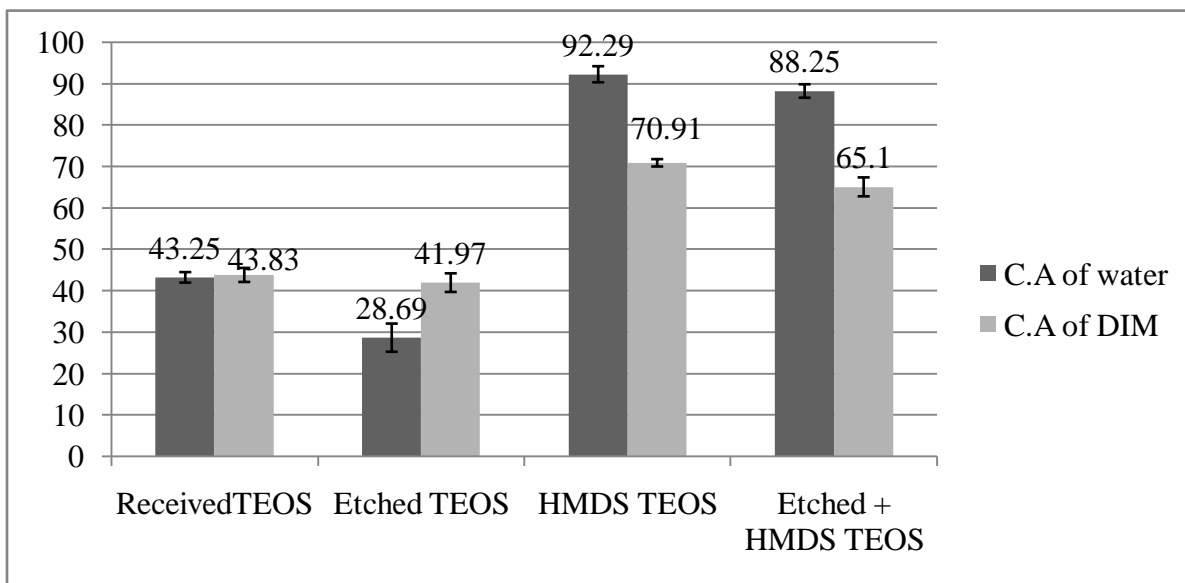


**Figure 5-17** Contact Angles for TEOS

**Table 5-13** Surface Energy for TEOS

SURFACE ENERGY	Polar ( $\frac{J}{m^2}$ )	Dispersive ( $\frac{J}{m^2}$ )	Total ( $\frac{J}{m^2}$ )
Geometric of Received TEOS	$23.09 \pm .24$	$37.63 \pm .24$	$60.66 \pm .23$
Harmonic of Received TEOS	$26.77 \pm .18$	$38.38 \pm .21$	$65.16 \pm .22$
Geometric of Etched TEOS	$30.32 \pm .45$	$38.61 \pm .3$	$68.93 \pm .43$
Harmonic of Etched TEOS	$33.32 \pm .38$	$39.26 \pm .26$	$72.56 \pm .41$
Geometric of HMDS TEOS	$3.25 \pm .17$	$22.37 \pm .13$	$25.61 \pm .19$
Harmonic of HMDS TEOS	$6.52 \pm .21$	$25.22 \pm .11$	$31.74 \pm .22$
Geometric of Etched + HMDS TEOS	$3.77 \pm .17$	$25.65 \pm .33$	$29.42 \pm .29$
Harmonic of Etched + HMDS TEOS	$7.45 \pm .19$	$28.00 \pm .29$	$35.45 \pm .28$

### 5.3.2 TEOS FTIR/GATR

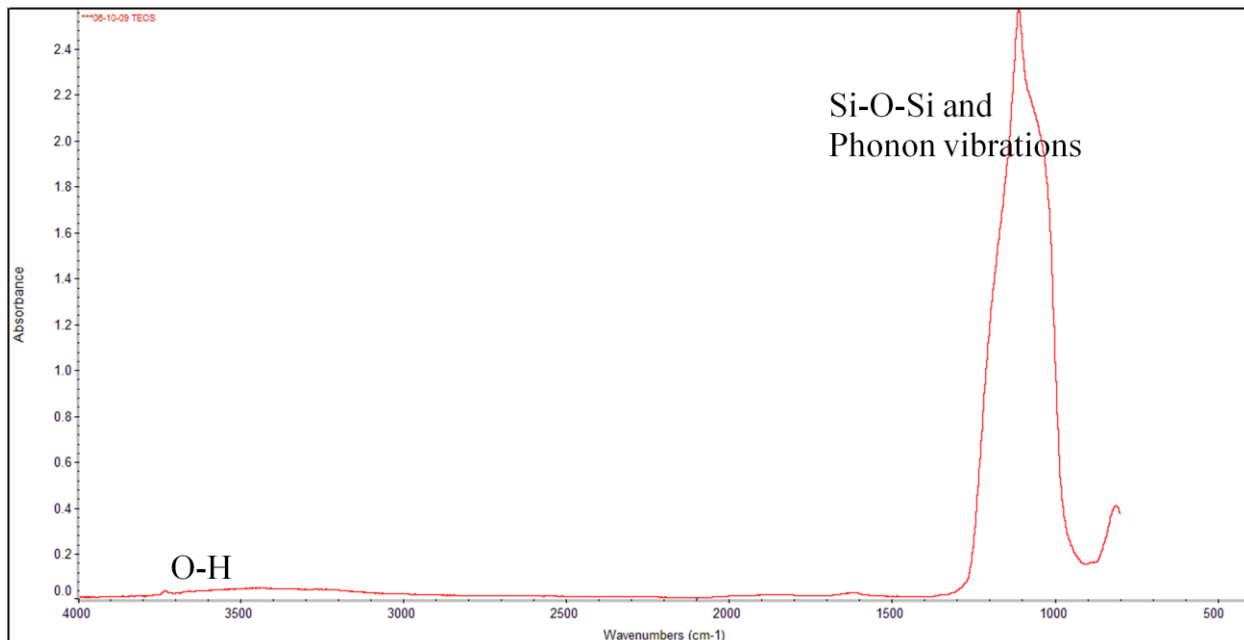


**Figure 5-18 a)** Received TEOS FTIR/GATR Spectrum

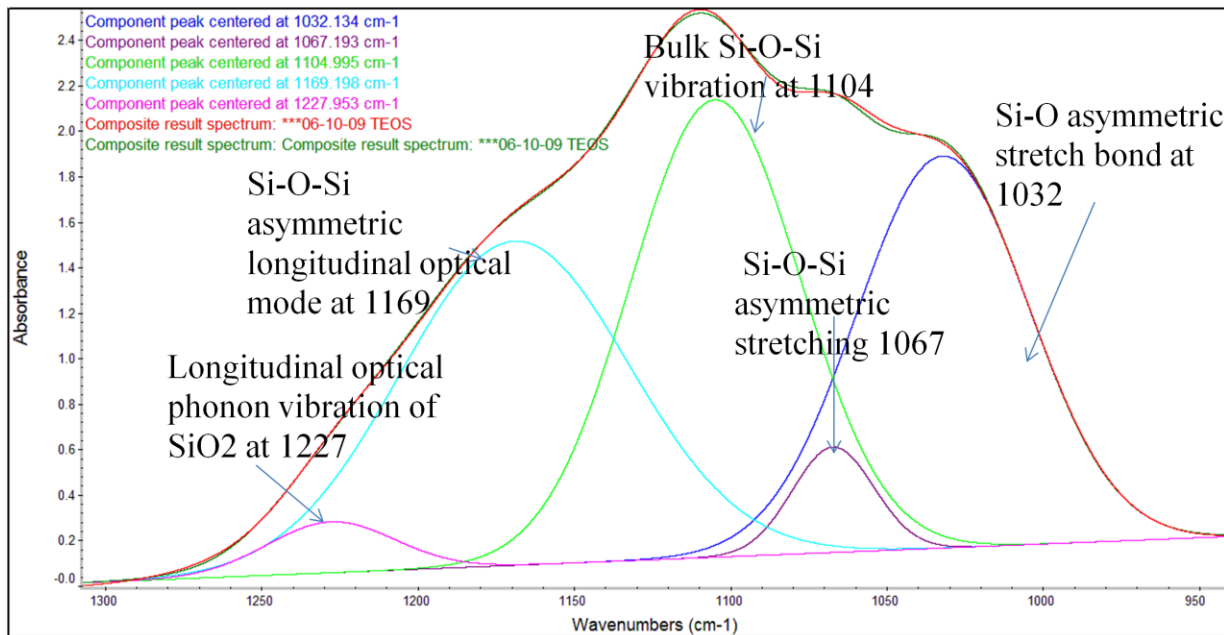


**Figure 5-18 b)** Received TEOS FTIR/GATR Spectrum Wavelengths 900 cm<sup>-1</sup>-1300 cm<sup>-1</sup>

The FTIR data for the received TEOS (figure 5-18 a-b) indicates the presence of hydroxyls at the peak  $3733\text{ cm}^{-1}$  (Si – OH terminal group) [65-66]. The figure 5-19 b gives a better picture of the  $\text{SiO}_2$  peaks: at  $1032\text{ cm}^{-1}$  [61-62],  $1067\text{ cm}^{-1}$  [68-72],  $1104\text{ cm}^{-1}$  [84],  $1169\text{ cm}^{-1}$  [32, 60] and  $1227\text{ cm}^{-1}$  [78-81]. At  $1032\text{ cm}^{-1}$ , it is considered an Si–O asymmetric stretch bond [61-62]. At  $1067\text{ cm}^{-1}$ , it is an Si – O – Si asymmetric stretching [68-72]. The  $1104\text{ cm}^{-1}$  peak is a bulk Si – O – Si vibration [84]. The  $1170\text{ cm}^{-1}$  peak shows that there is Si – O – C asymmetric stretching vibration [32, 60]. The  $1227\text{ cm}^{-1}$  peak shows that there is longitudinal optical phonon vibration of  $\text{SiO}_2$  [78-81].

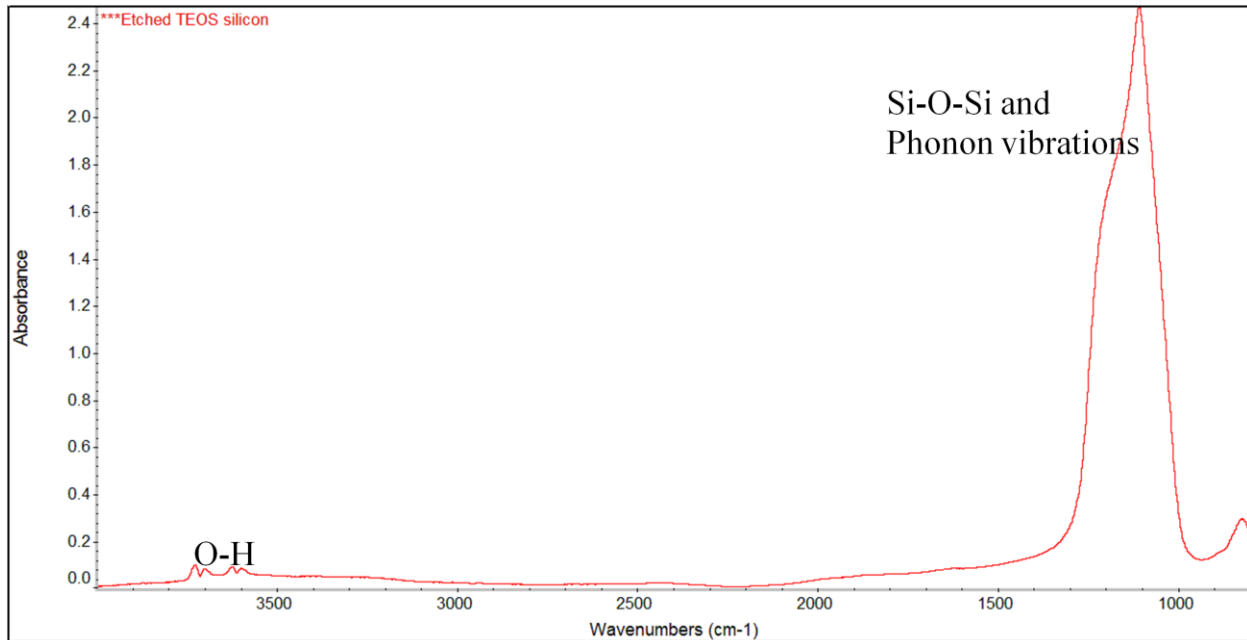


**Figure 5-19 a)** Etched TEOS FTIR/GATR Spectrum

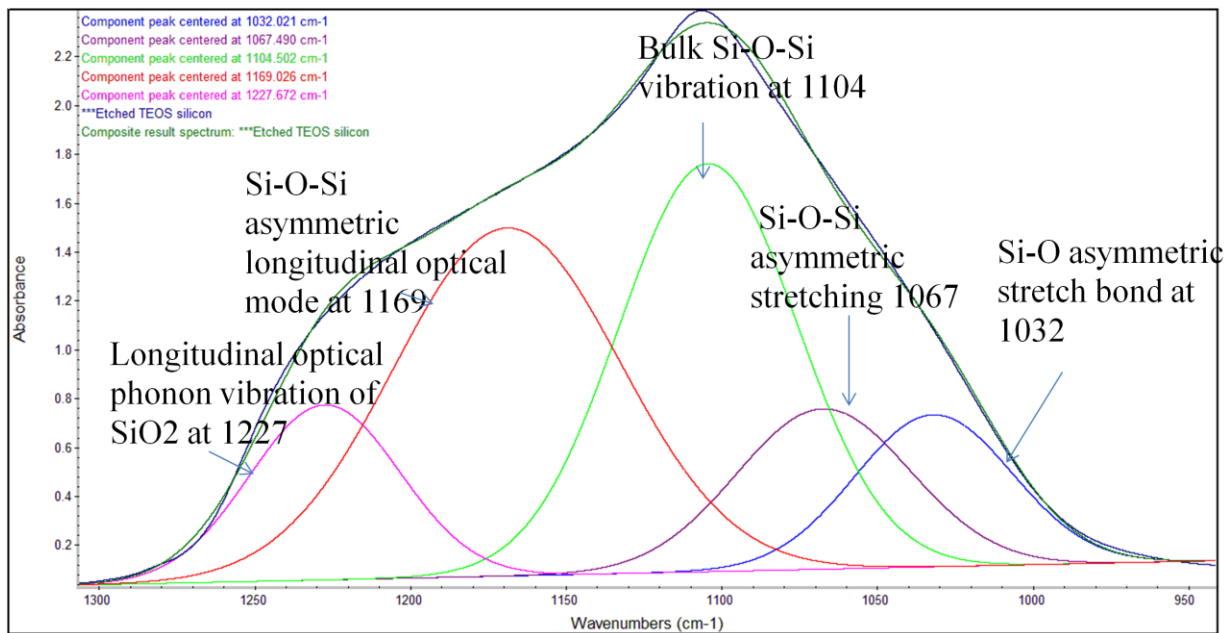


**Figure 5-19 b)** Etched TEOS FTIR/GATR Spectrum Wavelengths  $950 \text{ cm}^{-1}$ - $1300 \text{ cm}^{-1}$

The FTIR data for the etched TEOS sample shows that it still has some hydroxyls left on the surface (figure 5-19 a-b). However, there is a difference between the hydroxyls in this sample as compared to the received TEOS. The peaks at  $3730\text{ cm}^{-1}$  and  $3700\text{ cm}^{-1}$  correspond to the Si – OH terminal group [65-66]. The peaks at  $3600\text{ cm}^{-1}$  and  $3626\text{ cm}^{-1}$  are considered hydrogen bonded OH groups [82-83]. The silicon dioxide is definitely present because the Si – O – Si peaks are very clearly shown. These peaks are the same as for the received TOX; they are at  $1032\text{ cm}^{-1}$  [61-62],  $1067\text{ cm}^{-1}$  [68-72],  $1104\text{ cm}^{-1}$  [84],  $1169\text{ cm}^{-1}$  [32, 60] and  $1227\text{ cm}^{-1}$  [78-81]. There were no Si – H peaks suggesting that etching did not leave a hydrogen terminated surface. These peaks are expected to be from range  $2000\text{ cm}^{-1} – 2300\text{ cm}^{-1}$ . This might explain why the contact angle was low.

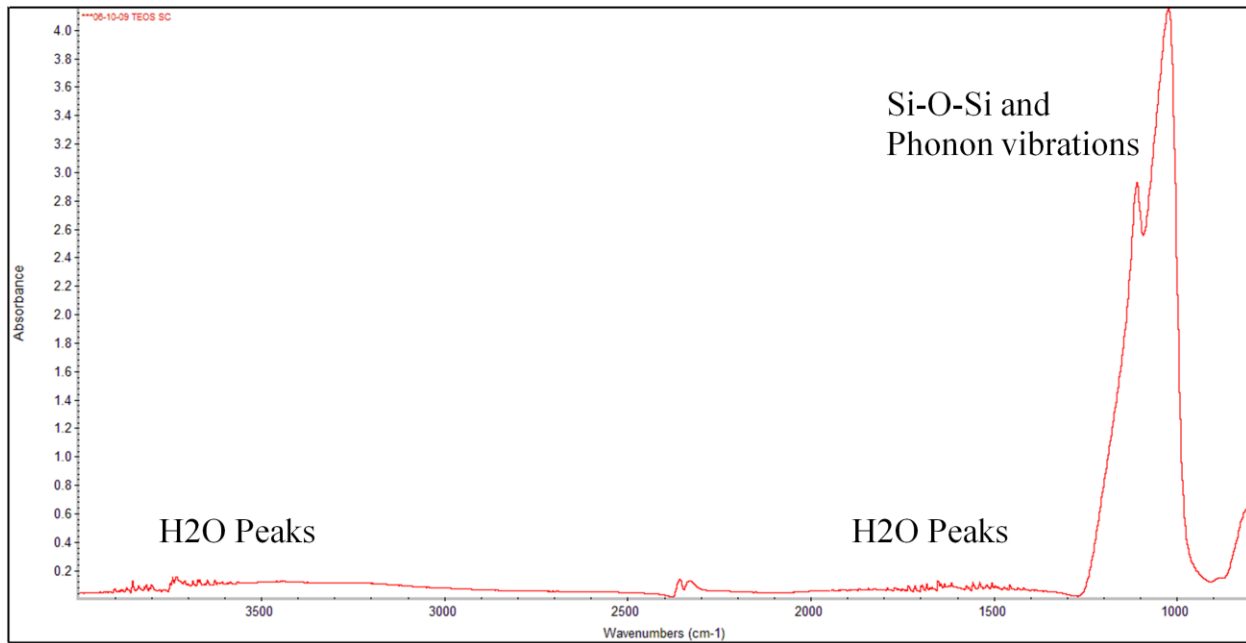


**Figure 5-20 a)** HMDS TEOS FTIR/GATR Spectrum

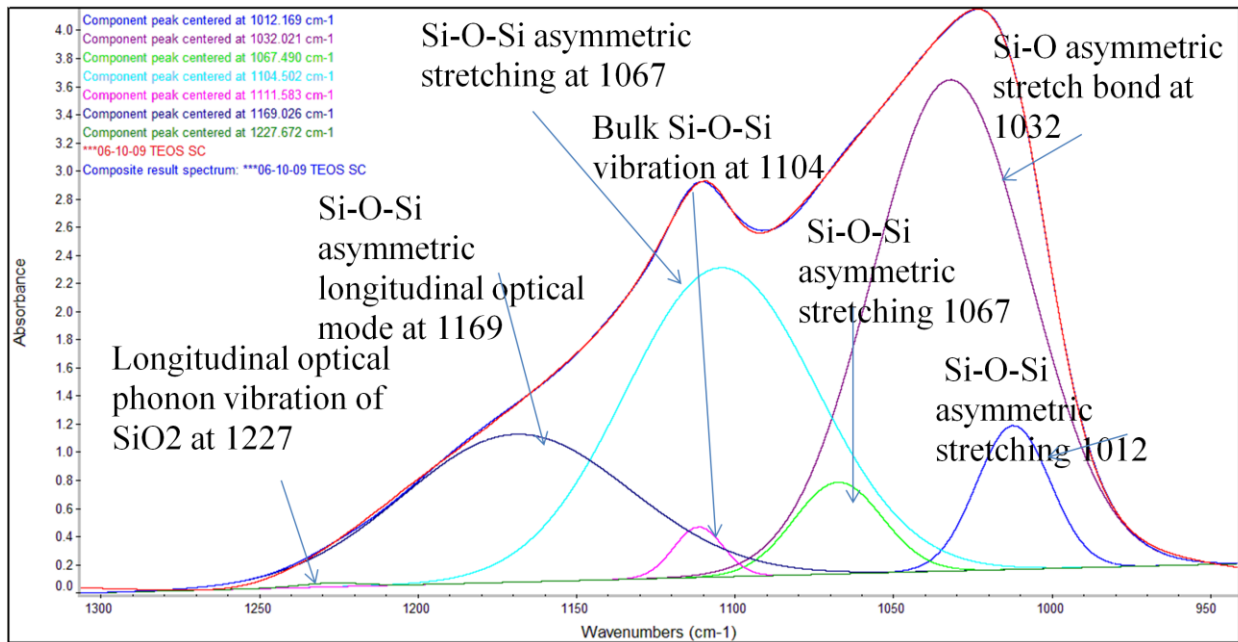


**Figure 5-20 b)** HMDS TEOS FTIR/GATR Spectrum Wavelengths  $900 \text{ cm}^{-1}$ - $1300 \text{ cm}^{-1}$

The FTIR data for the HMDS TEOS are given figure-20a and figure-20b. There are water peaks at  $3500\text{ cm}^{-1}$  to  $4000\text{ cm}^{-1}$  wavelengths, and at wavelengths  $1300\text{ cm}^{-1}$ - $2000\text{ cm}^{-1}$ . The peaks observed here are the same peaks as for the received TEOS: they are at  $1032\text{ cm}^{-1}$  [61-62],  $1067\text{ cm}^{-1}$  [68-72],  $1104\text{ cm}^{-1}$  [84],  $1169\text{ cm}^{-1}$  [32, 60] and  $1227\text{ cm}^{-1}$  [78-81]. However, there are two extra peaks observed. They are the  $1111\text{ cm}^{-1}$  [84] and the  $1012\text{ cm}^{-1}$  [86] peaks. Both of these peaks correspond to the bulk Si – O – Si vibration. There was no peak that showed signs of trimethylsilyls. However, XPS will be analyzed to find evidence of trimethylsilyls.

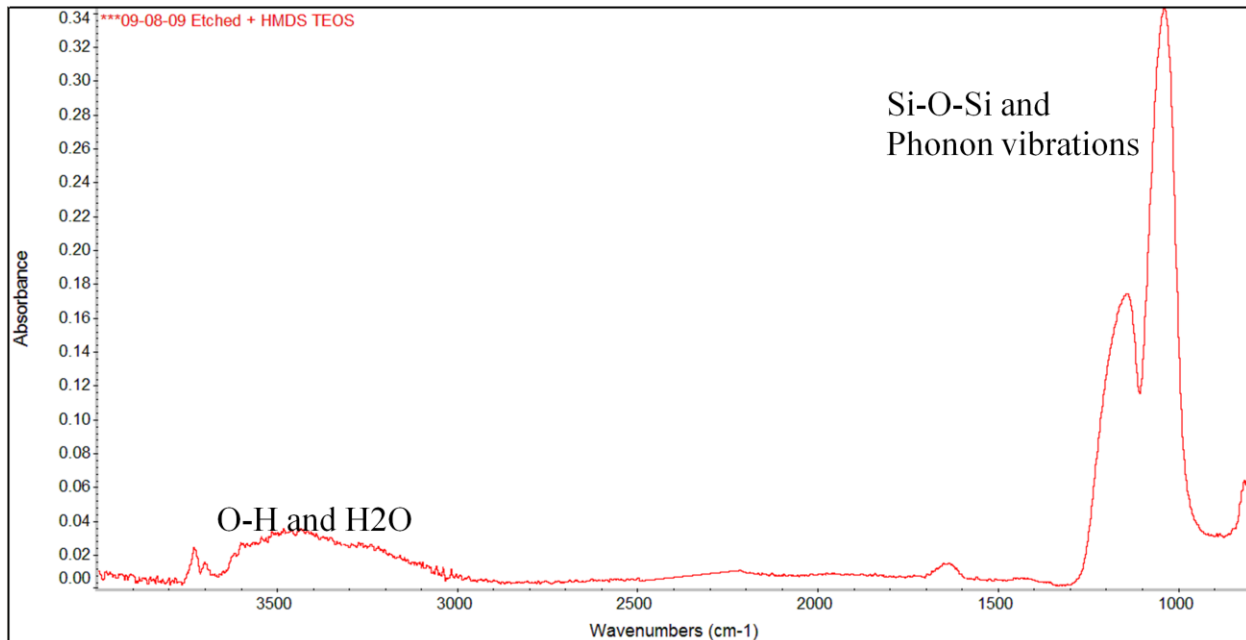


**Figure 5-21 a)** Etched + HMDS TEOS FTIR/GATR

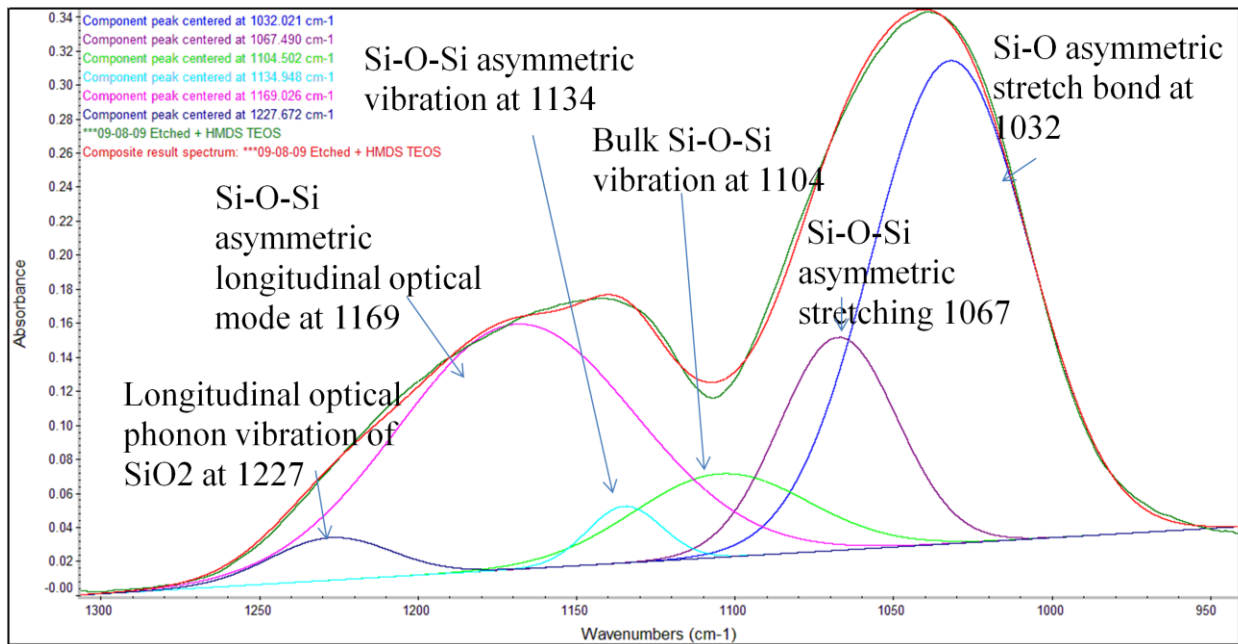


**Figure 5-21 b)** Etched + HMDS TEOS FTIR/GATR Spectrum Wavelengths

900 cm<sup>-1</sup>-1300 cm<sup>-1</sup>

The FTIR data for the etched + HMDS TEOS is given in figure 5-21a, and figure 5-21b. The peaks observed here are the same peaks as for the received TEOS; they are at  $1032\text{ cm}^{-1}$  [61-62],  $1067\text{ cm}^{-1}$  [68-72],  $1104\text{ cm}^{-1}$  [84],  $1169\text{ cm}^{-1}$  [32, 60] and  $1227\text{ cm}^{-1}$  [78-81]. However, there is an extra peak observed. It is the  $1134\text{ cm}^{-1}$  [78, 84] peak. It corresponds to the Si – O – Si asymmetric stretching vibration. I was expecting to see a Si – CH<sub>3</sub> peak, but there was none observed. XPS will be analyzed to find evidence of trimethylsilyls on the sample.

The FTIR data showed no evidence of trimethylsilyls present for the HMDS TEOS or the etched + HMDS TEOS. Also there were no Si – H peaks present for the etched TEOS sample. However, the low concentration used for the HMDS could be the reason why the FTIR/GATR is not peaking up these peaks. The equipment is not sensitive enough to pick up such a thin layer. The reason why there are no Si – H peaks is because the etching did not leave a hydrogen terminated surface. The XPS data will be used in the next section to find evidence of trimethylsilyls. The band assignments and wavenumbers are summarized in table 5-14.

**Table 5-14** Wavenumber and Band Assignment for TEOS Samples

Wavenumber cm <sup>-1</sup>	Band assignment	Reference
1012	Bulk Si – O – Si vibration	[86]
1032	Si – O – Si asymmetric stretching	[61-62]
1067	Si – O – Si asymmetric stretching	[68-72]
1104	Bulk Si – O – Si vibration	[84]
1134	Si – O – Si asymmetric stretching	[78, 84]
1169	Si – O – Si asymmetric stretching	[32, 60]
1227	Longitudinal optical phonon vibration of SiO <sub>2</sub>	[78-81]
3600 & 3626	Hydrogen bonded OH groups	[78-81]
3700 & 3730	Terminal Si – OH group	[82-83]
3733	Terminal Si – OH group	[65-66]

### 5.3.3 TEOS XPS

The surface chemistries are shown in table 5-15. The TEOS and the etched TEOS have less carbon than the etched + HMDS TEOS sample and the HMDS TEOS. The additional carbon in these two samples is due to trimethylsilyl ( $\text{CH}_3)_3\text{Si} - \text{O}$  addition. The etched TEOS has slightly less oxygen than the received TEOS. However, it is not significant so it can be assumed to be the same. Also the XPS data shows that the etched TEOS had more carbon. This could have come from impurities.

The HMDS TEOS and the HMDS TEOS sample that was sputter cleaned show that sputtering removed some of the carbon species. It is not clear if all of the trimethylsilyls are removed from the surface or if only some of them are removed by sputtering. This was also observed with the sputter cleaned etched + HMDS TEOS. However, since there was an addition of carbon for HMDS TEOS and etched + HMDS TEOS, XPS is showing that there were trimethylsilyls present.

**Table 5-15** XPS Data for TEOS

Samples	C 1s	O 1s	Si 2p	O/Si
Received TEOS	0.6	69.5	29.9	2.32
Etched TEOS	2	68	30	2.26
HMDS TEOS(No sputter)	2.4	67	30.7	2.18
HMDS TEOS (Sputter clean)	1.9	67.5	30.5	2.21
Etched + HMDS TEOS (No sputter)	4.7	65.9	29.4	2.24
Etched + HMDS TEOS (sputter clean)	4.1	66	29.9	2.21

### 5.3.4 TEOS AFM

An AFM image for the received TEOS is given below (figure 5-22). There were 5 different scans of the sample taken and their data were averaged. The number of events vs. height graph describes the distribution of peak heights. The wavelength for this case is 9.94 nm, and the average Root Mean Square roughness is .72 nm. The wavelength tells us that the asperities are reasonably close. The RMS roughness tells us that it is somewhat rougher than the etched Si and the received TOX. The wavelength, RMS roughness, and peak heights are given in the table below.

**Table 5-16** Wavelength, RMS, Peak Heights of Received TEOS

Scan	Wavelength (nm)	RMS (nm)	Peak Heights (nm)
1	9.3	1.23	4.2
2	9.95	0.80	2.9
3	9.25	0.86	3.7
4	10.13	0.68	3.9
5	11.05	0.65	4
Average	$9.94 \pm .73$	$0.72 \pm .23$	$3.74 \pm .50$

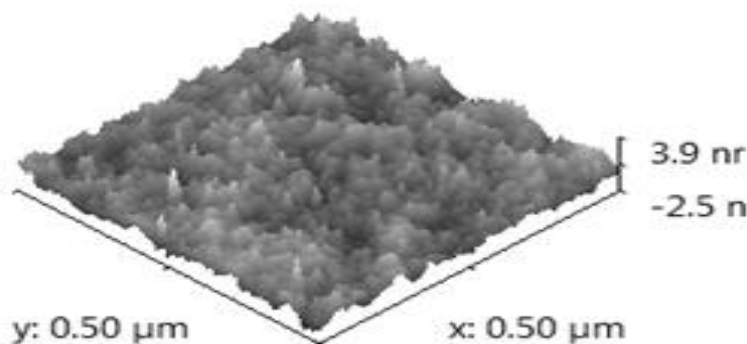


**Figure 5-22** Peak Heights for Received TEOS

An AFM image for the etched TEOS is shown below (figure 5-23). Interestingly, roughness decreased after etching. The wavelength for this sample is 13.17 nm which increased relative to the received TEOS. The average Root Mean Square roughness is .66 nm. This is a very interesting result because the film surface is smoothed during etching instead of roughening it up. This could be due to selective etching of asperities—this is suggested by the reduction of peak height with respect to received TEOS. The wavelength, RMS roughness, and peak heights are given in the table below (table 5-17).

**Table 5-17** Wavelength, RMS, Peak Heights of Etched TEOS

Scan	Wavelength (nm)	RMS (nm)	Peak Height (nm)
1	12.98	0.68	2.8
2	12.65	0.68	2.7
3	13.23	0.66	2.9
4	13.08	0.66	2.8
5	13.9	0.66	2.5
Average	$13.17 \pm .46$	$0.66 \pm .01$	$2.74 \pm .15$

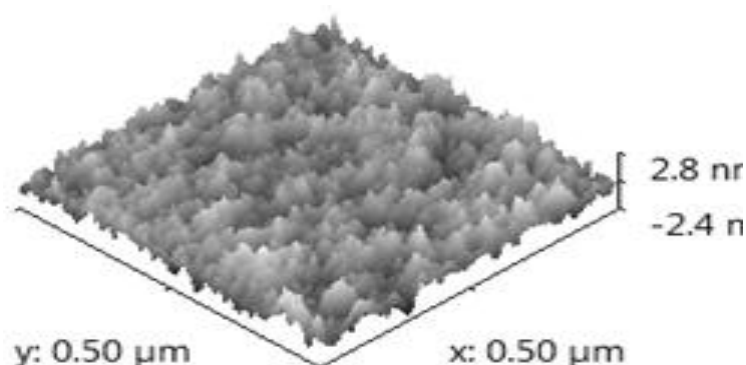


**Figure 5-23** Peak Heights for Etched TEOS

The AFM for the HMDS TEOS is given below (figure 5-24). The heights of the peaks are greater than the etched TEOS, but only slightly larger than the received TEOS. (In this case the 31.9 nm peak height will be excluded since this is due to dust.) This means that the trimethylsilyls are being placed on the peaks, thus, increasing the height difference between peaks and valleys. This difference in height between received and HMDS TEOS, 0.5 nm is only slightly larger than the length of a trimethylsilyl group (0.3 nm). The wavelength for this case is 14.34 nm, which is greater than the received TEOS. This is in contrast to the height increase; consequently, it is unclear where and if silylation is preferential to any site. The average Root Mean Square roughness is .65 nm. In comparison to the received TEOS sample, this is actually smoothing the surface more. The wavelength, RMS roughness, and peak heights are given in the table below (table 5-18).

**Table 5-18** Wavelength, RMS, Peak Heights of HMDS TEOS

Scan	Wavelength (nm)	RMS (nm)	Peak height (nm)	Peak Height (nm) Excluding 31.9
1	14.63	0.65	4.1	4.1
2	14.85	0.69	31.9	
3	14.47	0.65	4.6	4.6
4	14.38	0.64	4.2	4.2
5	13.38	0.61	4	4
Average	$14.34 \pm .57$	$0.65 \pm .03$	$9.76 \pm 12.4$	$4.23 \pm .27$

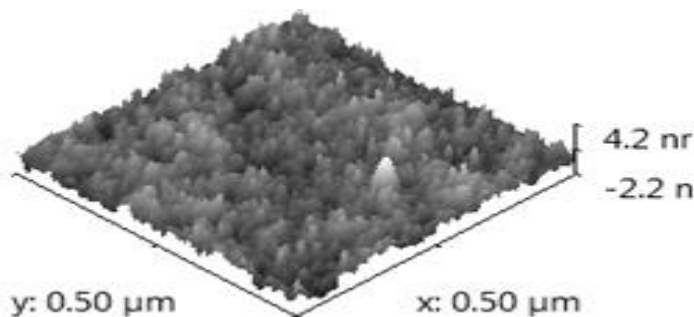


**Figure 5-24** Peak Heights for HMDS TEOS

The AFM image for the etched + HMDS TEOS is shown below (figure 5-25). The peak heights are greater than the etched TEOS. The wavelength for this case is 12.33 nm—slightly less than the etched TEOS. This might be due to fact that silylation occurs on the surface of the peaks, thus increasing height and lowering wavelength. The average Root Mean Square roughness is 0.67 nm—very similar to etched TEOS. The wavelength, RMS roughness, and peak heights are given in the table 5-19.

**Table 5-19** Wavelength, RMS, Peak Heights of Etched + HMDS TEOS

Scan	Wavelength (nm)	RMS (nm)	Peak Heights (nm)
1	12.1	0.68	7.2
2	12.65	0.66	16.2
3	11.93	0.68	9.8
4	12.65	0.65	10.3
5	12	.56	2.1
Average	$12.33 \pm .35$	$0.67 \pm .05$	$10.85 \pm 5.12$

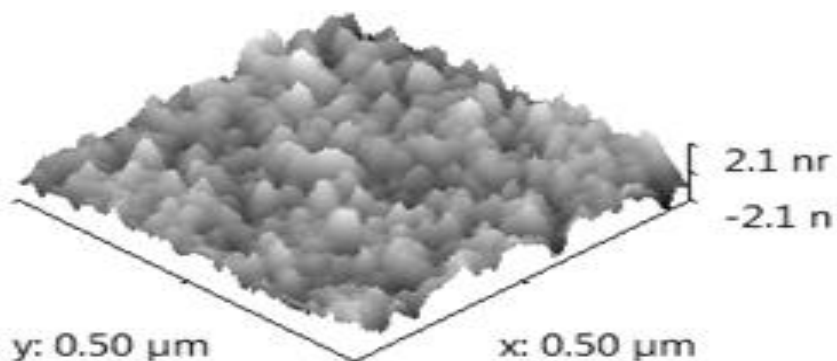


**Figure 5-25** Peak Heights for Etched + HMDS TEOS

The number of events vs. height for all the TEOS samples is given below. This data shows that TEOS is smoothed by etching, by adding HMDS, and by etching and adding HMDS. It is unclear why this occurs. One possibility is that the etching process selectively etches peaks leading to smoothing. Silylation can be conformal and not roughen the surface. Silylation of the TEOS may not occur on the top of peaks but on the sides of the peak surfaces.

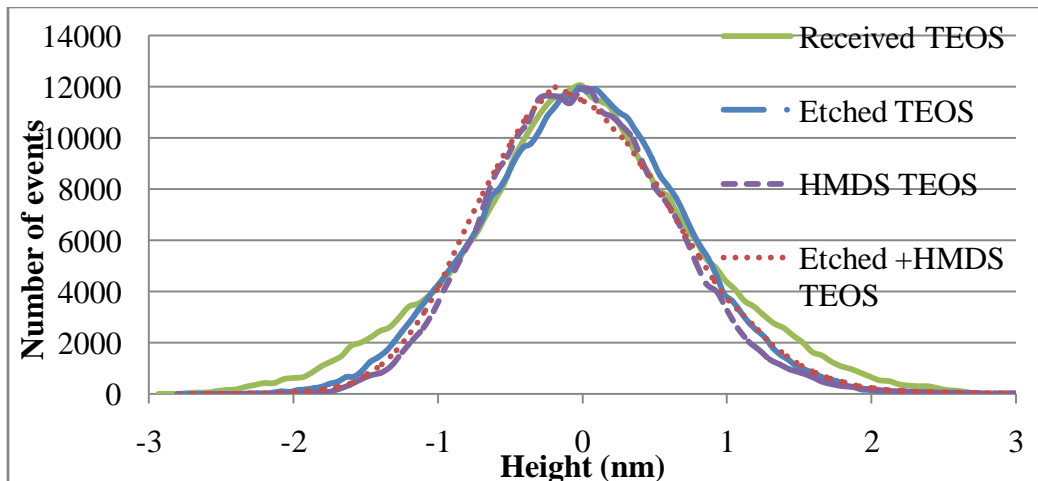


**Figure 5-26** Number of Events vs. Height for TEOS

### 5.3.5 Conclusions for TEOS

There is a clear correlation between the contact angle and surface chemistries. The FTIR/GATR indicated that there were more hydroxyls after the etching. It is safe to conclude at if there are more hydroxyls on the surface of a sample the more attractive it is to water. XPS showed evidence of trimethylsilyls groups on the surface of the samples. It shows that as trimethylsilyls are placed on the surface, the more it repels a liquid. The AFM data showed that the roughness decreased as the samples were etched and as they were functionalized with HMDS. It seems that the etching was selective and this is why it smoothed the surface. While it appeared that the HMDS could have placed the trimethylsilyls on the sides of the peaks rather than directly on top. There was no clear correlation between the roughness and the contact angle. The roughness reduced as it was etched, functionalized, and etched + functionalized.

## 5.4 OSG Results

In this section the results for an organosilicate glass, made through a plasma enhanced chemical vapor deposition (PECVD) fabrication (OSG), will be given. OSG was used because it offers a rougher surface compared to the surfaces presented earlier. OSG is of interest because of its current use as interlayer dielectrics. Four different sets of samples were used in this case. One OSG set was used as-received (received OSG). One OSG set was etched in HF/de-ionized water (1:50) mixture for 30 sec (etched OSG). The purpose of etching the sample was to see if it would remove hydroxyls and replace them with hydrogen. A second set was placed on the supercritical chamber as they came and functionalized with HMDS (HMDS OSG). This was done to replace hydroxyls with trimethylsilyls. The third set was etched and functionalized with HMDS in supercritical CO<sub>2</sub> (etched + HMDS OSG). This was done to see if the etching would replace the hydroxyls with hydrogen, and the functionalization was done to replace any remaining hydroxyls with trimethylsilyls. The purpose of doing this was to see if how the contact angle of a liquid would get affected after removing all the hydroxyls from the OSG and replacing them with hydrogen and trimethylsilyls.

### 5.4.1 OSG Contact Angle and Surface Energy

The water contact angle for the received and etched OSG samples were 92.71°, and 68.19°, respectively. My speculation of what is going on here is that the water is actually penetrating the sample, similar to the Wenzel model. Ekaterina Vinogradova points out in her paper that it is possible for OSG to absorb moisture [87]. The HMDS OSG (83.09°) had a lower water contact angle compared to the received OSG. As for the etched + HMDS OSG (81.57°) sample, the water contact angle is higher relative to the etched OSG, but it is a little lower than the HMDS OSG. However, it is only one degree lower than HMDS OSG so it is going to be

considered the same contact angle as the HMDS OSG. The reason the contact angle is less for both of these cases than the received OSG may have to do with unintended residues left after supercritical treatments. This is what caused the lowering in contact angle for the HMDS OSG and the etched + HMDS OSG.

The DIM contact angle followed similar results. However, the changes in contact angles were not drastic. The DIM contact angle for received OSG is  $55.34^\circ$ , and for the etched OSG is  $51.61^\circ$ . The DIM contact angle for the HMDS OSG was  $53.67^\circ$ . This is lower than the received OSG but slightly higher than the etched OSG. As for the etched + HMDS OSG sample, the DIM contact angle was  $55.56^\circ$  which is higher than the HMDS OSG by 2 degrees. This result is only 2 degrees higher, so it can be considered to be equal to the HMDS OSG DIM contact angle. Again, the reason the contact angle for the HMDS treated samples were less than the received OSG may also be the result of HMDS functionalization residue that was left on the sample after it was placed on the supercritical chamber.

Surface energies for the OSG samples are given above in table 5-20. The surface energy values correlate well with the observed contact angles. The etched OSG is of interest because it has a high surface energy relative to the other OSG samples. This high surface energy is due to the fact that the etched OSG absorbed moisture.

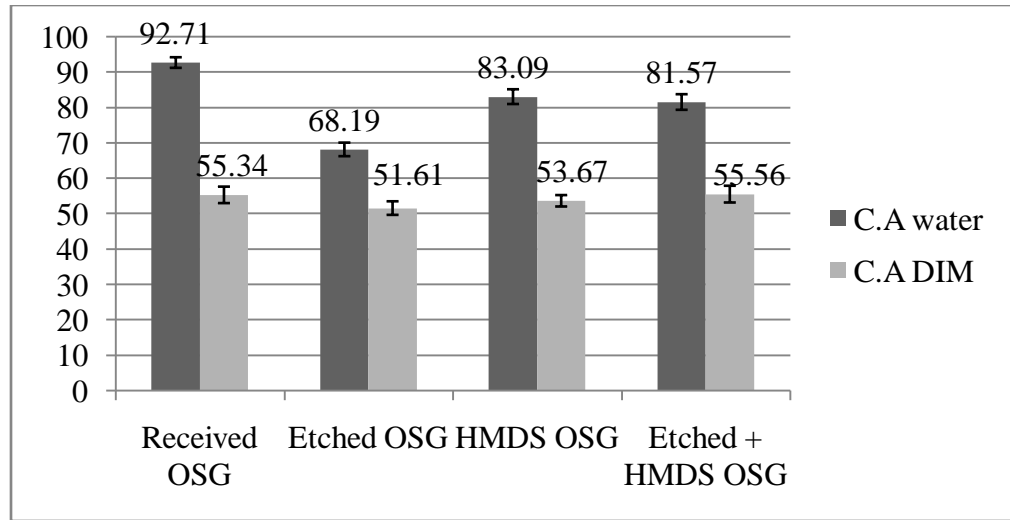


**Figure 5-27** Contact Angles for OSG

**Table 5-20** Surface Energy for OSG

SURFACE ENERGY	Polar ( $\frac{J}{m^2}$ )	Dispersive ( $\frac{J}{m^2}$ )	Total ( $\frac{J}{m^2}$ )
Geometric of Received OSG	$1.44 \pm .1$	$31.25 \pm .35$	$32.69 \pm .31$
Harmonic of Received OSG	$4.63 \pm .14$	$32.77 \pm .29$	$37.40 \pm .27$
Geometric of Etched OSG	$10.32 \pm .42$	$33.38 \pm .42$	$43.71 \pm .46$
Harmonic of Etched OSG	$14.99 \pm .36$	$34.62 \pm .36$	$49.61 \pm .44$
Geometric of HMDS OSG	$4.01 \pm .29$	$32.21 \pm .34$	$36.21 \pm .39$
Harmonic of HMDS OSG	$8.35 \pm .34$	$33.6 \pm .3$	$41.95 \pm .42$
Geometric of Etched + HMDS OSG	$4.84 \pm .35$	$31.13 \pm .51$	$35.96 \pm .41$
Harmonic of Etched + HMDS OSG	$9.21 \pm .38$	$32.67 \pm .42$	$41.88 \pm .5$

### 5.4.2 GATR/FTIR for OSG

The FTIR data for the received OSG, etched OSG, HMDS OSG, and etched + HMDS OSG are given in the graphs below. The FTIR/GATR data was used to determine the chemical makeup of the samples. All of the samples showed the same peaks at the same wavelengths. This is saying that the chemical makeup of the films was not significantly affected by the chemical treatments that were done to it. The peaks and their band assignments are given in table 5-21.

**Table 5-21** Wavenumber and Band Assignment for OSG Samples

Wavenumber cm <sup>-1</sup>	Band assignment	Reference
1021	Si – CH <sub>2</sub> – Si wagging vibration	[68, 72]
1060	Si – O – Si asymmetric stretching	[68-72]
1143	Si–O – Si asymmetric stretching	[35, 77]
1273	Si – CH <sub>3</sub> symmetric deformation	[28-31, 35, 46, 50, 60, 69]
1359	Bending C – H <sub>2</sub>	[35, 45]
1410	Bending asymmetrical C – H <sub>3</sub>	[35, 45-46]
1642	OH bending of absorbed water	[88]
3600 & 3626	Hydrogen bonded OH groups	[82-83]
3700 & 3730	Terminal Si – OH group	[65-66]

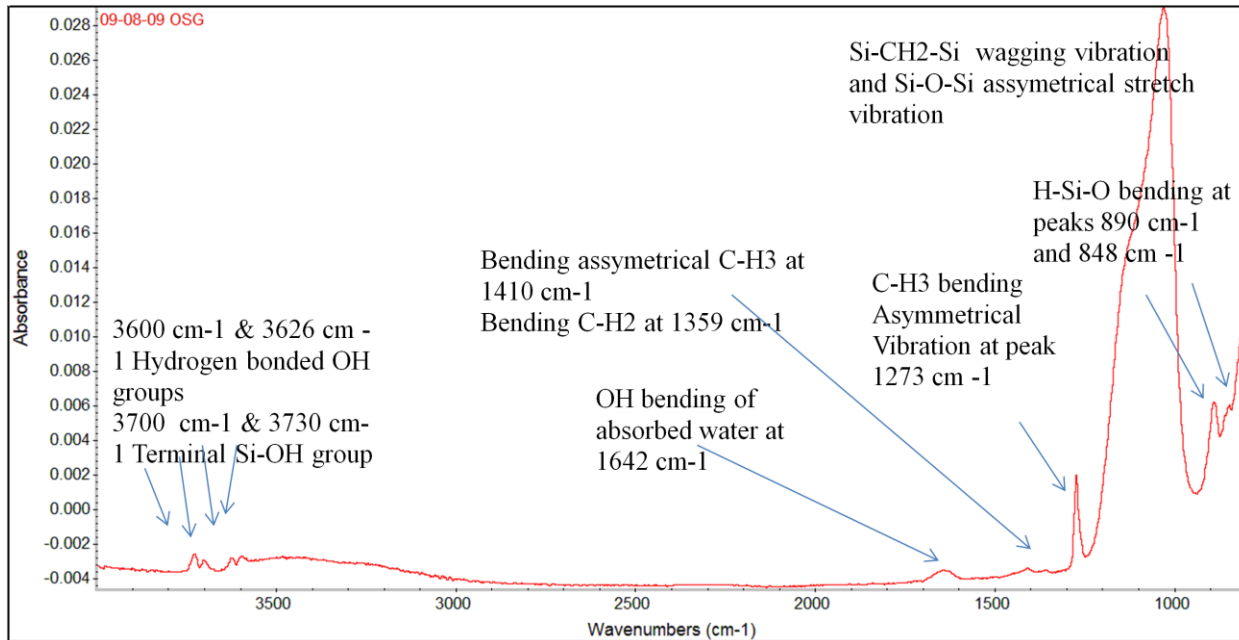


**Figure 5-28 a)** Received OSG FTIR/GATR Spectrum

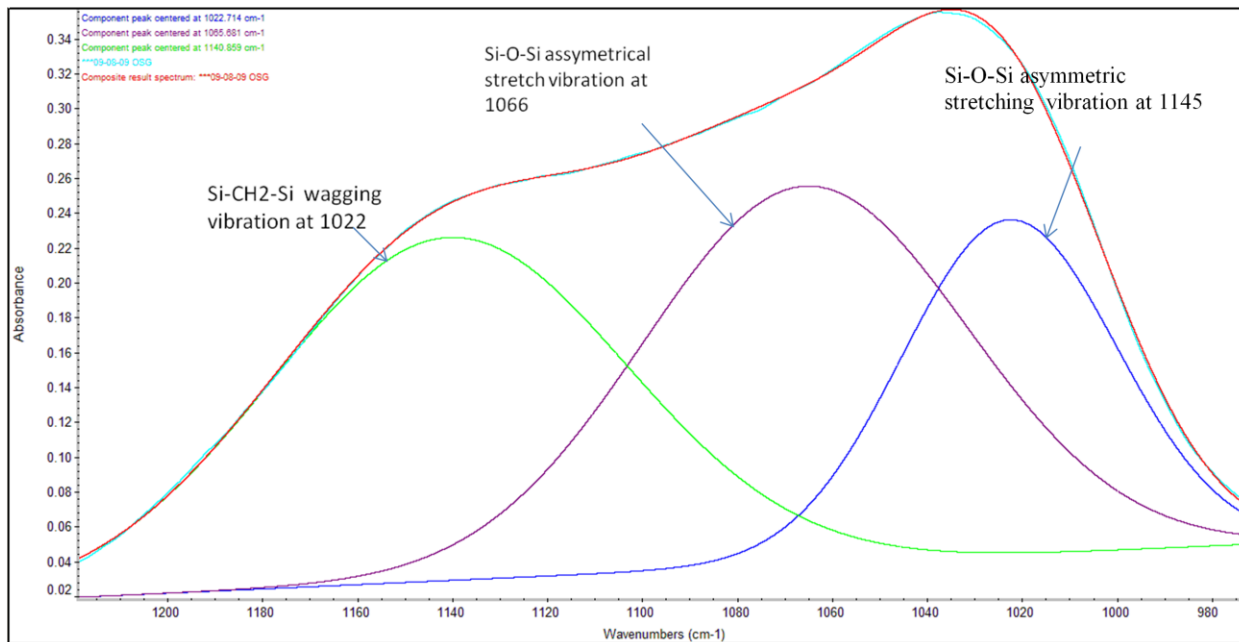


**Figure 5-28 b)** Received OSG FTIR/GATR Spectrum Wavelengths  $900 \text{ cm}^{-1}$ - $1300 \text{ cm}^{-1}$

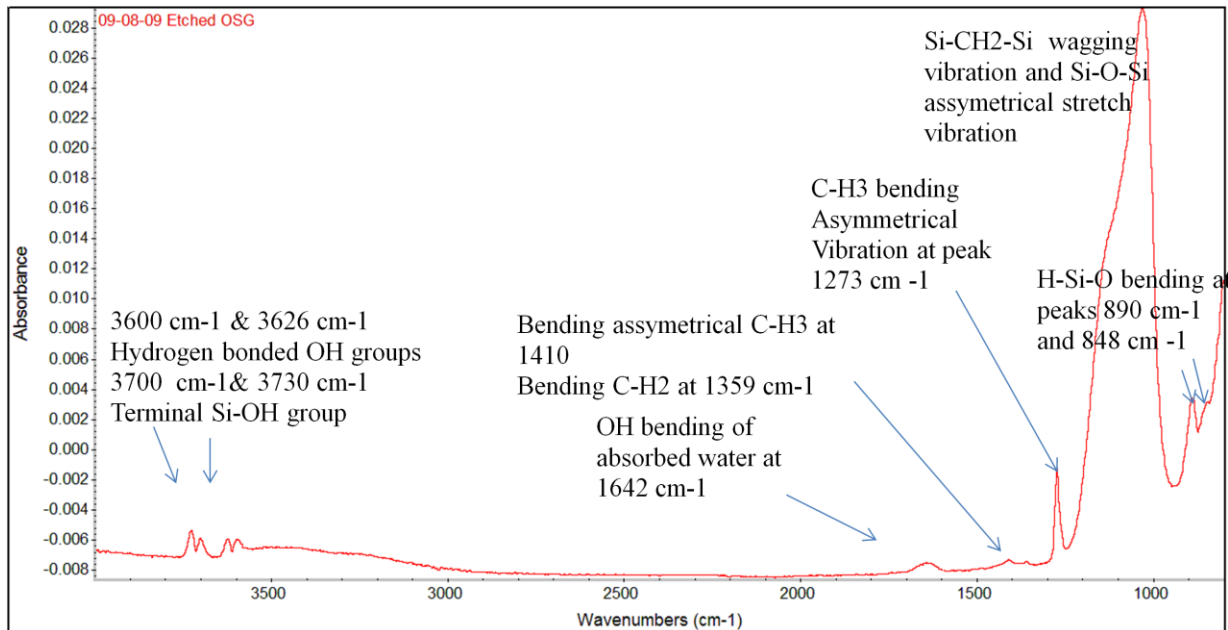


**Figure 5-29 a)** Etched OSG FTIR/GATR Spectrum

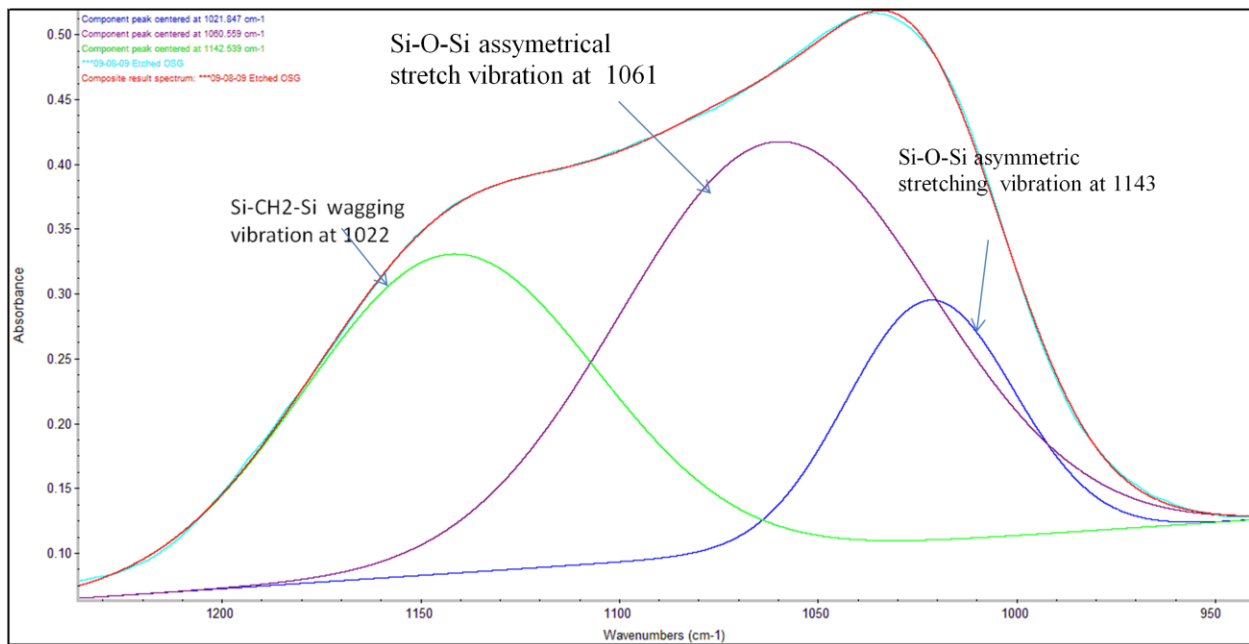


**Figure 5-29 b)** Etched OSG FTIR/GATR Spectrum Wavelengths  $950\text{ cm}^{-1}$ - $1300\text{ cm}^{-1}$

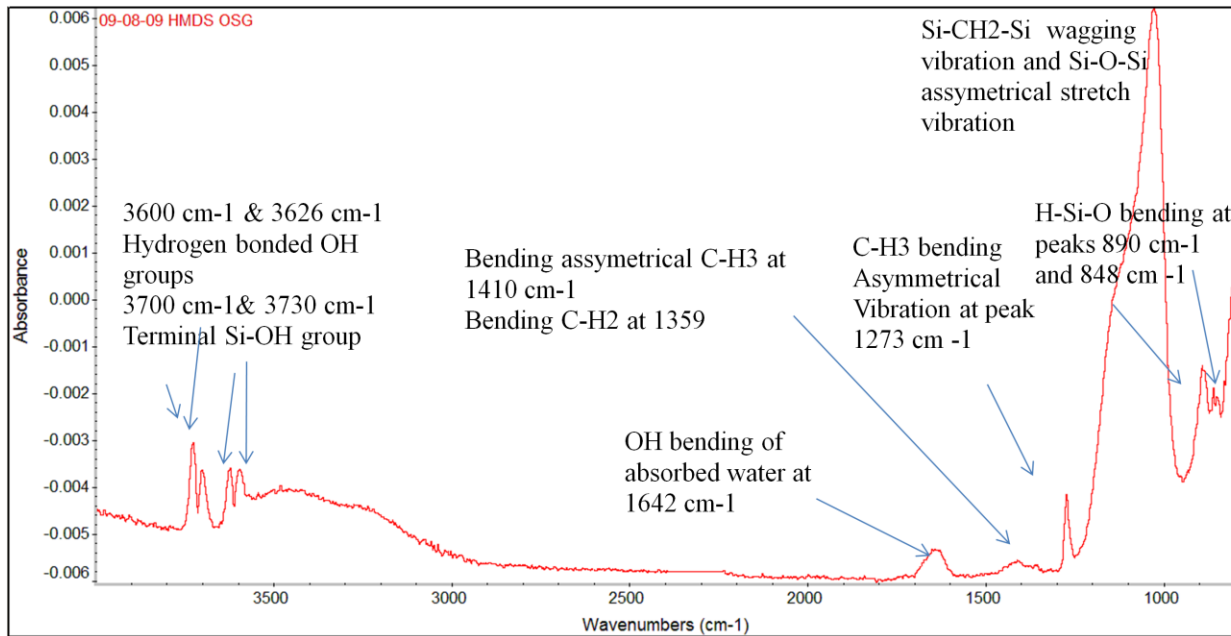


**Figure 5-30 a)** HMDS OSG FTIR/GATR Spectrum

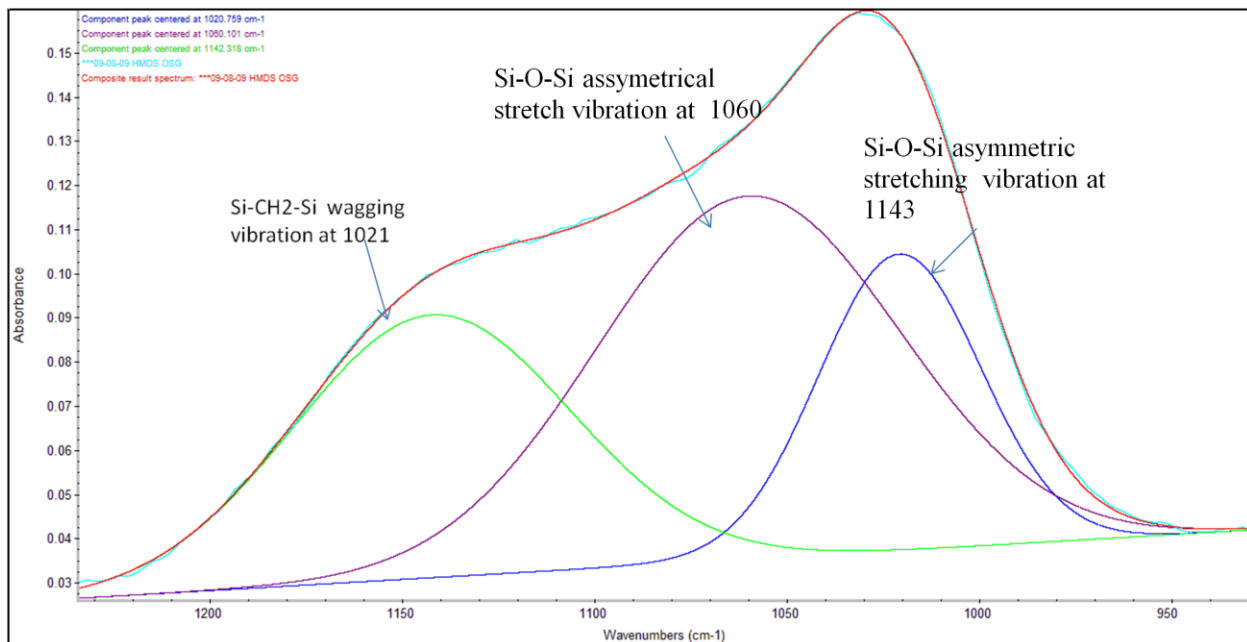


**Figure 5-30 b)** HMDS OSG FTIR/GATR Spectrum Wavelengths  $950 \text{ cm}^{-1}$ - $1300 \text{ cm}^{-1}$

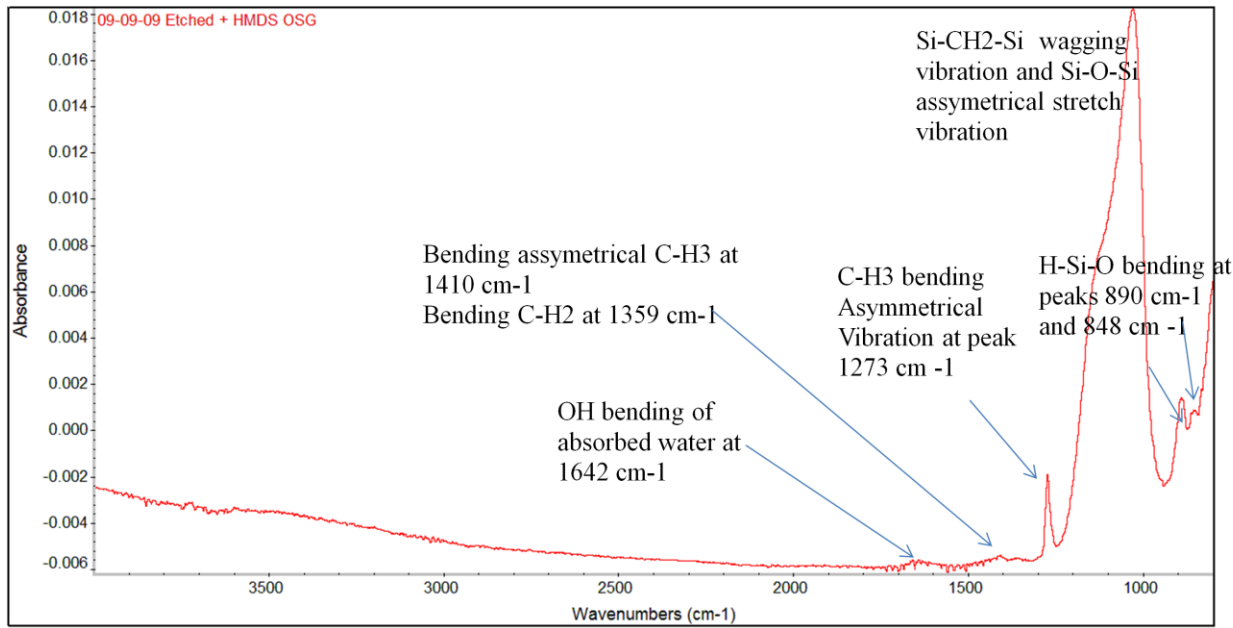


**Figure 5-31 a)** Etched + HMDS OSG FTIR/GATR Spectrum

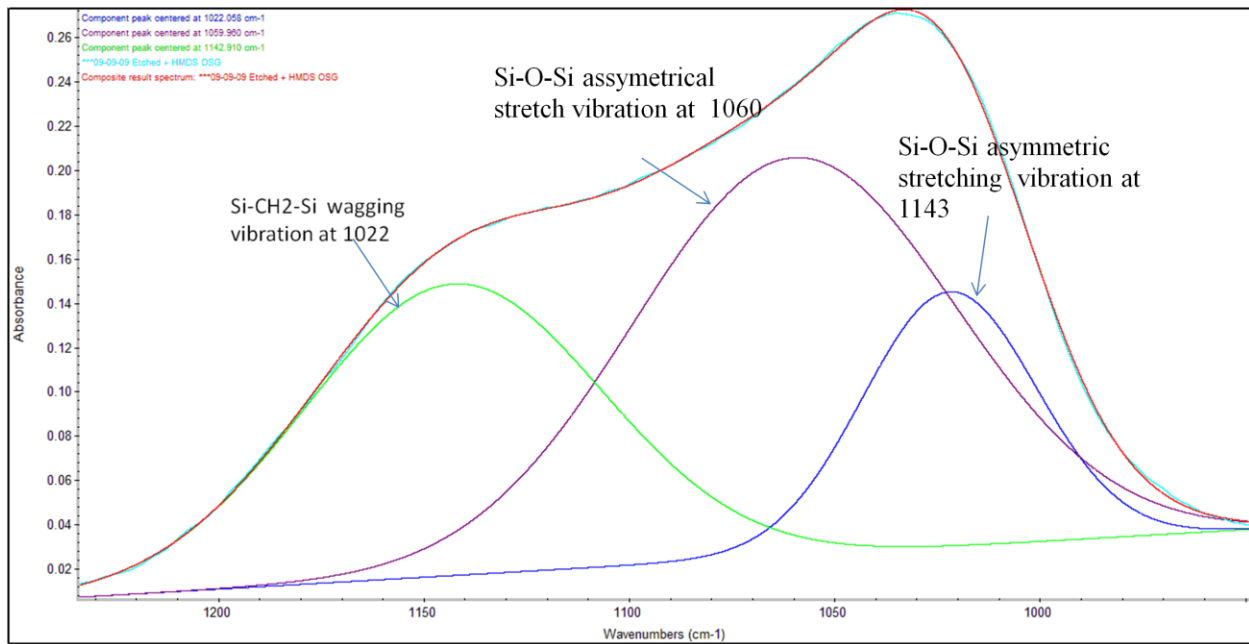


**Figure 5-31 b)** Etched + HMDS OSG FTIR/GATR Spectrum Wavelengths

$$900 \text{ cm}^{-1} - 1300 \text{ cm}^{-1}$$

### 5.4.3 OSG XPS

The XPS data showed that there is a significant amount of carbon in all of the samples. The table below shows the concentrations of carbon, silicon, and oxygen present in each film. The chemistries are very interesting for these samples. The received OSG, etched OSG, and HMDS OSG have virtually the same compositions. What this is saying is that the chemical procedures that were done to the samples had no affect on the surface of the samples. However, the etched + HMDS OSG showed significantly more carbon, and less oxygen and silicon compared to the first three samples. This may be due to reasonably efficient silylation of the OSG sample after it has been etched with HF/water mixture. These results are showing that it is possible to modify the surface of the samples, but the sample has to be etched in order for HMDS to functionalize it.

The FTIR showed that there was no change in the surface of the samples as etching and supercritical treatments were done to it. The XPS data supports this conclusion, with the exemption of the etched + HMDS OSG. As can be seen in the table 5-22 the carbon content for the etched + HMDS OSG increased by 9 percent as compared to the OSG, etched OSG, and HMDS OSG.

**Table 5-22 XPS Data for OSG**

Samples	C 1s	Si 2p	O 1s	O/Si
OSG	25.9	27	47.1	1.74
Etched OSG	25.7	27.1	47.2	1.74
HMDS OSG	25.6	27	47.5	1.76
Etched + HMDS OSG	34.5	23.4	42.1	1.79

#### 5.4.4 OSG AFM

A representative AFM image of the received OSG is shown below (figure 5-32). The average height of the peaks was 3.5 nm. The wavelength for this sample is 12.24 nm, and the average Root Mean Square roughness is .78 nm. This RMS value is rougher than the silicon, TOX, and TEOS samples. The wavelength, RMS roughness, and peak heights for OSG are given in the table 5-23.

**Table 5-23** Wavelength, RMS, Peak Heights of Received OSG

Scan	Wavelength (nm)	RMS (nm)	Peak Heights (nm)
1	14.23	0.79	4.3
2	13.88	0.77	2.9
3	13.58	0.77	3.2
4	12.38	0.75	3.2
5	12.13	0.83	3.9
Average	$13.24 \pm .93$	$0.78 \pm .03$	$3.5 \pm .58$

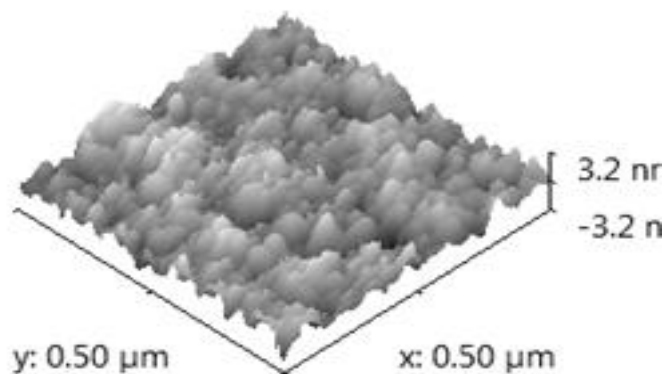


**Figure 5-32** Peak Heights for the Received OSG

An AFM image of the etched OSG is shown below (figure 5-33). The wavelength for this case is 12.44 nm, and the average Root Mean Square roughness is .86 nm. The wavelength, RMS roughness, and peak heights are given in the table 5-24.

**Table 5-24** Wavelength, RMS, Peak Heights of Etched OSG

Scan	Wavelength (nm)	RMS (nm)	Peak height (nm)
1	13.65	0.86	2.8
2	12	0.82	2.7
3	13.2	0.84	2.9
4	11.1	0.87	2.8
5	12.23	0.88	2.5
Average	$12.44 \pm 1$	$0.85 \pm .02$	$2.74 \pm .15$

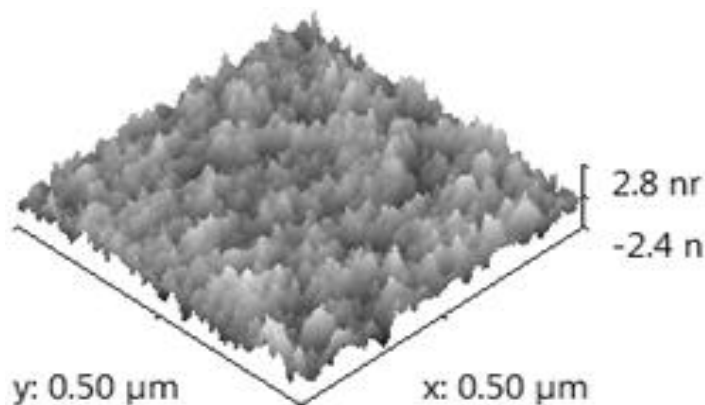


**Figure 5-33** Peak Heights for the Etched OSG

An AFM for the HMDS OSG is show below (figure 5-34). The heights of the peaks are higher than the etched OSG, but it is just a little higher than the received OSG. This could be coming from the residue left over after the supercritical treatment. The wavelength for this case is 13.74 nm, and the average Root Mean Square roughness is .81 nm. This sample is somewhat rougher than the received OSG; this is rougher but less rough than the etched OSG. The roughening is likely due to HMDS residue left on the sample. That is why it is rougher than Received OSG but smoother than the etched OSG. The wavelength, RMS roughness, and peak heights are given in table 5-25.

**Table 5-25** Wavelength, RMS, Peak Heights of HMDS OSG

Scan	Wavelength (nm)	RMS (nm)	Peak Heights (nm)
1	13.88	0.85	4.9
2	15.08	0.4	4.8
3	13.55	0.79	3.5
4	12.53	0.78	3.7
5	13.65	0.78	3.2
Average	$13.74 \pm .91$	$0.81 \pm .18$	$4.02 \pm .78$

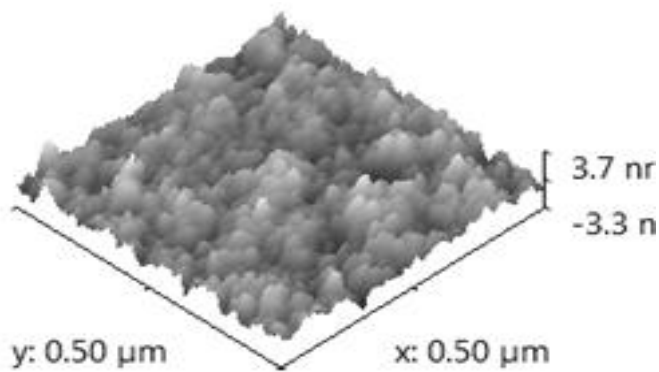


**Figure 5-34** Peak Heights of HMDS OSG

The AFM for the etched + HMDS OSG is given below (figure 5-35). The heights of the peaks are a lot higher than the other OSG samples, but this can be due to the residue in the samples. The wavelength for this case is 13.18 nm, and the average Root Mean Square roughness is .85 nm. This sample is rougher than the Received OSG and the HMDS OSG, but not rougher than the etched OSG. The wavelength, RMS roughness, and peak heights are given in the table 5-26.

**Table 5-26** Wavelength, RMS, Peak Heights of Etched + HMDS OSG

Scan	Wavelength (nm)	RMS (nm)	Peak height (nm)
1	15.4	0.85	300
2	12.43	0.85	4
3	12.88	0.87	7.2
4	12.9	0.85	110
5	12.28	0.85	18
Average	$13.18 \pm 1.27$	$0.85 \pm .01$	$87.84 \pm 126$

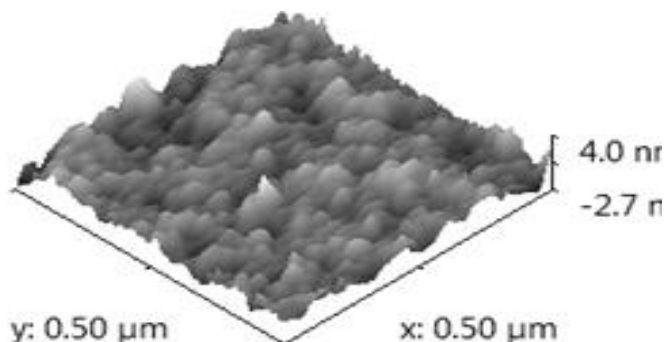


**Figure 5-35** Peak Heights for Etched + HMDS OSG

The number of events vs. height for the OSG samples is given below (figure 5-36). This data shows that the peaks did increase after etching. When the samples were etched and etched + supercritical treated, the peak heights are almost identical. Furthermore, the peak for the HMDS treated sample was virtually the same height as the received OSG. It appears that etching the sample caused it to increase in peak heights.

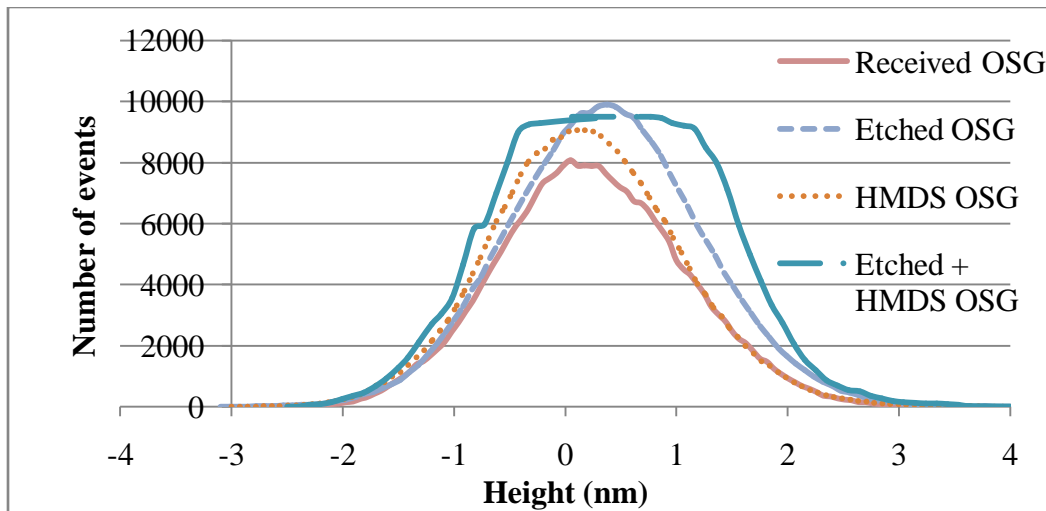


**Figure 5-36** Number of Events vs. Height for OSG

#### 5.4.5 Conclusions for OSG

There does not appear to be a clear correlation between the contact angles and surface chemistries. The etched OSG sample reduced the contact angle for water and for DIM. This is most likely due to moisture absorption after the etching process. The XPS showed no difference in the elemental makeup of the samples. Only the etched + HMDS OSG showed an increase in carbon. This could have come from some silylation of the OH in the sample. What this shows is that etching and supercritical treatments had no effect on the samples. However, it is possible to functionalize the OSG sample but after it has been etched. The AFM showed no correlation between the roughness and the contact angle.

## CHAPTER 6

### FURTHER EXPERIMENTATION

#### 6.1 Wetting after Dynamic Contact

Additional experiments were conducted to see if the liquids actually penetrated the surface of these films using dynamic contact angle measurements. DI water and DIM was added and removed from the surface of the samples. Movies of this process were made using the goniometer. The contact angle was then measured from the separate still images. The point was to see if the contact angle changed after repeating this dynamic process.

The results are given in figure 6-1a and figure 6-1b. All samples showed that water penetrated their surface. This can be concluded because most of the samples showed a reduction in contact angle after the dynamic contact, with the exemption of a few. However, those that didn't show a change in contact angle showed very similar contact angles as before the dynamic contact mechanism was done to them.

We see that for the water contact angle before and after the dynamic contact for the etched TOX gave values of 18.44 before and 18.15 after. These two values are identical so what happened here is that the contact angle was already very low. So doing a dynamic contact would not do anything to it. As for the HMDS TEOS, we see that the contact angle was 92.29 before the dynamic contact and 92.1 after the dynamic contact. This could have been either because the trimethylsilyls repelled the water after the dynamic contact, or the dynamic contact didn't cause the water to penetrate the valleys.

The DIM contact angle after the dynamic contact caused all the samples to wet except for the received TOX and etched TOX. We see that for the DIM contact angle before and after the dynamic contact for the received TOX gave values of 50.18 before dynamic contact and 51.6

after dynamic contact. What happened here is that the DIM didn't penetrate the surface. The contact angle after dynamic contact is higher but it is still with error of the contact angle before the dynamic contact. The DIM contact angle for the etched TOX showed that after the dynamic contact the contact angle increased by 3 degrees;  $41.77^\circ$  for the DIM contact angle before dynamic contact and  $44.9^\circ$  after dynamic contact. From this observation it is obvious that the DIM didn't penetrate the surface of the etched TOX, and the reason the contact angle was higher after the dynamic contact is probably because of impurities on the sample.

As has already been mentioned, the Cassie-Baxter model makes the assumption that air can be trapped between the peaks or pillar of a material while the liquid rests on top of the air/peaks. While the Wenzel model makes the assumption that the liquid penetrates the surface of the sample. What happens in this mechanism is that when the liquid touches the surface of the samples there is a transition from the Cassie-Baxter model to the Wenzel model. When the liquid is placed on the sample and a dynamic contact mechanism is done to it, the mechanism will wet the sample. And if the sample is wet already, forming another droplet will cause the contact angle to reduce.

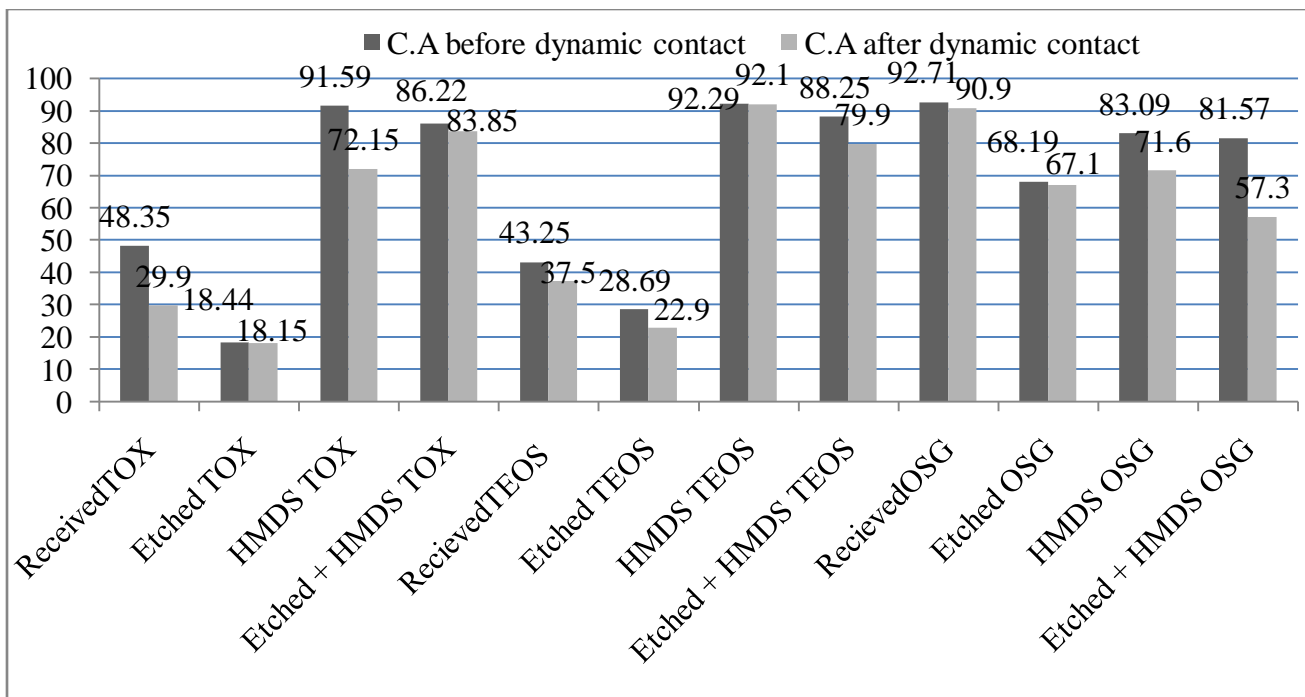


**Figure 6-1 a)** Water Contact Angle Before and After Dynamic Contact

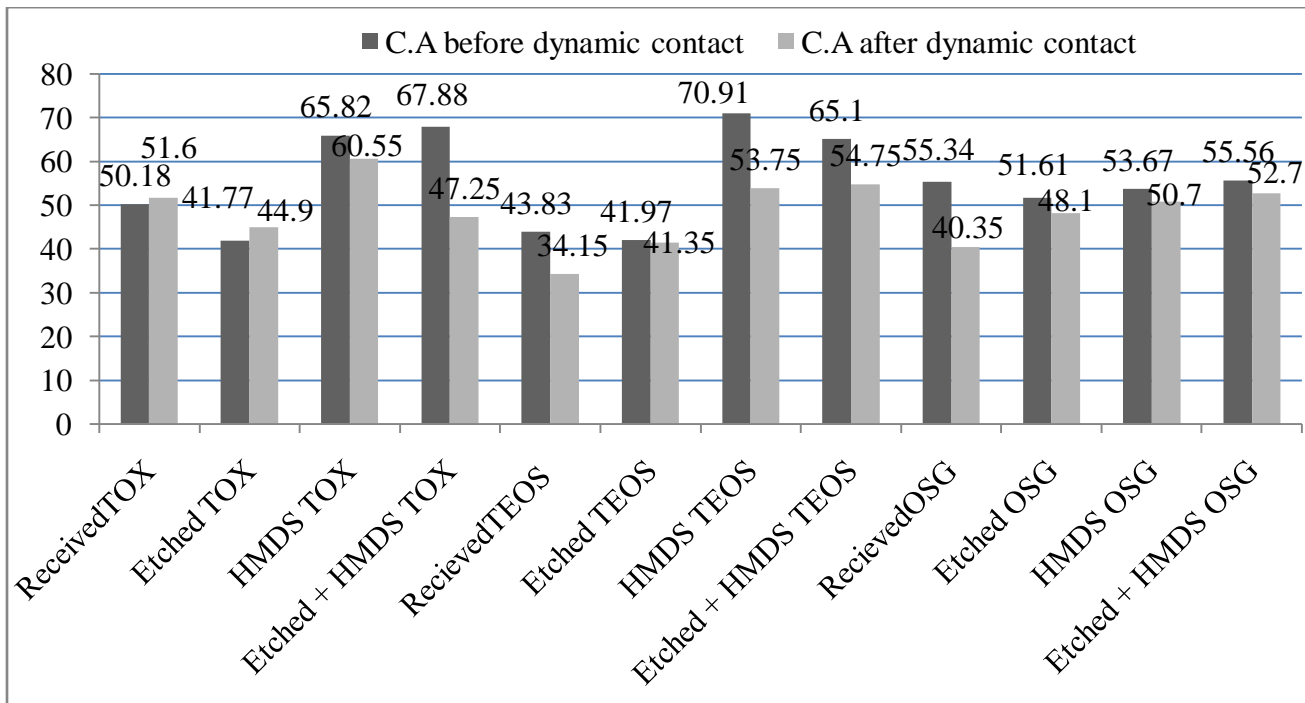


**Figure 6-1 b)** DIM Contact Angle Before and After Dynamic Contact

## 6.2 Wetting in ESEM vs. Goniometer

ESEM permitted the imaging of the formation of micro water droplets on the various surfaces. Additional experiments examined the effect of the weight of the water droplet (i.e., its size and height) on the measured contact angle. The measurements were taken in the environmental scanning electron microscope. The pressure was held at 6 Torr while the temperature was changed from 1 to 4 degrees Celsius. The point was to form water droplets on the sample surface such that the drops were on the 5 – 10 micron scale. The Image J software was used to calculate the contact angle. The results show that for smaller droplets, the contact angle increased for some and decreased for the others. The results are shown in the figure 6-2.

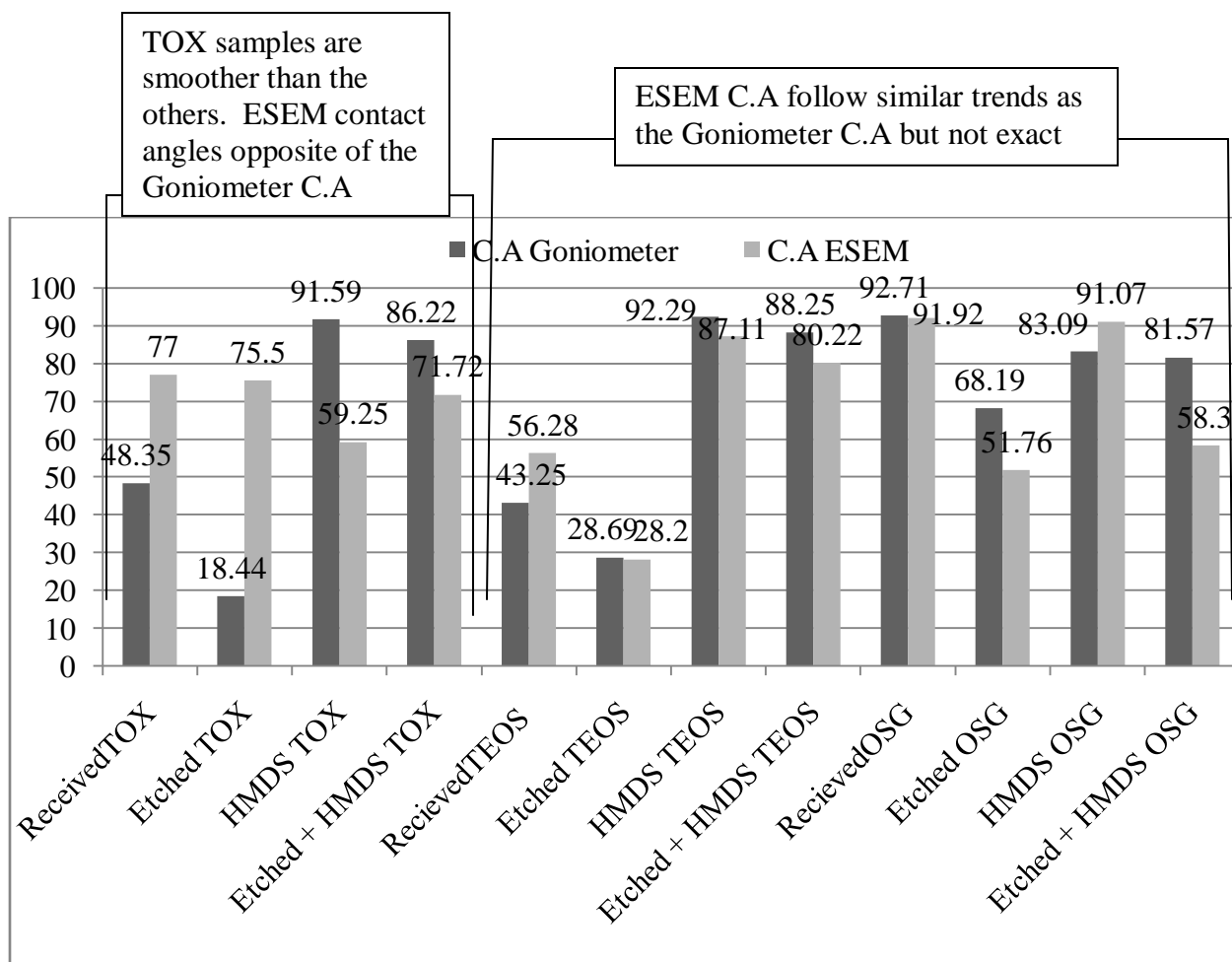


**Figure 6-2** Water Contact Angle on Goniometer and ESEM

It appears that the size of the water droplet, has an affect on the contact angle. However, there isn't a direct correlation between the roughness and chemistry on the contact angle for the micro droplets. For the Received TOX and etched TOX, the ESEM contact angle increases. But for the HMDS TOX and etched + HMDS TOX, the ESEM contact angle decreases. The TOX samples are smoother than the other samples and it appears that the contact angles are opposite as for the goniometer contact angle. For the received TEOS the ESEM contact angle increases, but for the etched TEOS the ESEM contact angle remains the same as for the goniometer contact angle. For the HMDS TEOS and the etched + HMDS TEOS, the ESEM contact angle decreases relative to the goniometer contact angle. The ESEM contact angle ( $91.92^\circ$ ) for the received OSG shows the same value as the goniometer contact angle ( $92.71^\circ$ ). For etched OSG and etched + HMDS OSG the ESEM contact angle decreases realitive to the goniometer contact angle. However, the HMDS OSG showed a reduction of the contact angle for the ESEM. One thing that appears to be happening, is that for the rougher samples the goniometer contact angle and the ESEM contact angle start to corralate. However, they are not exactly the same. Figure 6-3 a-d shows pictures of a droplet at the micro scale as it condenses on a surface.

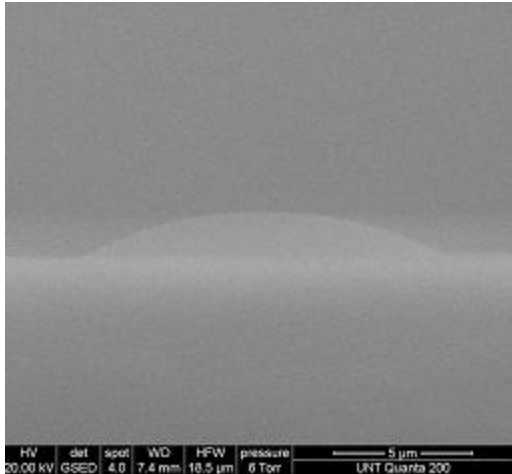


**Figure 6-3 a**

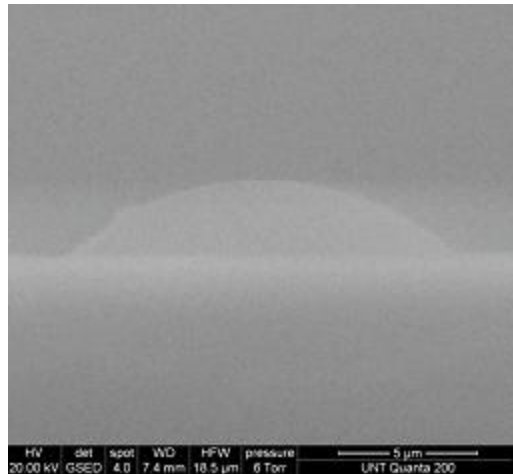


**Figure 6-3 b**

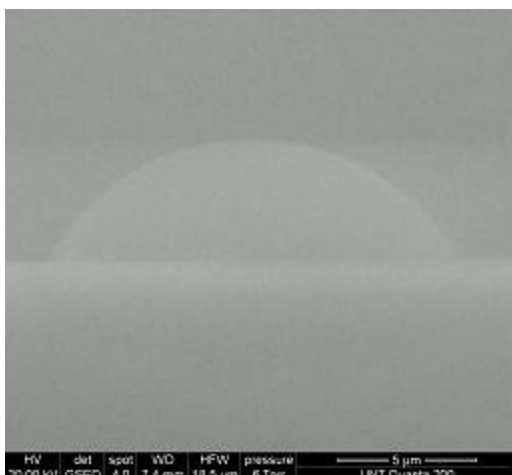


**Figure 6-3 c**

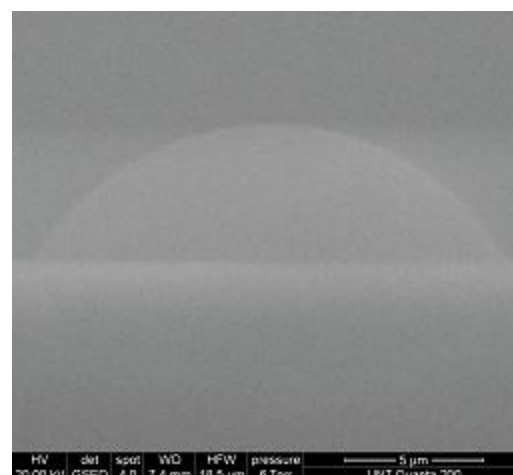


**Figure 6-3 d**

**Figure 6-3 a,b,c,d)** Images of Water Droplet on the Environmental Scanning Electron Microscope as the Drop Starts to Condense and Grow on the Samples

## CHAPTER 7

### CONCLUSIONS AND FUTURE WORK

#### 7.1 Conclusion

There is a clear correlation between the contact angle and surface chemistry. The more hydroxyls a surface has the more it attracts water. The trimethylsilyl groups on the sample increased the contact angle. DIM showed similar trends to the water contact angle but it showed that it is not heavily affected by the hydroxyls. There was no clear correlation between the RMS roughness and the contact angle. The OSG samples showed that etching and supercritical functionalization had no effect on the surface. However, it did show that etching + functionalization changed the surface. The dynamic contact measurements show that water can penetrate the surface of the samples. The DIM also shows that it can penetrate the surface of the samples. The ESEM contact angle does shows that size on the micro scale affects the water contact angle. One thing that was observed for the ESEM contact angle is that the ESEM contact angle and the goniometer contact angle appear to correlate as the samples were rougher. However, there is no direct correlation between micro scale contact angle with RMS roughness and surface chemistry.

#### 7.2 Future Work

The roughness effect on the contact angle for these samples should be further investigated since it showed no direct correlation between roughness and contact angle. The contact angle in the environmental scanning electron microscope needs to be further investigated. This preliminary work showed difference in the ESEM contact angle as compared to the goniometer contact angle. However, there was no direct correlation between the ESEM contact angle with the roughness or chemistry of the samples. The dynamic contact mechanism

should also be further investigated on the ESEM to see if at the microscopic level the surface allows the penetration of a fluid.

## BIBLIOGRAPHY

- [1] K. L. Mittal, Ed., *Contact Angle, Wettability and Adhesion* vol 2. Utrecht: VSP BV, 2002.
- [2] R. J. Stokes and D. F. Evans, *Fundamentals of Interfacial Engineering*. New York: Wiley-VCH, 1997.
- [3] Z. Yoshimitsu, A. Nakajima, T. Watanabe, and K. Hashimoto, "Effects of surface structure on the hydrophobicity and sliding behavior of water droplets." *Langmuir*, vol. 18, pp. 5818-5822, May. 2002.
- [4] P. Letellier, A. Mayaffre, and M. Turmine, "Drop size effect on contact angle explained by nonextensive thermodynamics. Young's equation revisited." *Journal of Colloid and Interface Science*, vol. 314, pp. 604-614, May. 2007.
- [5] D. Y. Kwok, T. Gietzelt, K. Grundke, H.-J. Jacobasch, and A. W. Neumann. "Contact angle measurements and contact angle interpretation. 1. Contact angle measurements by axisymmetric drop shape analysis and a goniometer sessile drop technique." *Langmuir*, vol. 13, pp. 2880-2894, Mar. 1997.
- [6] D. Aronov and G. Rosenman. "Wettability study of modified silicon dioxide surface using environmental scanning electron microscopy." *Journal of Applied Physics*, vol. 101, pp. 084901-5, Apr. 2007.
- [7] T. S. Meiron, A. Marmur and I. Saguy. "Contact angle measurement on rough surfaces." *Journal of Colloid and Interface Science*, vol. 274, pp. 637-644, Mar. 2004.
- [8] M. Nosonovsky and B. Bhushan, "Cassie-Wenzel wetting regime transition," in *Multiscale Dissipative Mechanisms and Hierarchical Surfaces Friction*,

*Superhydrophobicity, and Biomimetics*, Berlin Heidelberg New York: Springer, 2008, pp. 153-167.

- [9] N. A. Patankar, "On the modeling of hydrophobic contact angles on rough surfaces," *Langmuir*, vol. 19, pp. 1249-1253, Nov. 2003.
- [10] P. J. Ramón-Torregrosa, M.A. Rodríguez-Valverde, A. Amirfazli, and M.A. Cabrerozo-Vilchez. "Factors affecting the measurement of roughness factor of surfaces and its implications for wetting studies." *Colloids and Surfaces A: Physicochemical and Engineering Aspects*, vol. 323, pp. 83-93, Nov. 2008.
- [11] Y.J. Sheng, S. Jiang, H.K. Tsao, "Effects of geometrical characteristics of surface roughness on droplet wetting," *Journal of Chemical Physics*, vol. 127, pp. 234704-7, Dec. 2007.
- [12] T. Soeno, K. Inokuchi and S. Shiratori, "Ultra-water-repellent surface: fabrication of complicated structure of SiO<sub>2</sub> nanoparticles by electrostatic self-assembled films," *Applied Surface Science*, vol. 237, pp. 539-543, Sept. 2004.
- [13] D. M. Spori, T. Drobek, S. Zürcher, M. Ochsner, C. Sprecher, A. Mühlebach, and N. D. Spencer, "Beyond the lotus effect: Roughness influences on wetting over a wide surface-energy range." *Langmuir*, vol. 24, pp. 5411-5417, Apr. 2008.
- [14] F. K. Hansen. *The Measurement of Surface Energy of Polymers by Means of Contact Angles of Liquids on Solid Surfaces*. Available:  
[http://www.ramehart.com/goniometers/support/surface\\_energy\\_finn.pdf](http://www.ramehart.com/goniometers/support/surface_energy_finn.pdf)
- [15] S. Wolf, "Oxidation," in *Microchip Manufacturing*, Sunset Beach: Lattice Press, 2004, pp. 213-216.

- [16] F. Ample and C. Joachim, "The chemisorption of polyaromatic hydrocarbons on Si (1 0 0) H dangling bonds," *Surface Science*, vol. 602, pp. 1563-1571, Mar. 2008.
- [17] A. J. Bauer, B. Froeschle, M. Beichele, and H. Ryssel, "Characterization of oxide etching and wafer cleaning using vapor phase anhydrous hydrofluoric acid and ozone," *Microelectronics and Reliability*, vol. 39, pp. 311-316, Mar. 1999.
- [18] I. A. Dogel, S.A. Dogel, J.L. Pitters, G.A. DiLabio and R.A. Wolkow, "Chemical methods for the hydrogen termination of silicon dangling bonds," *Chemical Physics Letters*, vol. 448, pp. 237-242, Oct. 2007.
- [19] J. K. Kang and C. B. Musgrave, "The mechanism of HF/H<sub>2</sub>O chemical etching of SiO<sub>2</sub>," *Journal of Chemical Physics*, vol. 116, pp. 275-280, Jan. 2002.
- [20] G. A. C. M. Spierings, "Wet chemical etching of silicate glasses in hydrofluoric acid based solutions," *Journal of Materials Science*, vol. 28, pp. 6261-6273, Feb. 1993.
- [21] A. Witvrouw, B. Du Bois, P. De Moor, A. Verbist, C. Van Hoof, H. Bender, and Kris Baert, "Comparison between wet HF etching and vapor HF etching for sacrificial oxide removal," Available:  
[http://www.primaxxinc.com/products/literature/Wet-dry\\_etching\\_comparison.pdf](http://www.primaxxinc.com/products/literature/Wet-dry_etching_comparison.pdf)
- [22] K. A. Reinhardt and W. Kern, Eds., *Handbook of silicon wafer cleaning technology*. Norwich, NY: William Andrew Publishing, 2008.
- [23] T. Ohmi, Ed., *Scientific wet process technology for innovative LSI/FPD manufacturing*. Boca Raton: CRC Press Taylor & Francis Group, 2006.
- [24] C. E. Bunker, "Fundamental Properties of Supercritical Fluids," in *Supercritical Fluid Technology in Materials Science and Engineering Syntheses, Properties, and Applications*, Y. P. Sun, Ed., New York-Basel: Marcel Dekker, Inc, 2002, pp. 1-58.

- [25] K. W. Hutchenson, "Organic Chemical Reactions and Catalysis in Supercritical Fluid Media," in *Supercritical Fluid Technology in Materials Science and Engineering Syntheses, Properties, and Applications*, Y. P. Sun, Ed., New York-Basel: Marcel Dekker, Inc, 2002, pp. 87-188.
- [26] C. Erkey, "Homogeneous Catalysis in Supercritical Carbon Dioxide," in *Supercritical Fluid Technology in Materials Science and Engineering Syntheses, Properties, and Applications*, Y. P. Sun, Ed., New York-Basel: Marcel Dekker, Inc, 2002, pp. 189-226.
- [27] Y. P. Sun, Ed., *Supercritical Fluid Technology in Materials Science and Engineering Syntheses, Properties, and Applications*. New York-Basel: Marcel Dekker, Inc, 2002.
- [28] R.F. Reidy, E.C. Chaung, R.A. Orozco-Teran, P.P. Kadam, P.D. Matz, J.T. Rhoad, E.L. Busch, D.W. Mueller, "Supercritical pore sealing of porous MSQ," presented at Advanced Metallization Conference. San Diego, CA, Oct 19-21, 2004.
- [29] P. M. Capani, P.D. Matz, D.W. Mueller, M.J. Kim, E.R. Walter, J.T. Rhoad, E.L. Busch, and R.F. Reidy "Observation of intrusion rates of hexamethyldisilazane during supercritical carbon dioxide functionalization of triethoxyfluorosilane low-k films," in *Mater. Res. Soc. Symp. Proc.*, 2005, vol. 863, pp. 177–182.
- [30] P. D. Matz and R. F. Reidy, "Supercritical CO<sub>2</sub> applications in BEOL cleanin," *Solid State Phenomena*, vol. 103-104, pp. 315-322, Apr. 2005.
- [31] B.P. Gorman, R.A. Orozco-Teran, Z. Zhang, P.D. Matz, D.W. Mueller, and R.F. Reidy "Rapid repair of plasma ash damage in low-k dielectrics using supercritical CO<sub>2</sub>," *Journ. Vac. Sci. Technol. B: Microelectronics and Nanometer Structures*, vol. 22, pp. 1210-1212, May. 2004.

- [32] R. A. Orozco-Teran, "Functionalization and characterization of porous low- $\kappa$  dielectrics." Ph.D. dissertation, Mater. Sci. Eng., Uni. Nor. Tex. , Denton, TX, 2005.
- [33] S. Wolf, "Oxidation," in *Microchip Manufacturing*, Sunset Beach: Lattice Press, 2004, pp. 216-235.
- [34] S. Wolf, "CVD of amorphous and polycrystalline thin films," in *Microchip Manufacturing*, Sunset Beach: Lattice Press, 2004, pp. 269-302.
- [35] A. Grill, "Low and ultra dielectric constant films prepared by plasma enhanced chemical vapor deposition," in *Dielectric films for advanced microelectronics* M. Baklanov, Ed., West Susex: John Wiley & Sons 2007, pp. 1-32.
- [36] Z. Miao, H. Yu, W. Song, D. Zhao, L. Hao, B. Yi and Z. Shao, "Effect of hydrophilic SiO<sub>2</sub> additive in cathode catalyst layers on proton exchange membrane fuel cells," *Electrochim. Comm.*, vol. 11, pp. 787-790, Jan. 2009.
- [37] N. D. Hegde and A. Venkateswara Rao, "Organic modification of TEOS based silica aerogels using hexadecyltrimethoxysilane as a hydrophobic reagent," *Appl. Surf. Sci.*, vol. 253, pp. 1566-1572, Apr. 2006.
- [38] S. A. Mirji, "Octadecyltrichlorosilane adsorption kinetics on Si(100)/ SiO<sub>2</sub> surface: contact angle, AFM, FTIR and XPS analysis," *Surf. Interface Anal.*, vol. 38, pp. 158-165, Jan. 2006.
- [39] S. D. Bhagat and A. V. Rao, "Surface chemical modification of TEOS based silica aerogels synthesized by two step (acid-base) sol-gel process," *Applied Surface Science*, vol. 252, pp. 4289-4297, Aug. 2005.

- [40] F. Persson, L H Thamdrup, M.B.L. Mikkelsen, S.E. Jaarlgard, P. Skafte-Pedersen, H. Bruus, and A. Kristensen, "Double thermal oxidation scheme for the fabrication of SiO<sub>2</sub> nanochannels," *Nanotechnology*, vol. 18, pp. 245301-2553014, May. 2007.
- [41] L. D. Eske and D. W. Galipeau, "Characterization of SiO<sub>2</sub> surface treatments using AFM, contact angles and a novel dewpoint technique," *Colloids and Surfaces A: Physicoche. Eng. Aspects*, vol. 154, pp. 33-51, 1999.
- [42] A. Amirfazli, D. Chatain, and A.W. Neumann, "Drop size dependence of contact angles for liquid tin on silica surface: line tension and its correlation with solid-liquid interfacial tension," *Colloids and Surfaces A: Physicochem. Eng. Aspects*, vol. 142, pp. 183-188, Jan. 1998.
- [43] R. R. Thomas, F. B. Kaufman, J.T. Kirleis, and R.A. Belsky, "Wettability of polished silicon oxide surfaces," *J. Electrochem. Soc.*, vol. 143, pp. 643-648, Feb. 1996.
- [44] S. M.M. Ramos, A. Benyagoub, B. Canut, P. De Dieuleveult, and G. Messin, "Strong water repellency effect on SiO<sub>2</sub> films processed at a nanometric scale," *Euro. Phys. J. B - Condensed Matter and Complex Systems*, vol. 62, pp. 405-410, May 2008.
- [45] M.L. O'Neill, R.N. Vrtis, J.L. Vincent, A.S. Lukas, E.J. Karwacki, B.K. Peterson, and M.D. Bitner, "Optimized materials properties for organosilicate glasses produced by plasma-enhanced chemical vapor deposition," in *Mater. Res. Soc. Symp. Proc.*, 2003, vol. 766, pp. E8.17.1-E8.17.6.
- [46] S. Lee, J. Yang, S. Yeo, J. Lee, D. Jung, J. Boo, H. Kim, and H. Chae, "Effect of annealing temperature on dielectric constant and bonding structure of low-k SiCOH thin films deposited by plasma enhanced chemical vapor," *Jpn J Appl Phys*, vol. 46, pp. 536-541, Feb. 2007.

- [47] J. B. Vella, I.S. Adhiketty, K. Junker, and A.A. Volinsky, "Mechanical properties and fracture toughness of organo-silicate glass (OSG) low-k dielectric thin films for microelectronic applications," *International Journal of Fracture*, vol. 120, pp. 487-499, 2003.
- [48] B. Lahlouh, J. A. Lubguban, G. Sivaraman, R. Gale, and S. Gangopadhyay, "Silylation using a supercritical carbon dioxide medium to repair plasma-damaged porous organosilicate films," *Electrochemical and Solid-State Letters*, vol. 7, pp. G338-G341, Nov. 2004.
- [49] D. Shamiryan, M. R. Baklanov, G. Vereecke, S. Vanhaelemeersch, and K. Maex, "Modification of low-k SiCOH film porosity by a HF solution," *Solid State Phenomena*, vol. 76-77, pp. 135-138, 2001.
- [50] J. Liu, W. Kim, J. Bao, H. Shi, W. Baek, and P. S. Ho, "Restoration and pore sealing of plasma damaged porous organosilicate low k dielectrics with phenyl containing agents," *Journal of Vacuum Science & Technology B: Microelectronics and Nanometer Structures*, vol. 25, pp. 906-912, May. 2007.
- [51] J.L. Panza and E.J. Beckman , "Surfactants in supercritical fluids," in *Supercritical Fluid Technology in Materials Science and Engineering Syntheses, Properties, and Applications*, Y.P. Sun Ed., New York-Basel: Marcel Dekker, Inc, 2002. pp. 261-290
- [52] V. P. Tolstoy, I. V. Chernyshova, and V. A. Skryshevsky, Eds., *Handbook of infrared spectroscopy of ultrathin films*, Hoboken, New Jersey: John Wiley & Sons, 2003, pp. 1-710.

- [53] J. N. Cox, "Fourier transform infrared spectroscopy," in *Encyclopedia of Materials Characterization - Surfaces, Interfaces, Thin Films*, C. R. Brundle, Ed., Greenwich, CT: Manning Publications, 1992, pp. 416-427.
- [54] C. R. Brundle, "X-Ray Photoelectron Spectroscopy," in *Encyclopedia of Materials Characterization - Surfaces, Interfaces, Thin Films*, C. R. Brundle, Ed., Greenwich, CT: Manning Publications, 1992, pp. 282-299.
- [55] C. D. Wagner, W. M. Riggs, L.E Davis, J.F. Moulder, and G.E Muilinberg, *Handbook of X-Ray Photoelectron Spectroscopy*, Eden Praire, MN: Perkin Elmer Corporation, 1979.
- [56] F. A. Stevie, "Surface Roughness Measurement, Formation by Sputtering, Impact on Depth," in *Encyclopedia of Materials Characterization - Surfaces, Interfaces, Thin Films*, C. R. Brundle, Ed., Creenwich, CT: Manning Publications, 1992, pp. 698-710.
- [57] S. N. Magonov and M.H. Whangbo, *Surface Analysis with STM and AFM*, New York, NY: VCH Publishers, Inc., 1996.
- [58] A. M. Donald, "The use of environmental scanning electron microscopy for imaging wet and insulating materials," *Nat Mater*, vol. 2, pp. 511-516, Aug. 2003.
- [59] J. B. Bindell, "Scanning electron microscopy." in *Encyclopedia of Materials Characterization - Surfaces, Interfaces, Thin Films*, C. R. Brundle, Ed, Greenwich, CT: Manning Publications, 1992, pp. 70-84.
- [60] R. A. Orozco-Teran, B. P. Gorman, D. W. Mueller, M. R. Baklanov, and R. F. Reidy, "Effect of silylation on triethoxyfluorosilane xerogel films by means of atmospheric pressure drying," *Thin Solid Films*, vol. 471, pp. 145-153, Jun. 2004.

- [61] B. Narayanan, R. Kumar, and P. D. Foo, "Properties of low-k SiCOH films prepared by plasma-enhanced chemical vapor deposition using trimethylsilane," *Microelectronics Journal*, vol. 33, pp. 971-974, Aug. 2002.
- [62] J. Serra, P. González, S. Liste, C. Serra, S. Chiussi, B. León, M. Pérez-Amor, H. O. Ylänen, and M. Hupa, "FTIR and XPS studies of bioactive silica based glasses," *Journal of Non-Crystalline Solids*, vol. 332, pp. 20-27, Nov. 2003.
- [63] K. Choi, T.J Eom and C. Lee, "Comparison of the removal efficiency for organic contaminants on silicon wafers stored in plastic boxes between UV/O<sub>3</sub> and ECR oxygen plasma cleaning methods," *Thin Solid Films*, vol. 435, pp. 227-231, Apr. 2003.
- [64] M. Deckwerth and C. Rüssel, "A new polymeric route to silicon carbide and silicon nitride using elementary silicon as starting material," *Journal of Materials Science*, vol. 29, pp. 4500-4504, Feb. 1994.
- [65] G. Müller, J. Bódis, G. Eder-Mirth, J. Kornatowski, and J. A. Lercher, "In situ FT-IR microscopic investigation of metal substituted AlPO<sub>4</sub>-5 single crystals," *Journal of Molecular Structure*, vol. 410-411, pp. 173-178, Nov. 2003.
- [66] P Gupta, A.C Dillon, A.S Bracker, and S.M George, "FTIR studies of H<sub>2</sub>O and D<sub>2</sub>O decomposition on porous silicon surfaces," *Surface Science*, vol. 245, pp. 360-372, Apr. 1991.
- [67] E. Kondoh, T. Asano, H. Arao, A. Nakashima, and M. Komatsu, "Dehydration after plasma oxidation of porous low-dielectric-constant spin-on-glass films," *Japanese Journal of Applied Physics*, vol. 39, p. 3919-3923, May 2000.

- [68] S. Sahli, S. Rebiai, P. Raynaud, Y. Segui, A. Zenasni, and S. Mouissat, "Deposition of SiO<sub>2</sub>-like films by HMDSN/O<sub>2</sub> plasmas at low pressure in a MMP-DECR reactor," *Plasmas and Polymers*, vol. 7, pp. 327-340, Dec. 2002.
- [69] J. A. Roepsch, B. P. Gorman, D. W. Mueller, and R. F. Reidy, "Dielectric behavior of triethoxyfluorosilane aerogels," *Journal of Non-Crystalline Solids*, vol. 336, pp. 53-58, Feb. 2004.
- [70] M. J. Loboda, C. M. Grove, and R. F. Schneider, "Properties of a-SiOx:H thin films deposited from hydrogen silsesquioxane resins," *Journal of The Electrochemical Society*, vol. 145, pp. 2861-2866, Aug. 1998.
- [71] Mei Jia-Xin, Xu Jun, Ma Zhong-Yuan, Zhu-Da, Sui Yan-Ping, Li Wei, Li Xin, Rui Yun-Jun, Huang Xin-Fan, and Chen Kun-Ji, "Structural evolution of a-Si:H/ SiO<sub>2</sub> multilayers upon step by step thermal annealing," *Chinese Physics*, vol. 13, pp. 1365-1369, Aug. 2004.
- [72] A. Barranco, J. Cotrino, F. Yubero, T. Girardeau, S. Camelio, and A. R. González-Elipe, "A structural study of organo-silicon polymeric thin films deposited by remote microwave plasma enhanced chemical vapour deposition," *Surface and Coatings Technology*, vol. 180-181, pp. 244-249, Mar. 2004.
- [73] A. Belgorokhov and L. Belgorokhova, "Optical properties of porous silicon layers processed with a HF: HCl: C<sub>2</sub>H<sub>5</sub>OH electrolyte," *Semiconductors*, vol. 33, pp. 169-174, Feb 1999.
- [74] H. S. Quanli Hu, H. Gao, H. Araki, W. Yang and T. Noda, "High-frequency FTIR absorption of SiO<sub>2</sub>/Si nanowires," *Chemical Physics Letters*, vol. 378, pp. 299-304 Aug. 2003.

- [75] T. Noda, H. Suzuki, H. Araki, W. Yang, Ying Shi, and M. Tosa, "Microstructures and IR spectra of long amorphous SiO<sub>2</sub>/Si nanowires," *Applied Surface Science*, vol. 241, pp. 231-235, Feb. 2005.
- [76] P. G. Pai, S.S Chao, Y. Takagi, and G. Lucovsky, "Infrared spectroscopic study of SiO<sub>x</sub> films produced by plasma enhanced chemical vapor deposition," *Journal of Vacuum Science & Technology A: Vacuum, Surfaces, and Films*, vol. 4, pp. 689-694, May. 1986.
- [77] K. Y. Yang, W.J. Yoo, and A. Krishnamoorthy, "Effect of electric field on chemical bonds of carbon-doped silicon oxide as evidenced by in situ Fourier transform infrared spectroscopy," *Journal of Vacuum Science & Technology B: Microelectronics and Nanometer Structures*, vol. 23, pp. 433-436, Mar. 2005.
- [78] V. E. Vamvakas and D. Davazoglou, "Comparison of FTIR transmission spectra of thermally and LPCVD SiO<sub>2</sub> films grown by TEOS pyrolysis," *Journal of The Electrochemical Society*, vol. 151, pp. F93-F97, Mar. 2004.
- [79] J. Rappich and H. J. Lewerenz, "In situ FTIR investigation of the electrochemical microstructuring of n-Si(111)," *Electrochimica Acta*, vol. 41, pp. 675-680, Apr. 1996.
- [80] M. K. Gunde, "Vibrational modes in amorphous silicon dioxide," *Physica B: Condensed Matter*, vol. 292, pp. 286-295, Nov. 2000.
- [81] M. J. Martin Kopani, H. Kobayashi, M. Takahashi, R. Brunner, M. Mikula, K. Imamura, S. Jurecka, and E. Pincik, "On determination of properties of ultrathin and very thin silicon oxide layers by FTIR and X - ray reflectivity," in *Mater. Res. Soc. Symp. Proc.*, 2008, vol. 1066, pp. A07-031-A07-036.

- [82] P. J. Tonge, R. Fausto, P.R. Carey, "FTIR studies of hydrogen bonding between  $\alpha,\beta$  unsaturated esters and alcohols," *Journal of Molecular Structure*, vol. 379, pp. 135-142, Jun. 1996.
- [83] P. Chiniwalla, Y. Bai, E. Elce, R. Shick, W. C. McDougall, S. A. B. Allen, and P. A. Kohl, "Crosslinking and decomposition reactions of epoxide-functionalized polynorbornene. II. Impact of reactions on mechanical properties," *Journal of Applied Polymer Science*, vol. 91, pp. 1020-1029, Nov. 2003.
- [84] D. B. Mawhinney, J. A. Glass Jr, J. T. Yates Jr, "FTIR study of the oxidation of porous silicon," *Journal of Physical Chemistry B*, vol. 101, pp. 1202-1206, Feb. 1997.
- [85] K.T. Queeney, M.K. Weldon, J.P. Chang, Y.J. Chabal, A.B. Gurevich, J. Sapjeta, R.L. Opila, "Infrared spectroscopic analysis of the Si/  $\text{SiO}_2$  interface structure of thermally oxidized silicon," *Journal of Applied Physics*, vol. 87, pp. 1322-1330, Feb. 2000.
- [86] F. R. F. Razi , and A. Irajizad, "Fourier transform infrared spectroscopy and scanning tunneling spectroscopy of porous silicon in the presence of methanol," *Elsevier*, vol. 132 pp. 40-44, May. 2008.
- [87] E. Vinogradova, C. E. Smith, D.W. Mueller, A.J. McKerrow, and R.F. Reidy, "Moisture adsorption in plasma-damaged porous low-k dielectrics," in *Mater. Res. Soc. Symp. Proc*, 2008, vol. 1079, pp. N02-091-N02-096
- [88] Q. Wang, X. Fan, W. Gao, and J. Chen, "Characterization of bioscoured cotton fabrics using FT-IR ATR spectroscopy and microscopy techniques," *Carbohydrate Research*, vol. 341, pp. 2170-2175, Sept. 2006.